ISSN 1408-7073

RMZ – MATERIALS AND GEOENVIRONMENT

PERIODICAL FOR MINING, METALLURGY AND GEOLOGY

RMZ – MATERIALI IN GEOOKOLJE

REVIJA ZA RUDARSTVO, METALURGIJO IN GEOLOGIJO

RMZ-M&G, Vol. 57, No. 1 pp. 001–158 (2010)
Ljubljana, March 2010

Historical Rewiev

More than 80 years have passed since in 1919 the University Ljubljana in Slovenia was founded. Technical fields were joint in the School of Engineering that included the Geologic and Mining Division while the Metallurgy Division was established in 1939 only. Today the Departments of Geology, Mining and Geotechnology, Materials and Metallurgy are part of the Faculty of Natural Sciences and Engineering, University of Ljubljana.

Before War II the members of the Mining Section together with the Association of Yugoslav Mining and Metallurgy Engineers began to publish the summaries of their research and studies in their technical periodical Rudarski zbornik (Mining Proceedings). Three volumes of Rudarski zbornik (1937, 1938 and 1939) were published. The War interrupted the publication and not untill 1952 the first number of the new journal Rudarsko-metalurški zbornik - RMZ (Mining and Metallurgy Quarterly) has been published by the Division of Mining and Metallurgy, University of Ljubljana. Later the journal has been regularly published quarterly by the Departments of Geology, Mining and Geotechnology, Materials and Metallurgy, and the Institute for Mining, Geotechnology and Environment.

On the meeting of the Advisory and the Editorial Board on May 22nd 1998 Rudarsko-metalurški zbornik has been renamed into "RMZ - Materials and Geoenvironment (RMZ -Materiali in Geookolje)" or shortly RMZ - M&G.

RMZ - M&G is managed by an international advisory and editorial board and is exchanged with other world-known periodicals. All the papers are reviewed by the corresponding professionals and experts.

RMZ - M&G is the only scientific and professional periodical in Slovenia, which is published in the same form nearly 50 years. It incorporates the scientific and professional topics in geology, mining, and geotechnology, in materials and in metallurgy.

The wide range of topics inside the geosciences are wellcome to be published in the RMZ -Materials and Geoenvironment. Research results in geology, hydrogeology, mining, geotechnology, materials, metallurgy, natural and antropogenic pollution of environment, biogeochemistry are proposed fields of work which the journal will handle. RMZ - M&G is co-issued and co-financed by the Faculty of Natural Sciences and Engineering Ljubljana, and the Institute for Mining, Geotechnology and Environment Ljubljana. In addition it is financially supported also by the Ministry of Higher Education, Science and Technology of Republic of Slovenia.

Editor in chief

Table of Contents – Kazalo

Original Scientific Papers – Izvirni znanstveni članki

Inverse determination of viscoelastic properties of human fingertip skin

Inverzno določanje viskoelastičnih lastnosti človeške kože na prstu

Silvia Giavazzi[1], Marco Francesco Ganatea[1], Mitja Trkov[2], Primož Šuštarič[3] & Tomaž Rodič[2, 3, *]

[1]Politecnico di Milano, Facoltà di Ingegneria dei Processi Industriali, Piazza Leonardo da Vinci, 26, 20133 Milano, Italy
[2]University of Ljubljana, Faculty of Natural Sciences and Engineering, Aškerčeva cesta 12, SI-1000 Ljubljana, Slovenia
[3]C3M, d. o. o., Centre for Computational Continuum Mechanics, Tehnološki park 21, SI-1000 Ljubljana, Slovenia

*Corresponding author. E-mail: tomaz.rodic@ntf.uni-lj.si

Received: December 11, 2009 **Accepted:** February 23, 2010

Abstract: This paper presents a combined experimental-numerical procedure to determine viscoelastic properties of human skin at the tip of an index finger. The in-vivo biomechanical test was performed by a non-intrusive suction instrument Cutometer® MPA 580 (Courage-Khazaka). The measurements of the fingertip skin deflections performed at various levels of negative pressures were analysed by an inverse finite element based procedure in order to determine parameters of the Fung material model, including a non-linear elastic part and a linear viscous part represented by a five-term Prony series. The constitutive parameters of the fingertip skin are applicable for computer modeling of biophysical phenomena that govern tactile sensations as well as for setting the target viscoelastic properties for developing biomimetic materials for hand prostheses and humanoid robotics.

Izvleček: Namen članka je predstavitev kombiniranega eksperimentalno-numeričnega postopka za določanje viskoelastičnih lastnosti človeške kože na konicah prstov kazalcev. Biomehanski preizkus

Original scientific paper

je bil narejen v živo s podtlačno napravo Cutometer® MPA 580 (Courage-Khazaka). Merili smo deformacije kože pri različnih podtlakih ter jih nato analizirali z inverzno analizo po metodi končnih elementov, kjer je bil za kožo uporabljen Fungov snovni model, ki vključuje nelinearni elastični del in linearni viskozni del, predstavljen s petimi parametri vrste Prony. Konstitutivni parametri kožnega tkiva na prstnih blazinicah so uporabni za računalniške analize biofizikalnih pojavov med dotikom, kakor tudi kot ciljne vrednosti viskoelastičnih lastnosti za biomimetične materiale, ki se uporabljajo za proteze in humanoidno robotiko.

Key words: human skin, suction test, viscoelasticity, finite element method, inverse analysis
Ključne besede: človeška koža, podtlačni preizkus, viskoelastičnost, metoda končnih elementov, inverzna analiza

Introduction

The human skin is highly nonlinear, inhomogeneous and anisotropic material which is in vivo subjected to a pre-stress. Its biomechanical behaviour may be affected by several dermatological and systemic state variables that vary with the age, body site, race, sex, mood as well as environmental conditions including temperature, humidity, chemical environment etc (Wilkes et al., 1973 [1]; Fung, 1972 [2]).

To characterize biomechanical properties of skin and understand its non-linear behaviour specially designed biomechanical tests can be performed where skin is thermo-mechanically stimulated by suction, indentation, tangential tractions and other load combinations (Diridollou et al., 2001 [3]; Israelowitz et al., 2005 [4]). The stress-strain response of skin surface can be measured under controlled loading programme and the experimental recordings can be processed by inverse numerical methods in order to determine fundamental viscoelastic parameters for constitutive models proposed by Arruda & Boyce, 1993 [5]; Yeoh, 1990 [6]; Fung, 1993 [7]; Holzapfel, 1996 [8]; Rees & Govindjee, 1998 [9]; Perić & Dettmer, 1998 [10]; De souza et al., 2008 [11]; Dupaix & Boyce, 2007 [12] and Lubiner, 1990 [13].

The main motivation for the research considered in this paper is to determine viscoelastic properties of human skin at the fingertip in order to derive constitutive parameters for numerical modeling of tactile sensations and related mechanotransduction phenomena than govern neural responses when

exploring textured surfaces by touch (Jiyong et al., 2007 [14]; Wang & Hayward, 2007 [15]).

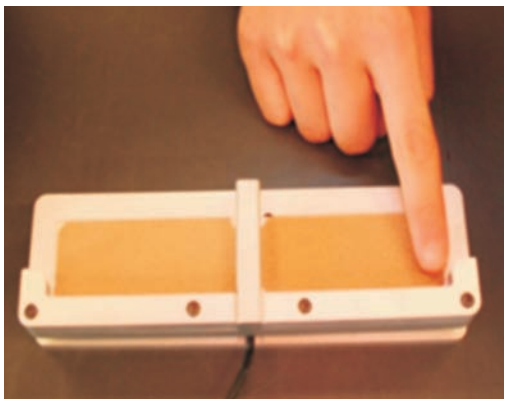

Figure 1. Tactile sensations and exploration of textured surfaces

Characterization of the Biomechanical Properties of Fingertip Skin

Characterization of the mechanical properties of skin was performed by sampling human skin at the fingertip of an index-finger. The experimental testing was performed in vivo by using a Cutometer® MPA 580 device (Courage + Khazaka Electronic GmbH, Koeln, Germany). This dermatological device is primarily used to evaluate the viscoelasticity of the skin by measuring its deflection at various levels of negative pressure. The testing principle is shown in Figure 2.

Suction test device

The device consists of a vacuum pump with a tank and a probe connected to it through a valve. Before the start of the test the pump decreases the pressure in the tank to the set value. When the test starts the skin is sucked into the probe's opening by the negative pressure created by the pump. During the test the pump generates a prescribed temporal evolution of pressure to evaluate transient deformation response of the skin.

A light sensor inside the probe measures the highest level reached by the skin sucked into the hole. The device is set to 0 mm which is the level observed when the negative pressure starts to pull the sample. This means that the possible increased level at the beginning, when the probe was pressed on the material due to the spring inside the probe, was not considered in the plotted result curve.

The probe's geometry shown in Figure 3 is composed of inner and outer concentric cylinders that are axially connected through a spring. The sensor is in the internal cylinder in which the skin is sucked.

Suction test method

In preliminary testing the identification of factors influencing the skin's mechanical response was made. The following factors were analyzed: load (pressure level imposed by the device), person (two different subjects were tested), hand (left or right) and various

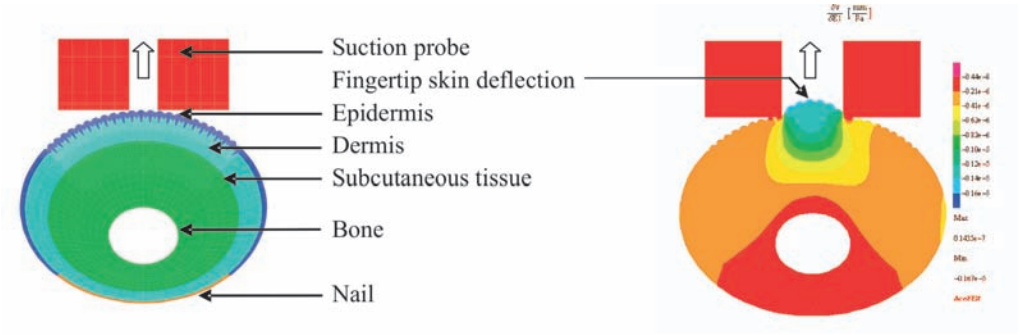

Figure 2. A crossection of a finger with different biological tissues and suction probe in undeformed (left) and deformed (right) configuration.

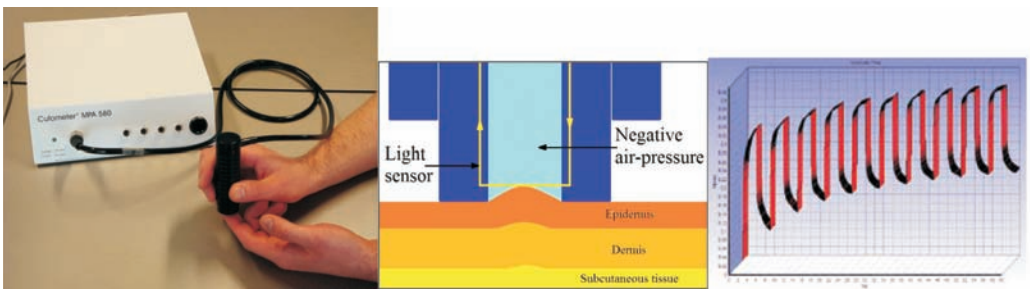

Figure 3. Experimental setup with the Cutometer® suction device

finger-tips (five fingers on each hand). The measurements for statistical analyses were acquired over a period of 15 days in both morning and afternoon sessions.

The results were analyzed using the one-way ANOVA statistical method. The results were further analyzed to compare the load, person, hand and various finger-tip results as defined by two different parameters. The first parameter was the mean value of the time interval between 49 s and 51 s for 200 data sets (MICHALERIS et al, 1994 [16]). This value is related to the response characteristics and their approximation. Note, that for the investigated stationary loading conditions, when the negative pressure was constant (see Figure 6 for loading conditions), the steady state response was not reached in the feasible time frames. The second parameter analyzed to represent how far the curve is from the steady state, was chosen as the mean value of the curve estimated derivatives in the time interval from 40 s to 50 s and represented the displacement rate at the end of the test. Statistics did not show any

significant differences between left and right hand fingers. Furthermore, no significant variations were observed with respect to the sampling time over the period of 15 days.

A standard protocol of index fingertip skin characterization was defined. For the skin suction test a probe with an opening radius 2 mm was used. The probe was positioned perpendicularly to the index fingertip and fixed with the other hand of the testing subject. When holding the probe between the fingers it was loaded using just the fingers' weight so that the spring retracted minimally into the device. This handling method is shown in Figure 2. The loading curve used was a pressure step. Seven different pressures were consecutively applied (150, 200, 250, 300, 350, 400, 450) mbar each of them for 60 s followed with a 15 s break. 10 cycles of measurements were performed on both of the index fingers of two different subjects while increasing the pressure from 150 mbar to 450 mbar.

Experimental test results with Cutometer®

Test experimental results for the characterization of index finger skin are presented in Figure 4 as an average response for each pressure level. The confidence interval of the average response was statistically evaluated. The semi-length of the confidence interval (related to a p-value of 0.05) over the

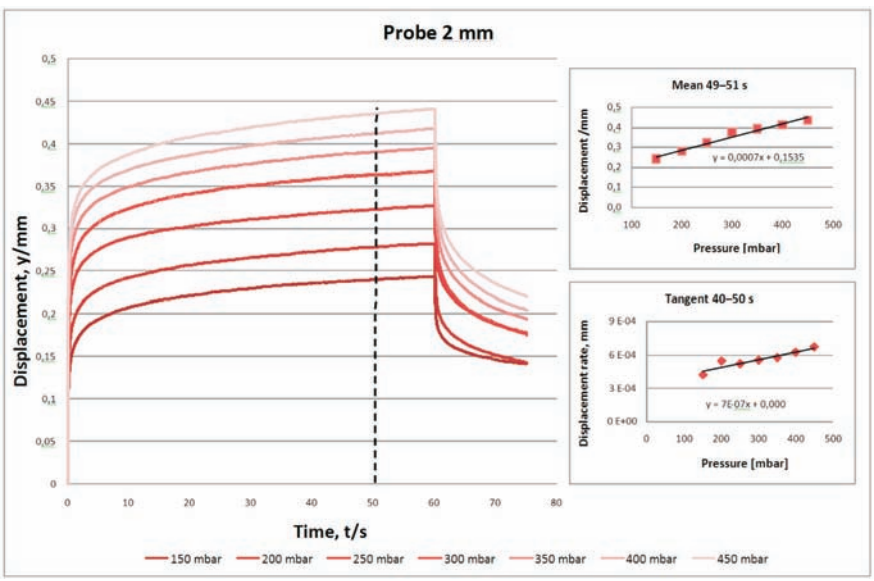

Figure 4. Average responses for each pressure levels for 2 mm hole radius of the test probe

average response is about 5 % for each test. In other word, it was affirmed with a probability of 95 %, that the estimation obtained for the average response is not more than 5 % from the real value of the estimated average response.

Finite Element model of the suction test

A finite element model of the suction tests was developed by AceGen system (KORELC, 2009 [17]) and implemented into AceFEM software (KORELC, 2009 [18]; Wolfram Research Inc Mathematica, 2008 [19]). The discretized numerical model of a finger cross-section with epidermal and dermal skin layers, subcutaneous tissue as well as bone and nail structure is presented in Figure 5. The spatial resolution of the model resembles the shape and size of fingerprint asperities. The probe was modeled by Neo-Hookian model with the stiffness much higher than the stiffness of the sample. The position of the probe was fixed. At the contact between the sample and the probe a Coulomb friction with a value of 0.35 was applied. The contact force generated due to the spring inside the probe was simulated as a pressure generated at the bottom of the bolster. The material law used for the sample was the Fung (FUNG, 1993 [7]) model.

The simulation was divided into four parts, enabling us to assign a different time step to each part, while considering both the computational time and the accuracy of the results. The loading phase was divided into two parts, the first from 0 s to 5 s and the second from 5 s to 60 s. The unloading phase was sectioned from 60 s to 65 s and from 65 s to 75 s into the test. During the loading phase both the probe's force and the negative pressure were considered. During the unloading phase the pressure load was zero and only the probe's force remained acting on the sample. The loading curve of applied negative pressure in respect to time is shown in Figure 6.

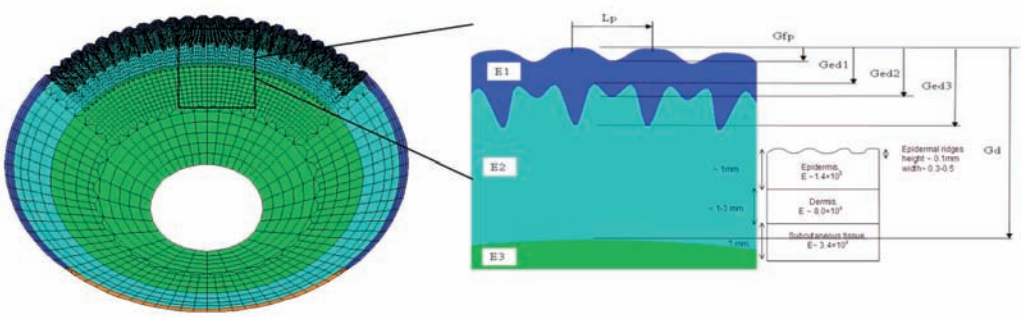

Figure 5. Finite element model of the finger cross-section and of the fingerprint asperities in skin layers

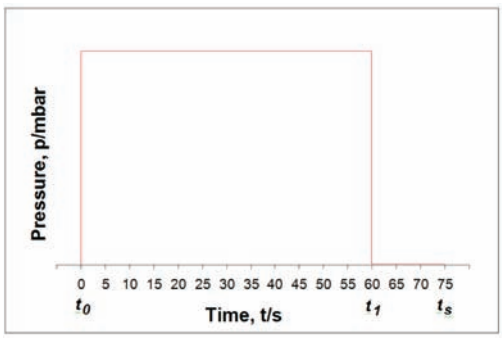

Figure 6. Loading curve used in the suction test

In order to perform the simulation of the FE model it was necessary to assign some values to the unknown parameters. The first such parameter was loading velocity, which was used to describe the function of increasing pressure load to the set value, since the implemented load was not a real step and depended on the performance of the pump, the volume that it had to move and the pressure that it had to maintain. Three different velocities (10^3, 10^5 and 10^7) mbar/s were analyzed, showing no difference between the results of the test, so the value was set as 10^5 mbar/s.

Other parameters set were the coefficients of friction between the probe and the sample and between the sample and the bolster. However, the friction coefficient does not significantly influence the response of the model and was set based on a literature search and on our preliminary research to the value 0.35. The spring force of the probe was set using balance as a 0.55 N. An error in the estimation of this value could cause different responses of the model by shifting the curves, without changing their shapes. The spring force does not influence the proportionality between the load and the displacement. Another parameter "ZeroDisp" was assigned as a displacement at the beginning of the test that represented a quantity of displacement due to the spring force. It was evaluated as an applying force to the model due to the probe. This value, obviously, shifted the response of the curves. The last parameter needed to be set was the thickness of the sample, which was the most important parameter for the characterization of the real skin. Changing the thickness of the sample minimally influenced the shape of the curve, but it had a significant impact on the maximum level reached by the sample into the probe.

Parameters sensitivity analysis

The sensitivity analyses reveal how model responses vary with model parameters. The numerical model for primal analysis was analytically differentiated by using the automatic differentiation facilities in the AceGen system (Korelc, 2009 [17]; Korelc, 2009 [20]; Korelc, 2002 [21]) in order to enable very accurate sensitivity analyses of the model and efficient inverse analysis procedure. In Figure 7 the sensitivity of the maximum fingertip deflection with respect to the elastic modulus of epidermal (a), dermal (b) and subcu-

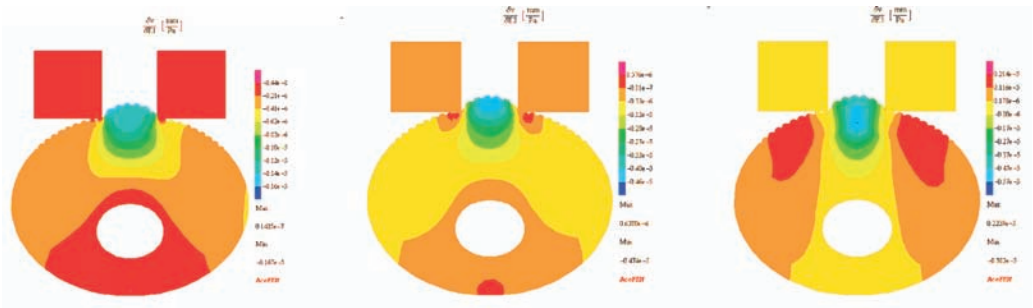

Figure 7. Sensitivity of the maximum fingertip deflection with respect to the elastic modulus of epidermal (a), dermal (b) and subcutaneous (c) tissue.

taneous (c) tissue is shown. Note that variations of the Bulk modulus shift curves up or down, while decreasing the Poisson's coefficient increased the fingertip displacement differences for a given pressure increment.

Inverse analysis procedure

Inverse analyses were used to determine unknown constitutive parameters of fingertip skin (TARANTOLA, 2004 [22]; GREŠOVNIK, 2000 [23]; C3M home page [24]). This was performed by an iterative procedure where the parameters of the model were automatically updated in such a way that the discrepancies between experimental and numerical results were minimized in a least square sense. The inverse approach combines the Finite Element Method with an optimization algorithm in order to find a set of parameters for which the fit between the numerical results and the experimental measurements is optimal (Kauer, 2001 [25]; Seshaiyer & Humprey, 2003 [26]; Kim & Srinivasan, 2005 [27]; Einstein et al., 2005 [28]). The optimum set of parameters x for the model was measured by the user-defined Objective Function $f(x)$ for $x \in R^n$. Constraint functions are defined as $c_i(x) \leq 0$ for $i \in I$. The physical consistency of lower (l_k) and upper (u_k) bounds of the set of parameters x, is ensured by $l_k \leq x_k \leq u_k$ condition for $k = 1, 2,..., n$.

Material model

The skin's behavior was described in terms of the Fung model (FUNG, 1993 [7]) as a quasi-linear viscoelastic (QLV). It was decoupled into a time-dependent elastic response and a linear viscoelastic stress relaxation response, which can be separately determined from the experimental results. The stresses in the tissues, which may be linear or nonlinear, were linearly superposed with respect to time. Rheological scheme of implemented constitutive viscoelastic model is shown in Figure 9. The three-dimensional constitutive relationship in the framework of QLV is given by

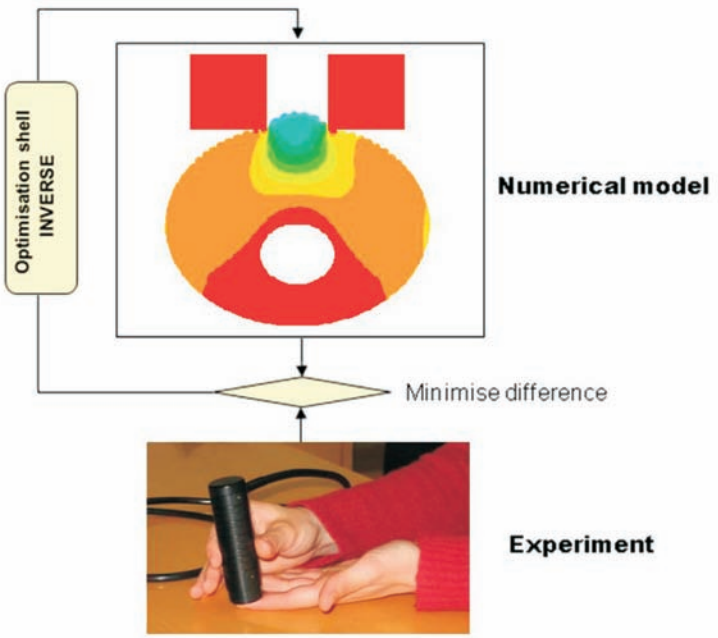

Figure 8. Inverse parameter identification concept based on iterative minimization of discrepancies between numerical results and experimental measurements.

equation:

$$S(t) = G(t)S^e(0) + \int_0^t G(t-\tau)\frac{\partial S^e(E)}{\partial \tau}d\tau \quad (1)$$

where $S(t)$ is the second Piola-Kirchhoff stress tensor, that does not change with material orientation, t is time and $G(t)$ is called the reduced relaxation function, which can be additively split in isochoric ${}^{iso}G(t)$ and volumetric ${}^{vol}G(t)$ part. $S^e(E)$, which is defined by the Green-Lagrange strain tensor E, is called the pure elastic response of the material and can be nonlinear or linear. The reduced isochoric relaxation function ${}^{iso}G(t)$ is a scalar function of time and can be often expressed by the Prony series:

$${}^{iso}G(t) = \sum_{i=0}^{n} {}^{iso}g_i \cdot e^{-t/{}^{iso}\tau_i}$$

$${}^{iso}\tau_0 = \infty \quad (2)$$

where ${}^{iso}g_i$ are the Prony series parameters (Soussou et al., 1970 [29]) and ${}^{iso}\tau_i$ are the relaxation times.

For the nonlinear elastic response a nearly-incompressible hyperelastic material representation was used, which is commonly applied for living

tissues that are in general assumed to be incompressible, due to their high water content.

The material properties of the hyperelastic material can be determined by the strain energy function W. Ideally this function is defined with only as many parameters as required to make a FEM model. Many specific material models could be used, depending on how the strain energy function is approximated. In this work the Yeoh energy potential was considered, with a maximum of 5 elastic coefficients c_{i0}, because it best fitted the experimental curves; also, it is quoted in literature that this strain energy potential has often been used for the characterization of nearly incompressible hyperelastic rubber (YEOH, 1990 [6]).

$$W = \sum_{i=1}^{N} c_{i0} \cdot \left(\tilde{I}_1 - 3\right)^i + \frac{k}{2} \cdot \left(J_{el} - 1\right)^2$$

$$S^e\left(E\right) = \frac{\partial W}{\partial E} \qquad (3)$$

where c_{i0} are material elastic parameters (having units of stress) and $\tilde{I}_1$ is the first principal invariant of isochoric Cauchy-Green tensor.

Since the analytical solution considering the above material law and experimental conditions is very difficult, the simulation using FEM has been widely used. Simulation of the test using the QLV approach gives the simulated force F_s, which depends of material parameters ${}^{iso}g_i$, ${}^{iso}\tau_i$ and c_{i0} containing the viscoelasticity and nonlinear elasticity. Elastic parameters are c_{20}, c_{30}, c_{40}, c_{50}. Viscous parameters are ${}^{iso}g_1$, ${}^{iso}g_2$, ${}^{iso}g_3$, ${}^{iso}\tau_1$, ${}^{iso}\tau_2$, ${}^{iso}\tau_3$. Shear modulus was defined as $G = \mu = 2 \times c_{10}$.

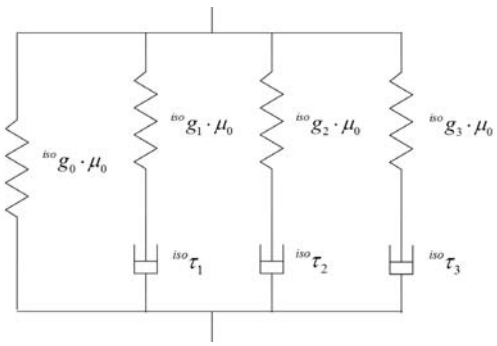

Figure 9. Rheological scheme of implemented constitutive viscoelastic model

Inverse algorithm

For inverse evaluation of skin parameters the FSQP algorithm was applied (YUUNG-HWA et al., 2006 [30]; FSQP home page [31]; FLETCHER, 1980 [32]). It is based on the concept of Feasible Sequential Quadratic Programming (FSQP). It is usually used for problems without nonlinear equality constrains. The algorithm starts with a feasible point, which is provided by the user or generated automatically and produces successive iterates that all satisfy the constraints. Algorithms in FSQP have global and two-step superlinear convergence properties. They also include

a special scheme for efficiently handling problems with more objectives or constrains than variables, thus greatly reducing computational efforts.

Parameters evaluated by the inverse procedure were shear modulus G, Poisson's coefficient ν (Raveh Tilleman et al., 2004 [33]), displacement at the start of the test ("ZeroDisp") and coefficients ($^{iso}g_1$, $^{iso}g_2$, $^{iso}g_3$). Parameter "ZeroDisp" was defined as a value of 0.07 mm. Based on our previous experience of testing various biomimetic materials in which the values were in the range between 0.05 mm and 0.09 mm the average value was taken to define "ZeroDisp".

First analysis of experimental and simulated suction skin testing revealed that experimental data are more dispersed as compared to the predictions of the FEM model. A new and important aspect observed in experimental fingertip testing was the presence of a high residual displacement after unloading. The thickness of human skin sucked into the probe could not easily exit from the probe's opening after unloading, probably because of irreversible slip. The other reasons may be attributed to the deep skin layers that have lower elastic properties, and due to microvascular responses in the living skin, which change the water content of the tissues during and after testing. The last aspect that had to be taken into account was the volume of the attached tissue also mobilized during the test that is described with an index of non-elasticity of the skin.

Estimation of the viscous parameters

Three viscous parameters ($^{iso}g_1$, $^{iso}g_2$, $^{iso}g_3$) and three deviatoric relaxation times ($^{iso}\tau_1$, $^{iso}\tau_2$, $^{iso}\tau_3$) were inversely analyzed. Only four levels of pressures (150, 250, 350, 450) mbar were used for this first optimization. The objective function was defined as

$$ObjFunc = \frac{a_1}{N_1} \cdot \sum_{i=1}^{N_1} \left(\tilde{d}_i - d_i\right)^2 + \frac{a_2}{N_2} \cdot \sum_{i=1}^{N_2} \left(\tilde{d}_i - d_i\right)^2 + \frac{a_3}{N_3} \cdot \sum_{i=1}^{N_3} \left(\tilde{d}_i - d_i\right)^2 + \frac{a_4}{N_4} \cdot \sum_{i=1}^{N_4} \left(\tilde{d}_i - d_i\right)^2 \quad (4)$$

where $\tilde{d}_i$ represents the simulation displacement and d_i the experimental displacement. Coefficients a_1, a_2, a_3 and a_4 represent weights for different parts of the tests (0–5 s, 5–60 s, 60–65 s, 65–75 s) that enable us to define the importance of a specific part of the test to ensure a better fit of simulation results to the experimental curve.

Estimation of the elastic parameters

The parameters that influence the elastic part of the response curve were in-

versely analyzed: shear modulus G and Poisson's coefficient ν. Three values of pressure (200, 300, 400) mbar were used. The differences between the displacement values recorded at the end of the loading phase (after 60 s) for FEM simulation and the experimental data were evaluated. The objective function used was the same as for the estimation of viscous parameters. The process of determination of elastic and viscous parameters was iterative and the final optimization was done simultaneously in order to get optimal values for both parameters.

Results and discussion

Comparison of experimental results and results of inverse analysis

Comparisons between experimental results and results from inverse analysis using FEM simulation are shown in Figure 10. They are shown as a correlation between displacement and time for different loads for probe with opening radius of 2 mm. The results of the simulation were fit on the experimental curves by the inverse analysis procedure.

In the tests with the probe with 2 mm of opening radius the elastic parameters are better interpolated for the lowest load pressure. An explanation of such behavior is most likely because the boundary conditions at the lowest pressure load influence the response more strongly. The interpolations in the unloading curves deviate more for the high pressure loads.

Summary of the results

During the experimental phase and also during the parameter estimation process it was confirmed that the in-vivo response of human skin is rather com-

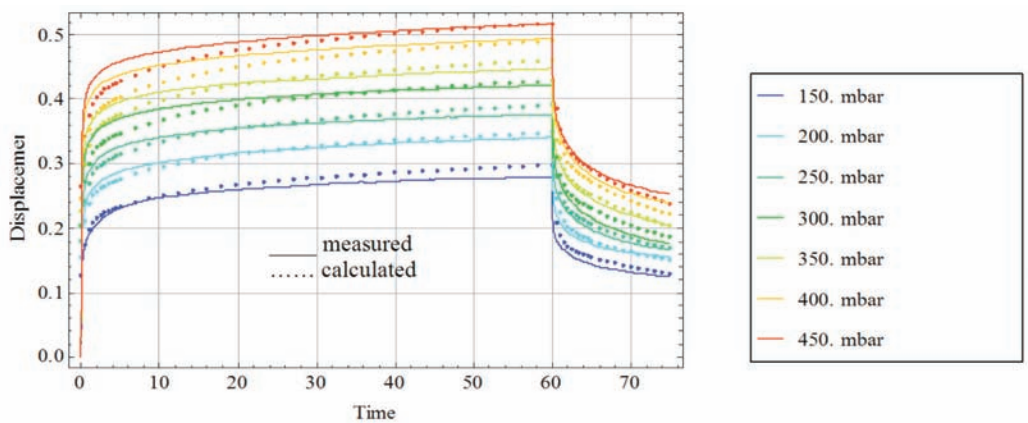

Figure 10. Results of optimization of viscous parameters for skin tested with 2 mm probe radius

plex. Our current viscoelastic model predicts the initial loading phases rather well while additional attention must be paid to the phenomena related to the unrestored energy that are currently not adequately captured.

The elastic parameters used in numerical model were Poisson's coefficient v (hypothesis of isotropic material), shear modulus G (material response to shear strains) and coefficients c_{i0}, which describe non-linearity in range of high strains.

Viscous parameters were ${}^{iso}g_i$, relaxation times ${}^{iso}\tau_i$ and a sum of viscous parameters $\Sigma_i {}^{iso}g_i$. The sum of viscous parameters was defined on a scale from 0 to 1 and represented the unit fraction of the modulus influenced by viscosity in respect to the equilibrium level. In fact its complement to value 1, represents the level of the elastic instantaneous response effect to the equilibrium level.

With reference to the Fung model the skin's parameters which were identified are shown in the Table 1.

In regard of the viscous characteristics, our attention was focused on the parameter ${}^{iso}g_3$, which represents the fastest viscous contribution in our material model. Even though it was still related to a rather long time constant, it is the most relevant parameter in reproducing tactile sensitivity within our model.

Table 1. Optimal parameters set obtained for the index fingertip skin.

ELASTIC parameters of fingertip skin	
v	0.489
k/MPa	59.29
G/MPa	1.30398
C_{10}	0.65199
C_{20}	5.39103
C_{30}	0
C_{40}	0
C_{50}	0
${}^{iso}g_0$	0.207428
VISCOUS parameters	
${}^{iso}g_1$	0.131161
${}^{iso}g_2$	0.137995
${}^{iso}g_3$	0.523416
${}^{iso}\tau_1$/s	6.73678
${}^{iso}\tau_2$/s	60.073
${}^{iso}\tau_3$/s	0.334463
$\Sigma_i {}^{iso}g_i$	0.792572

Conclusions

This work describes a combined numerical-experimental procedure for the evaluation of the mechanical properties of the human skin at the fingertip of an index finger. In order to characterize the viscoelastic response of human skin a non-intrusive test done "in vivo" was applied by using MPA 580 Cutometer® instrument from Courage+Khazaka. To interpret the measurements in terms of biomechanical parameters an inverse

FEM based procedure was developed where skin's behavior was simulated by Fung's constitutive model. The constitutive parameters of the fingertip skin are applicable for computer modeling of tactile sensations as well as for setting the target viscoelastic properties for biomimetic materials for hand prostheses and humanoid robotics.

Acknowledgements

The experimental work of the first two authors from Italy was partially supported by the Leonardo In-Oltre3 project while the computation facilities were developed by the Slovenian postgraduate students in the scope of Slovenian research and technology agencies ARRS and TIA, respectively. The support from European Union, European Social Fund is gratefully acknowledged.

References

[1] Wilkes, G. L., Brown, I. A., Wildnauer, R. H. (1973): The biomedical properties of skin, *CRC Critical Reviews in Bioengineering*, pp. 453–495.

[2] Fung, Y. C. (1972): Stress-strain-history relations of soft tissues in simple elongation, *Biomechanics: Its Foundations and Objectives Edited by YC Yung, N Perrone, M Anliker*. Englewood Cliffs, NJ, Prentice Hall, pp 181–208.

[3] Diridollou, S., Patat, F., Gens, F., Vaillant, L., Black, D., Lagarde, J. M., Gall, Y., Berson, M. (December 2001): In vivo model of the mechanical properties of the human skin under suction, *Skin research and technology,* Vol. 6, Issue 4 , pp. 214–221.

[4] Israelowitz, M., Rizvil, S. W. H., Kramer, J., von Schroeder, H. P. (2005): Computational modeling of type I collagen fibers to determine the extracellular matrix structure of connective tissues, *Protein Engineering, Design & Selection*, Vol. 18, No.7, pp. 329–335.

[5] Arruda, E. M., Boyce, M. C. (1993): Evolution of plastic anisotropy in amorphous polymers during finite straining, *International Journal of Plasticity*, Vol. 9, No. 6, pp. 697–720.

[6] Yeoh, O. H. (1993), Some forms of the strain energy function for rubber, *Rubber Chemistry and Technology*, Vol. 66, Issue 5, November 1993, pp.754–771.

[7] Fung, Y. C. (1993): *Biomechanics: Mechanical Properties of Living Tissues*, Springer-Verlag, New York 1993, pp. 242–320.

[8] Holzapfel, G. A. (1996): On large strain viscoelasticity: continuum formulation and finite element applications to elastomeric structure, *International Journal for Numerical Methods in Engineering*, Vol. 39, pp. 3903–3926.

[9] Reese, S., Govindjee, S. (1998): A

theory of finite viscoelasticity and numerical aspects, *International Journal of Solids and Structures*, Vol. 35, pp. 3455–82.

[10] Perić, D., Dettmer, W. (2003): A computational model for generalized inelastic materials at finite strains combining elastic, viscoelastic and plastic material behaviour, *Engineering Computations*, Vol. 20, No. 5/6, pp. 768–787.

[11] De Souza Neto, E. A., D. Perić, Owen, D. R. J. (2008): *Computational Methods for Plasticity: Theory and Applications*, Wiley.

[12] Dupaix, R. B., Boyce, M. C. (2007): Constitutive modeling of the finite strain behavior of amorphous polymers in and above the glass transition, *Mechanics of Materials* 39, pp. 39–52.

[13] Lubliner, J. (1990): *Plasticity Theory*, MacMilan Publishing Company, New York.

[14] Jiyong, H., Ding, X., Rubin, W. (2007): Dependence of tactile sensation on deformations within soft tissues of fingertip, *World Journal of Modeling and Simulation*, Vol. 3, No. 1, pp. 73–78.

[15] Wang, Q., Hayward, V. (2007): In vivo biomechanics of the fingerpad skin under local tangential traction, *Journal of Biomechanics*, Vol. 40, Issue 4, pp. 851–860.

[16] Michaleris, P., Tortorelli, D. A., Vidal, C. A. (1994): Tangent operators and design sensitivity formulations for transient non-linear coupled problems with applications to elastoplasticity, *International Journal for Numerical Methods in Engineering*, 37:2471–2499.

[17] Korelc, J. (2009): "*AceGen – Users manual*", Accessible on Internet: http://www.fgg.uni-lj.si/symech/.

[18] Korelc, J. (2009): "*AceFEM – Users manual*", Accessible on Internet: http://www.fgg.uni-lj.si/symech/.

[19] Wolfram Research, Inc., *Mathematica*, Version 7.0, Champaign, IL, 2008.

[20] Korelc, J. (2009): Automation of primal and sensitivity analysis of transient coupled problems, *Computational Mechanics*, Vol. 44, 631–649.

[21] Korelc, J. (2002): Multi-language and Multi-environment Generation of Nonlinear Finite Element Codes, *Engineering with Computers*, Vol. 18, No. 4, 312–327.

[22] Tarantola, A. (2004): *Inverse Problem Theory and Methods for Model Parameter Estimation*, SIAM.

[23] Grešovnik, I. (2000): *A General Purpose Computational Shell for Solving Inverse and Optimisation Problems - Applications to Metal Forming Processes*, Ph. D. thesis, University of Wales Swansea, Chapter 3, U. K..

[24] C3M home page, Optimization Shell Inverse, Accessible on Internet: www.c3m.si/inverse.

[25] Kauer, M. (2001): *Inverse Finite Element Characterization of Soft Tissues with Aspiration Experiment*, Ph. D. Thesis, Swiss federal institute of technology, Zurich.

[26] Seshaiyer, P., Humphrey, J. D. (2003): A Sub-Domain Inverse Finite Ele-

ment Characterization of Hyperelastic Membranes Including Soft Tissues, *Journal of Biomechanical Engineering*, Transaction of the ASME, Vol. 125, pp. 363–371.

[27] Kim, J., Srinivasan, M. A. (2005): *Characterization of Viscoelastic Soft Tissue Properties from In vivo Animal Experiments and Inverse FE Parameter Estimation*, Springer Berlin / Heidelberg.

[28] Einstein, D. R., Freed, A. D., Stander, N., Fata, B., Vesely, I. (December 2005): Inverse Parameter Fitting of Biological Tissues: A Response Surface Approach, *Annals of Biomedical Engineering*, Vol. 33, No. 12, pp. 1819–1830.

[29] Soussou, J. E., Moavenzadeh, F., Gradowczyk, M. H. (December 1970): Application of Prony Series to Linear Viscoelasticity, *Journal of Rheology*, Vol.14, Issue 4, pp. 573–584.

[30] Yuung-Hwa, L., Fung-Huei, Y., Ching-Lun, L. (2006): Application of FSQP to inverse estimation of the constitutive constants and friction coefficient in the nosing process, *Materials Science Forum,* Vol. 505–507, pp 685–690.

[31] FSQP home page, Accessible on Internet: www.aemdesign.com.

[32] Fletcher, R. (1980): *Practical Methods of Optimization, Vol. 1 - Unconstrained Optimization and Vol. 2 - Constrained Optimization*, John Wiley and Sons.

[33] Raveh Tilleman, T., Tilleman, M. M., Neumann, M. H. A. (2004): The elastic properties of cancerous skin: Poisson's ratio and Young's modulus, *IMAJ Israel Medical Association Journal*, Israel, Vol. 6, No.12, pp. 753–755.

Critical inclusion size in spring steel and genetic programming

Kritična velikost vključka v vzmetnem jeklu in genetsko programiranje

Miha Kovačič[1, 2, *], Sandra Senčič[3]

[1]ŠTORE STEEL, d. o. o., Štore, Slovenia
[2]University of Nova Gorica, Laboratory for Multiphase Processes, Nova Gorica, Slovenia
[3]KOVA, d. o. o., Celje, Slovenia

*Corresponding author. E-mail: miha.kovacic@store-steel.si

Received: October 9, 2009 **Accepted:** January 11, 2010

Abstract: In the paper the genetic programming method was used for critical inclusion size determination. At first the mathematical model according to dynamically testing results of the seven broken 51CrV4 springs has been obtained and after the optimization with the model was performed. For the modeling of the spring life the inclusion size of the inclusion found at the breakage surface and the distance of the inclusion from the spring tensile surface were used. The results show that the critical inclusion (the inclusion at the spring tensile surface) size in our case is 0.14 mm. The results of the proposed concept can be used in practice.

Izvleček: V članku je bila za določevanje kritične velikosti vključka uporabljena metoda genetskega programiranja. Najprej se je na podlagi eksperimentalnih podatkov sedmih prelomljenih vzmeti iz 51CrV4 izdelal matematični model, ki se je kasneje uporabil za optimizacijo. Za modeliranje trajnostne dobe vzmeti sta se uporabila velikost vključka, najdenega na prelomu, in njegova oddaljenost od natezne površine vzmeti. Rezultati kažejo, da je kritična velikost vključka (na natezni strani vzmeti) v našem primeru 0,14 mm. Rezultate predloženega koncepta lahko uporabimo v praksi.

Key words: spring steel, inclusions, modeling, genetic programming

Original scientific paper

Ključne besede: vzmetno jeklo, vključki, modeliranje, genetsko programiranje

INTRODUCTION

Spring life depends on steel and spring producers activities. Each producer part contribute to mechanical behavior of the produced spring.[1, 2]

The spring life is determined by dynamical testing. There are many different techniques for spring life determination.[1–4] In general the whole spring assembly or just a sample cutout is used for the spring life analysis. ŠUŠTARŠIČ et al. tried to determine the bend fatigue strength of selected spring steel with a resonant pulsator using standard Charpy V-notched specimens.[1–2] MURAKAMI et al. tried to predict the upper and the lower limits of fatigue strength from the Vickers hardness of a matrix and the maximum size of inclusions defined by the square root of the projected area of an inclusion.[3] MURAKAMI also introduces several spring steel quality determination techniques.[4]

In the present paper the dependence between inclusion size, inclusion location and spring life was discussed. The experimental data was collected after spring breakage between dynamic testing.

After the genetic programming method [5–7] was used to determine the correlation between spring tool life and inclusion size and inclusion location. With the genetically obtained mathematical model the critical inclusion size was determined.

The critical inclusion size information could be easily used for steel plant metallurgical processes design.

SPRING LIFE DYNAMIC TESTING

We were using the three-point flexural testing device. The spring life dynamic testing is schematically presented in figure 1. The tested material was 51CrV4. The chemical composition of the tested material is colected in the table 1. Test frequency was 40 r/min, test force (F) between 3.3 kN and 50 kN,

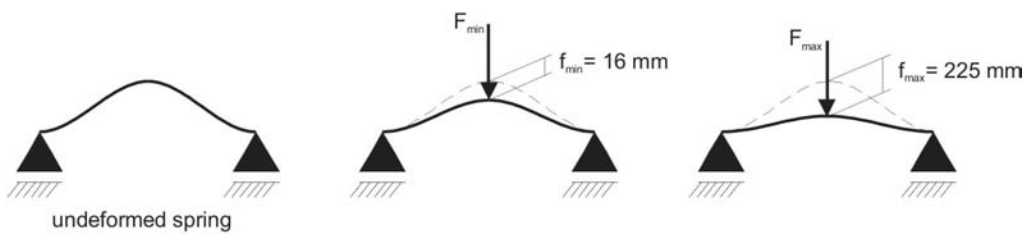

Figure 1. Spring life dynamic testing

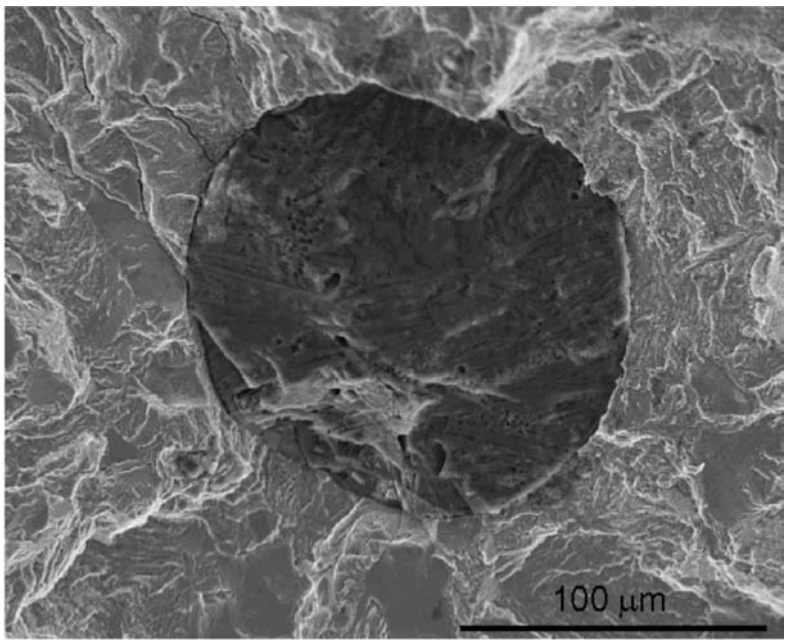

Figure 2. The inclusion found at the breakage surface of the spring number 2 (Table 3)

Table 1. 51CrV4 spring steel chemical composition (*w*/%)

C	Si	Mn	P	S	Cr	Mo	Ni	Al	Cu	Nb	Ti	V	Sn	Ca	B
0,51	0,34	0,96	0,014	0,003	1,07	0,06	0,08	0,012	0,13	0,001	0,004	0,17	0,01	0,0009	0,0002

Table 2. The inclusion (spring number 2) chemical composition (*w*/%)

O	Mg	Al	Si	S	Ca	Ti	Fe	Zn
43,42	3,26	19,77	2,91	1,08	24,47	0,20	4,69	0,21

Table 3. The spring life dynamic testing data

Spring number	Inclusion size, *S*/mm	Inclusion depth, *D*/mm	Spring life [cycles, *r*]
1	0.33	3.75	53667
2	0.16	1.34	96484
3	0.22	0.91	60157
4	0.26	3.87	62437
5	0.44	3.71	57454
6	0.38	3.09	53200
7	0.2	1.19	53062

spring sink (*f*) from 16 mm to 225 mm. It is easily to conclude that the load was pulsative and the bottom and top surface were tensile and compressed, respectively.

After the spring breakage the inclusion size of and the depth of the inclusion found at the breakage surface (distance from the bottom spring surface) were measured. The inclusion and spring life data is collected in the table 3. The inclusion found at the spring number 2 breakage surface (Table 3) and its chemical composition is presented in the figure 2 and table 2, respectively.

SPRING LIFE MODELING BY GENETIC PROGRAMMING

Genetic programming is probably the most general evolutionary optimization method.[5–7] The organisms that undergo adaptation are in fact mathematical expressions (models) for spring life prediction consisting of the available function genes (i.e., basic arithmetical functions) and terminal genes (i.e., independent input parameters, and random floating-point constants). In our case the models consist of: function genes of addition (+), subtraction (–), multiplication (*) and division (/), terminal genes of inclusion size (*S*) and inclusion depth (*D*).

Random computer programs of various forms and lengths are generated by means of selected genes at the beginning of simulated evolution. Afterwards, the varying of computer programs during several iterations, known as generations, by means of genetic operations is performed. After completion of varying of computer programs a new generation is obtained that is evaluated and compared with the experimental data, too.

For spring life prediction the fitness measure was defined as:

$$\Delta = \frac{\sum_{i=1}^{n} \Delta_i}{n} \tag{1}$$

where n is the size of sample data, Δ_i is a percentage deviation of single sample data. The percentage deviation of single sample data, produced by individual organism, is:

$$\Delta_i = \frac{|E_i - G_i|}{E_i} \cdot 100\ \% \tag{2}$$

where E_i and G_i are the actual spring life and the predicted spring life by a model, respectively. The smaller the values of equation (1), the better is adaptation of the model to the experimental data.

The process of changing and evaluating of organisms is repeated until the termination criterion of the process is fulfilled. This was the prescribed maximum number of generations.

For the process of simulated evolutions the following evolutionary parameters were selected: size of population of organisms 500, the greatest number of generation 100, reproduction probability 0.4, crossover probability 0.6, the greatest permissible depth in creation of population 6, the greatest permissible depth after the operation of crossover of two organisms 10 and the smallest permissible depth of organisms in generating new organisms 2. Genetic operations of reproduction and crossover were used. For selection of organisms the tournament method with tournament size 7 was used.

We have developed 100 independent civilizations of mathematical models for spring life prediction. Each civilization has the most succesfull organism – mathematical model for spring life prediction. The best most succesfull organism from all of the civilizations is presented here:

$$\left(8.32555+8.40678\left(8.23089+D\right)+\frac{8.23089+D}{D}+\frac{D}{3.48269\cdot D-\frac{0.85092}{S}}\right)\left(-\frac{8.55026}{8.32555-\frac{D}{S}}-\frac{\left(-29.777904+\frac{D}{8.32555-\frac{8.55026}{9.17647+\frac{8.23089+D}{D}}-\frac{D}{S}}+\frac{2}{S}\right)\left(6.66951+S\right)}{S}-27.21465\cdot S\left(S+D+\frac{-8.55026+\frac{D}{S}+S}{1+\frac{1}{S\cdot D}}\right)+S\left(\frac{8.23089+D}{D}+S+\frac{-8.55026+2D+S}{8.32555-\frac{D}{S}}\right)+\frac{D+\frac{D}{S}+S}{3.48269\cdot D-\frac{0.85092}{S}}\right) \tag{3}$$

with fitness measure (average percentage deviation) 0.64 %.

The calculated spring life and percentage deviations from experimental data is presented in the next table (Table 4).

Table 4. The calculated spring life and percentage deviations from experimental data

Spring number	Inclusion size *S*/mm	Inclusion depth *D*/mm	Spring life [cycles] *r*	Predicted spring life [cycles] *r*	Deviation
1	0.33	3.75	53667	53673	0.01 %
2	0.16	1.34	96484	95829	0.68 %
3	0.22	0.91	60157	59715	0.73 %
4	0.26	3.87	62437	62788	0.56 %
5	0.44	3.71	57454	57969	0.90 %
6	0.38	3.09	53200	53187	0.02 %
7	0.2	1.19	53062	53890	1.56 %

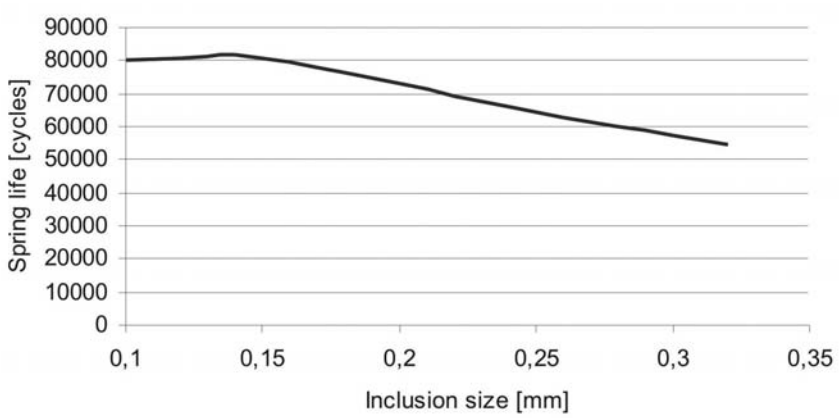

Figure 3. Spring life and inclusion size on the surface dependency

CRITICAL INCLUSION SIZE

According to the best genetically developed spring life model it is easily to calculate the critical size of inclusion on the spring surface. The spring life and inclusion size on the surface dependency is presented in the next figure (Figure 3).

The highest calculated spring value is at inclusion size 0.14 mm. After that value spring life rapidly decreases.

CONCLUSION

Spring life depends on many properties. One of the most important is inclusions size.

In the research 7 springs were dynamically tested on three-point flexural testing device. The tested material was 51CrV4. Test frequency was 40 r/min, test force between 3.3 kN and 50 kN, spring sink from 16 mm to 225 mm.

After the spring breakage the inclusion size and depth (distance from the bottom surface) were measured.

The genetic programming method was used to determine the correlation between spring tool life and inclusion size and inclusion location.

From the 100 runs (civilizations) the best predictive model for spring life was developed with average percentage deviation 0.64 %.

According to the best genetically developed spring life model it was easily to calculate the critical size of inclusion on the spring surface. The value is 0.14 mm.

With the help of genetic programming method the decision value was determined. According to known critical inclusion size value the right spring steel and steel plant technology could be easily selected. The results are compared with the similar more experimentaly-oriented research.[1]

References

[1] Šuštaršič, B., Senčič, B., Leskovšek, V. (2008): *Fatigue strength of spring steels and life-time prediction of leaf springs*, Assessment of reliability of materials and structures RELMAS'2008, St. Petersburg, Russia.

[2] Šuštaršič, B., Senčič, B., Arzenšek, B. (2006): *Notch effect on fatigue strength of 51CrV4Mo spring steel*, 6th International Conference on Fatigue and Fracture - NT2F6, Brdo pri Kranju, Slovenia.

[3] Murakami, Y., Kodama, S., Konuma, S. (1989): Quantitative evaluation of effects of non-metallic inclusions on fatigue strength of high strength steels. I: Basic fatigue mechanism and evaluation of correlation between the fatigue fracture stress and the size and location of non-metallic inclusions, *International Journal of Fatigue*, Vol. 11, No. 5, 291–298.

[4] Murakami, Y. (2002): Spring Steels, *Metal Fatigue*, pp. 163–183.

[5] Kovačič, M., Uratnik, P., Brezočnik, M., Turk, R. (2007): Prediction of the bending capability of rolled metal sheet by genetic programming, *Materials and manufacturing processes*, No. 22, 634–640.

[6] Kovačič, M., Šarler, B. (2009): Application of the genetic programming for increasing the soft annealing productivity in steel industry. *Materials and manufacturing processes*, Vol. 24, No. 3, 369–374.

[7] Koza, J. R. (1999): *Genetic programming III*., Morgan Kaufmann, San Francisco.

Bacterial indicators of faecal pollution and physiochemical assessment of important North Indian lakes

Bakterijski indikatorji fekalnega onesnaženja in fizikalno-kemijsko stanje pomembnih jezer v severni Indiji

Punam Sharma[1], Anchal Sood[1], Shivesh Sharma[2,*], Sandeep Bisht[1], Vivek Kumar[3], Piyush Pandey[1], Manju P. Gusain[4], Om P. Gusain[4]

[1]Department of Microbiology, SBS Post Graduate Institute of Bio-Medical Sciences and Research, Balawala, Dehradun, Uttarakhand, India
[2]Department of Applied Mechanics (Biotechnology), Motilal Nehru National Institute of Technology, Allahabad, Uttar Pradesh, India
[3]Microbiology Section, Department of Soil and Water Research, Public Authority of Agriculture & Fish Resources, PO Box 21422, Safat-13075, Kuwait
[4]Department of Zoology & Biotechnology, Hemwati Nandan Bahuguna Garhwal University, Srinagar-Garhwal, Uttarakhand, India

*Corresponding author. E-mail: dr.shiveshsharma@gmail.com

Received: Novembre 10, 2009 **Accepted:** February 4, 2010

Abstract: A study was conducted to investigate the water quality of seven important lakes in North India during the periods of summer, monsoon and winter seasons. All of these studied lakes are important recreational spots of India. Water samples were analyzed for various bacteriological parameters including total viable count (TVC), total coliform (TC), faecal coliform (FC) and faecal streptococci (FS). Also physico-chemical parameters like pH, conductivity, total dissolved solids (TDS), dissolved oxygen (DO), biological oxygen demand (BOD) and chemical oxygen demand (COD) were assessed. Total viable count exceeded the maximum permissible limits in all the lakes irrespective to different seasons. The high most probable number (MPN) values and presence of faecal coliforms and streptococci in the water samples suggests the potential presence of pathogenic microorganisms which might cause water borne diseases. A direct effect of season and human activities on the pollution status was ob-

Original scientific paper

served in all the lakes. The over all objective of this work was to investigate the incidence of these indicator organisms, coliform, faecal coliform, faecal streptococci and physiochemical parameters during different seasons in important north Indian lakes.

Povzetek: V članku so predstavljeni rezultati raziskave kakovosti vode sedmih pomembnih jezer v severni Indiji, ki so potekale v poletnem, monsunskem in zimskem času. Vsa raziskana jezera predstavljajo pomembna rekreacijska območja v Indiji. V vzorcih vode so bili določeni različni bakteriološki parametri, kot so število bakterijskih kolonij (TVC), skupni koliformi (TC), fekalni koliformi (FC) in fekalni streptokoki (FS), določeni pa so bili tudi fizikalno-kemijski parametri kot so pH, električna prevodnost, celotna suspendirana snov (TDS), raztopljeni kisik (DO), biokemijska potreba po kisiku (BOD) in kemijska potreba po kisiku (COD). Število bakterijskih kolonij presega maksimalne dovoljene vrednosti v vseh jezerih v vseh opazovanih obdobjih. Visoko najbolj verjetno število bakterij (MPN) in prisotnost fekalnih koliformov in streptokokov v vzorcih vode nakazujejo potencialno prisotnost patogenih mikroorganizmov, ki lahko povzročijo obolenja. Tudi neposredni učinek sezon in človeške dejavnosti na stanje onesnaženja je bil opažen v vseh jezerih. Glavni namen opravljenih raziskav je bil določiti obseg indikatorskih organizmov, koliformov, fekalnih koliformov in fekalnih streptokokov ter spreminjanje fizikalno-kemijskih parametrov v različnimi letnih časih v pomembnih jezerih v severni Indiji.

Key words: coliforms, seasons, physiochemical, lake water, India
Ključne besede: koliformi, sezone, fizikalno-kemijski, jezerska voda, Indija

Introduction

India is rich in surface water resources. Nearly 80 % of rural residents rely on untreated ground water for potable water supplies. Rivers and lakes are the major sources of fresh water supply, but almost 70 % of India's surface water resources and ground water reserves have been contaminated (Rao & Mamatha, 2004).

Lake Riwalsar is eutrophic in nature and is situated in lesser Himalayas, surrounded by middle Shivalik rocks with a catchments area of 4.8 km^2, the

surface area is 0.5 km^2 with maximum depth of 6.5 m. The lake Parashar is a high altitude lake with a catchment area of 8.9 km^2; the surface area is 0.23 km^2 with a maximum depth of 5.3 m. The Sukhna Lake is at the foot hills of Shivalik hills, the surface area is 3.0 km^2, the maximum depth is 9 m and catchments area is 14.9 km^2. The water flowing into the lake is heavily loaded with silt. Dul Lake is eutrophic in nature at foot hills of Himalayan range, which surrounds it on three sides. The catchments area is 316 km^2; surface area being 18 km^2 with maximum depth of 6 m. Lake Nainital is also eutrophic, a high altitude lake, situated in a valley surrounded by low and high hills. The total length of the drainage basin is about 42 km and lake has a catchments area of 11.8 km^2. The lake receives rain water and waste water from 24 permanent and temporary inlets coming from different sources and inhabited areas. The area of the lake is 0.46 km^2 and maximum depth is 26 m. The Bhimtal Lake is surrounded by high hills, with a catchments area of 12.3 km^2 and the surface area of the lake is 0.42 km^2. Maximum depth of the lake is 24.7 m and is of eutrophic nature. Lake Naukuchiatal is also surrounded by Himalayan hills. The lake has catchments area of 14.8 km^2, the surface area being 0.90 km^2 and maximum depth is 41.2 m and is of eutrophic nature (Central Water Commission, 2007).

In sub rural areas, water of lakes or ponds is sufficient to fulfill the water requirements of that area. In the present study, we collected water samples from important lakes of North India and examined to understand the outcome of seasonal variations on water quality. These lakes have different meanings to different people because they serve with different functions, such as drinking water to area residents nearby, recreation value, food protection for downstream residents, habitat for wild life, irrigation and water power generation. Some of these lakes are considered to be sacred. However, human activities have affected the water quality of the lakes. This type of eutrophication is called as 'cultural' eutrophication. The human activities include religious activities, tourism, bathing, washing, open defecation, cultivation, stone crushing, road construction, fishing, surface drainage, irrigation, drinking water uptake, rafting, discharges of industrial wastes and domestic wastewaters, and other similar activities.

Microorganisms are widely distributed in nature, and their abundance and diversity may be used as an indicator for the suitability of water (Okpokwasili & Akujobi, 1996). The use of bacteria as water quality indicators can be viewed in two ways, first, the presence of such bacteria can be taken as an indication of faecal contamination of the water

and thus as a signal to determine why such contamination is present, how serious it is and what steps can be taken to eliminate it; second, their presence can be taken as an indication of the potential danger of health risks that faecal contamination posses. The higher the level of indicator bacteria, the higher the level of faecal contamination and the greater the risk of water-borne diseases (Pipes, 1981). A wide range of pathogenic microorganisms can be transmitted to humans via water contaminated with faecal material. These include enteropathogenic agents such as salmonellas, shigellas, enteroviruses, and multicellular parasites as well as opportunistic pathogens like Pseudomonas aeroginosa, Klebsiella, Vibrio parahaemolyticus and Aeromonas hydrophila (Hodegkiss, 1988). It is not practicable to test water for all these organisms, because the isolation and identification of many of these is seldom quantitative and extremely complicated (Cairneross et al., 1980; World Health Organization (WHO), 1983). An indirect approach is based on assumption that the estimation of groups of normal enteric organisms will indicate the level of faecal contamination of the water supply (WHO, 1983). The most widely used indicators are the coliform bacteria, which may be the total coliform that got narrowed down to the faecal coliforms and the faecal streptococci (Kistemann et al., 2002; Pathak & Gopal, 2001; Harwood et al., 2001). Concurrently, contamination of water by enteric pathogens has increased worldwide (Islam et al., 2001; Pathak et al., 1991; Craun, 1986). However, to the best of our knowledge, no report is available on the bacterial as well as physiochemical parameters analysis of seven important lakes in North India. The overall objective of this work was to investigate the incidence of these indicator organisms, coliforms, faecal coliforms and faecal streptococci in relation with physiochemical parameters of north Indian lakes in different seasons.

Materials and methods

Collection of water samples

The lakes of the North Indian region were intensively surveyed to select different sites for sample collection from various lakes. Seven North Indian lakes which are renowned for recreational and tourism activities were selected (Table 1, Figure 1). Access to the individual sites was accomplished by way of boat. All the samples were collected just below the surface of lake water by plunging the open end of each sterile bottle before turning it upright to fill. Samples were collected during the summer, monsoon and winter seasons. Each lake was divided into four sampling sites and samples were collected in triplicate from each site, and were transported in ice boxes at 3 °C and brought to the laboratory for analysis (Sood et al., 2008). The results presented in the tables are average of all the four sites of a particular lake.

Table 1. Lakes of North India selected in the study

Lake	**State**	**Altitude** (from sea level)	**Latitude and longitude**	**Significance**
Riwalsar	Himachal Pradesh	754 m	30° 15' N 77° 50' E	Tourism, Religious
Prashar	Himachal Pradesh	754 m	30° 12' N 77° 47' E	Tourism, Religious
Sukhna	Punjab and Haryana	365 m	30° 50' N 76° 48' E	Tourism, Recreational
Dul	Jammu and Kashmir	1583 m	34° 18' N 74° 91' E	Tourism, Recreational
Nanital	Uttarakhand	1938 m	29° 34' N 79° 23' E	Tourism, Recreational, Irrigation, Drinking
Bhimtal	Uttarakhand	1371.6 m	29° 21' N 79° 34' E	Tourism, Recreational
Naukuchiatal	Uttarakhand	1219 m	29° 32' N 79° 21' E	Tourism, Recreational

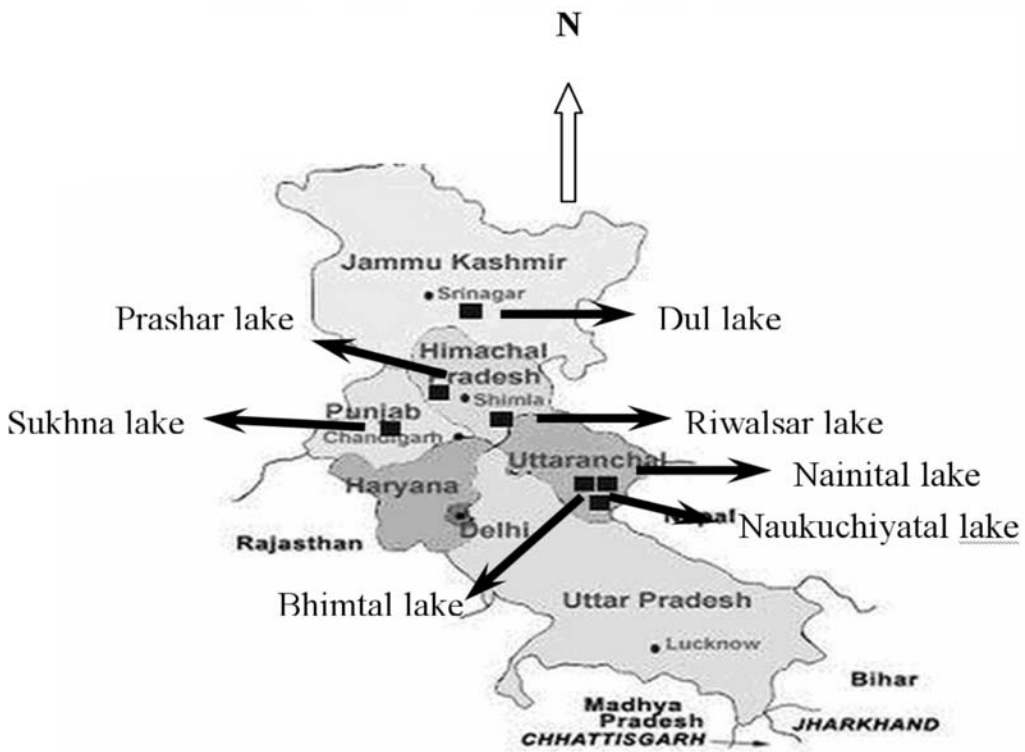

Figure 1. Map of study area of north Indian lakes

Bacterial analysis

The bacterial population (total viable count, TVC) in different samples was estimated by inoculating nutrient agar plates with 0.1 mL of suitable dilutions. The results were expressed as colony forming units (cfu)/mL, enumerated after 48 h of incubation. The water quality was determined by the standard most probable number (MPN) method. Coliforms were detected by inoculation of samples into tubes of MacConkey broth and incubation at (37 ± 1) °C for 48 h. The positive tubes were sub cultured into brilliant green bile broth (BGBB) and were incubated at (44.5 ± 1) °C. Gas production in BGBB at (44.5 ± 1) °C was used for the detection of faecal coliform after 48-h incubation. Faecal streptococci were detected by inoculation of water samples into Azide Dextrose broth and incubation at (37.5 ± 1) °C for 24–48 h (APHA, 1999). All the culture media were obtained from Hi-Media Pvt. Ltd., Mumbai, India.

Physiochemical analysis

Physicochemical parameters including total dissolved solids (TDS), conductivity and pH were analyzed on site at the time of sample collection by water analysis kit (Model LT-61, Labtronics, Guelph, Ontario, Canada) as per manufacturer instruction. Other parameters i.e. dissolved oxygen (DO), biological oxygen demand (BOD) and chemical oxygen demand (COD) were performed in laboratory by standard titrimetric method (Apha et al., 1999).

The data were analyzed statistically by using analysis of variance (ANOVA) to find out significance at 5 % levels. In figures, error bars indicate standard error of the mean, where error bars are not visible; they are smaller than the marker.

Results

The TVC values showed a regular trend (Figure 2). The values increased in summer season, thus generally highest counts were observed, intermediate in winter season and least in monsoon season, for each lake. The highest TVC was noted in the Dul lake water samples, where the values were as high as 189×10^6 cfu/mL in summer and the lowest values were recorded in case of Naukuchiyatal lake in monsoon season where values were 28×10^6 cfu/mL.

The total coliform count was high in all water samples (Figure 3), values ranged from 16/100 mL to 135/100 mL. The highest MPN (135/100 mL) was recorded during summer from Dul lake having peak tourist season. The least count MPN (16/100 mL) was obtained in monsoon from Naukuchiatal with less tourist or human activities. Even the water samples during less human activities in monsoon and winter seasons were found not suitable for drinking as per the Bureau of Indian Standards (BIS), (1991).

Figure 2. Total viable count (TVC) of different lake samples

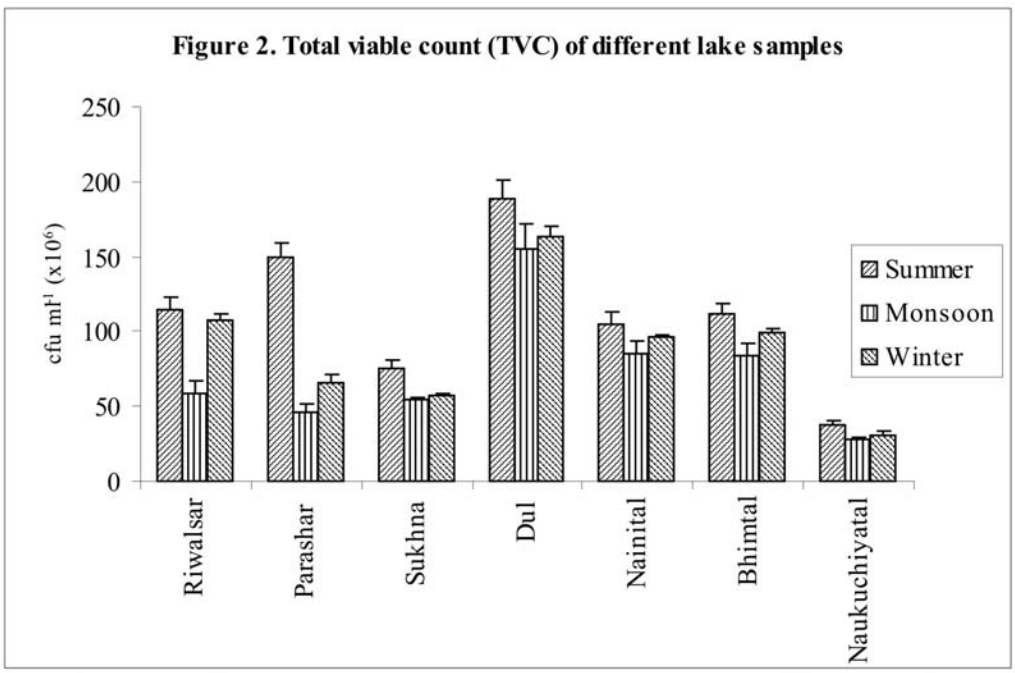

Figure 3. Total coliform (TC) count per100 ml of water sample

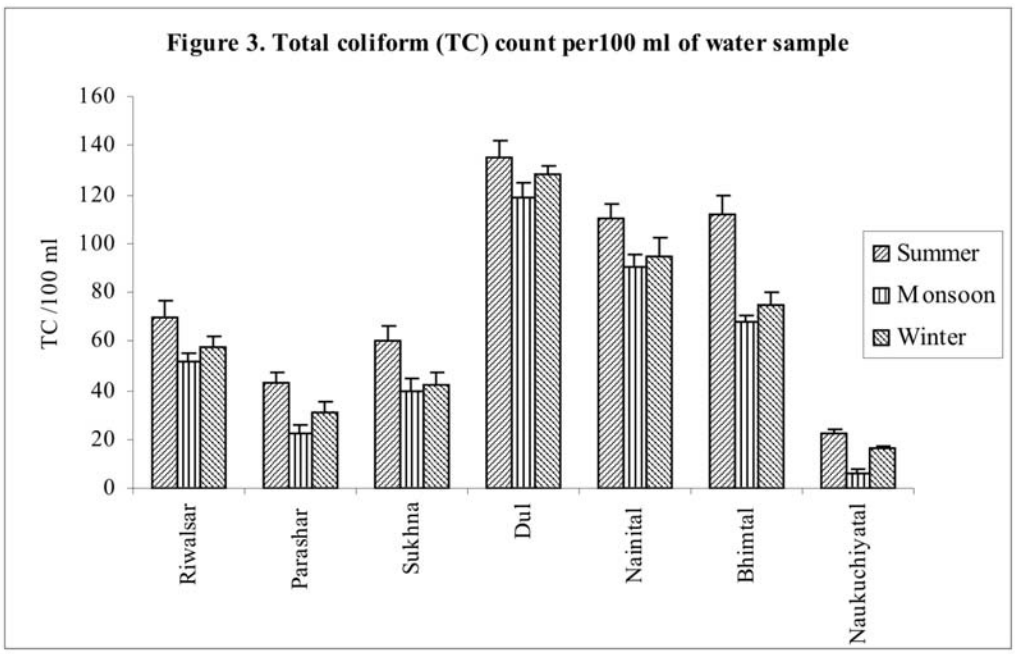

Figure 4. Faecal coliform (FC) count per 100 ml of water sample

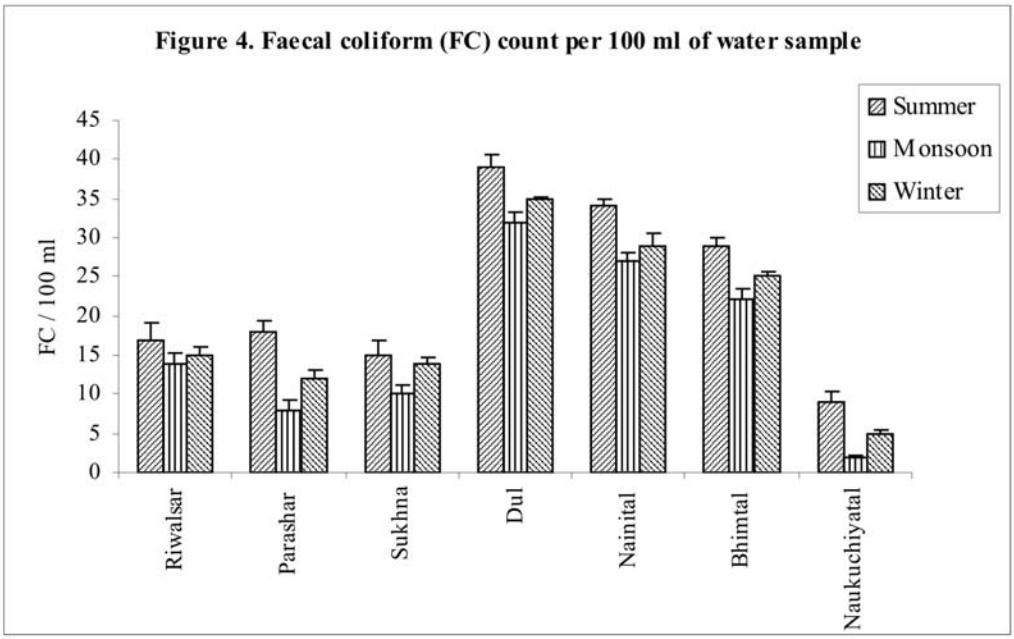

Figure 5. Faecal Streptococci (FS) count per 100 ml of water sample

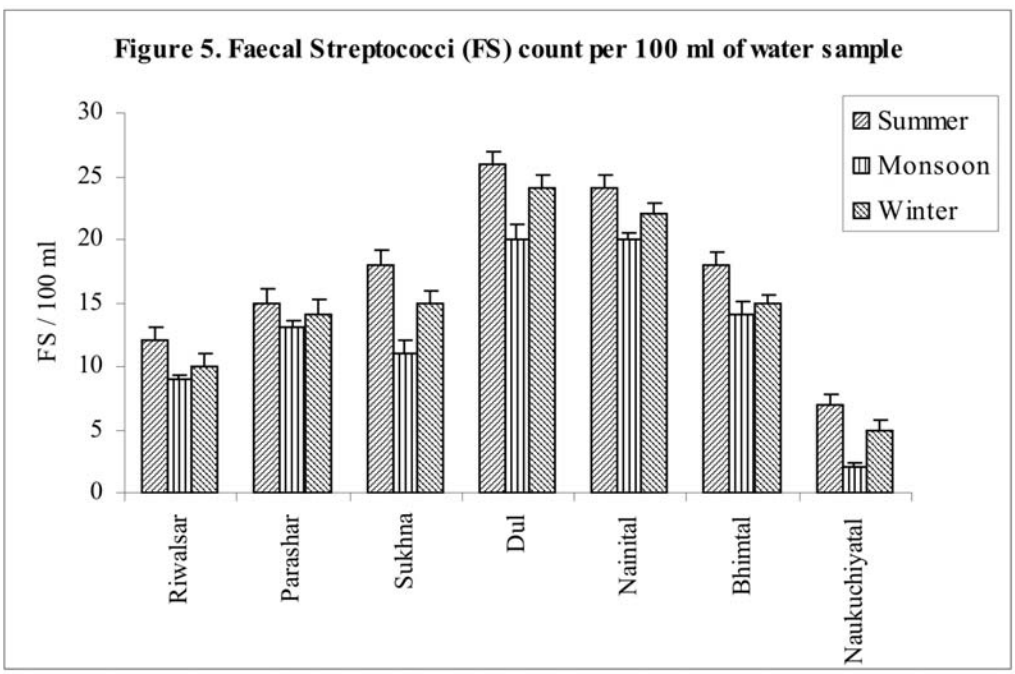

Results for FC and FS counts have also shown a similar trend to TVC and TC, i.e. higher in summer season, intermediate in winter season and least during monsoon season. (Figures 4 & 5). Highest FC count was observed in Dul lake (39, 32, 35)/100 mL and the lowest count (9, 2, 5)/100 mL was observed in Naukuchiatal lake during summer, monsoon and winter seasons, respectively. Lake Nainital and Bhimtal have also shown higher number of FC after Dul lake. Similar trend was also observed in FS, the higher count (26, 20, 24)/100 mL in Dul Lake followed by Nainital (24, 20, 22)/100 mL during summer, monsoon and winter seasons, respectively, while the least count (7, 2, 5)/100 mL was observed in lake Naukuchiatal.

Conductivity and TDS in all the sites were found to be well with in the minimum prescribed limits (APHA et. al. 1999) (Table 2). The TDS value for water samples ranged from 24.1 mg/L to 198.9 mg/L. The TDS values; though within minimum permissible limits showed a regular trend of increasing value during winter, monsoon and summer samples (except for Riwalsar and Sukhna lakes). Conductivity of samples ranged from 0.035 S/cm to 0.46 S/cm. pH value showed a decreasing trend during summer season but for monsoon and winter it was nearly same, though the values were found to be neutral for most of the samples, but overall the pH increased with decrease in temperature i.e. in winter season.

Table 2. Physicochemical characteristics of lake water samples

Sampling area (Lakes)	Seasons								
	Summer			Monson			Winter		
	TDS	Conductivity	pH	TDS	Conductivity	pH	TDS	Conductivity	pH
Riwalsar	139.9	0.207	7.3	130.8	0.194	7.2	131.90	0.217	7.1
Prashar	27.7	0.041	6.3	24.9	0.037	5.9	24.10	0.035	7.1
Sukhna	133.1	0.198	6.7	126.3	0.187	7.1	126.70	0.189	7.4
Dul	147.7	0.222	6.6	132.7	0.197	7.8	99.00	0.147	7.8
Nainital	190.5	0.460	7.8	188.3	0.460	7.9	186.60	0.450	8.0
Bhimtal	198.9	0.200	7.6	178.6	0.180	7.7	164.20	0.160	7.9
Naukuchiatal	133.7	0.130	7.4	133.4	0.130	7.6	132.20	0.120	7.6

TDS mg/e at 200 mg/kg; Conductivity (2M) (S/cm)
Values are average of triplicate

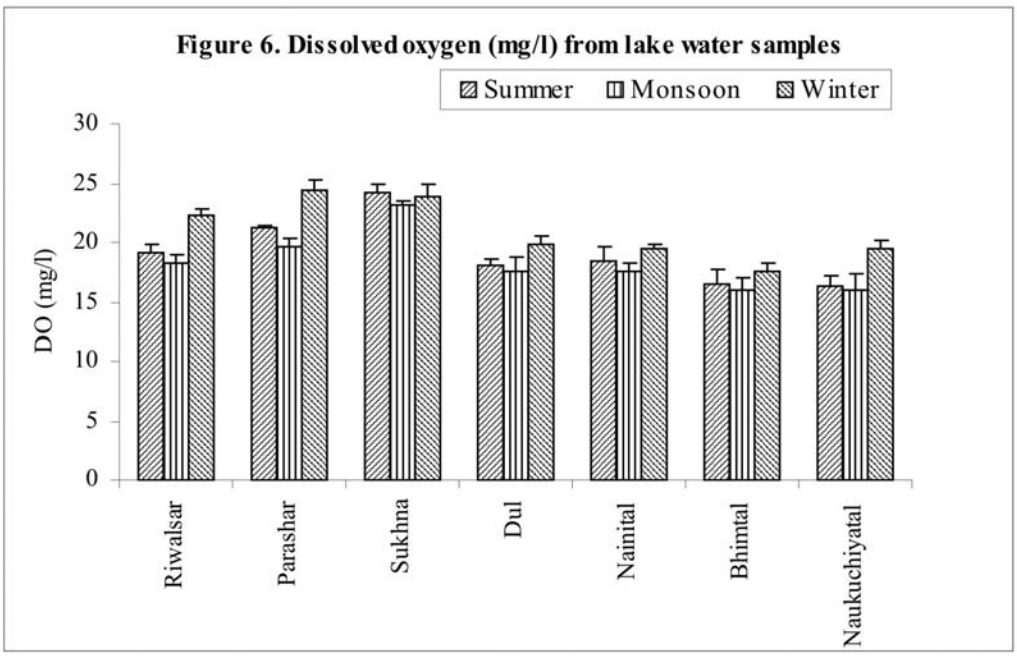

Figure 6. Dissolved oxygen (mg/l) from lake water samples

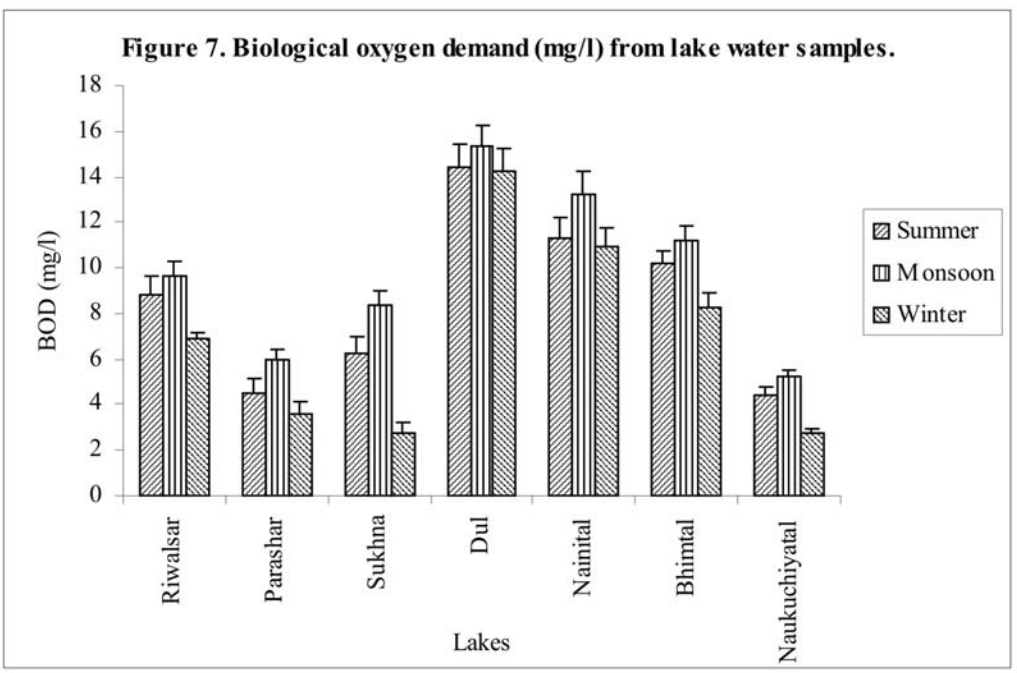

Figure 7. Biological oxygen demand (mg/l) from lake water samples.

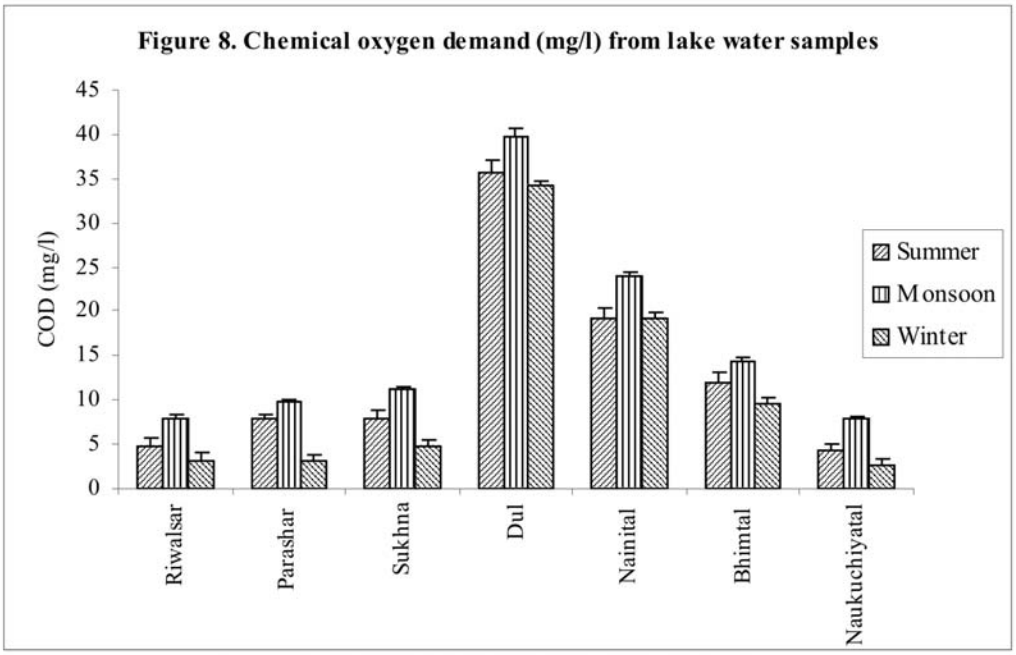

The DO values ranged from 13.2–16.8 mg/L in summer samples, 16.4–24.2 mg/L in monsoon samples and 17.1–24.4 mg/L in winter samples (Figure 6). Lake Prashar showed a remarkable increase in DO in winter season. Though, in general the DO content of all the lakes show a uniform trend with varying seasons i.e. least during summer and highest during winter and intermediate in monsoon season. However, all the samples were found to be saturated with oxygen and were fit for bathing, wild life and irrigation with respect to the amount of dissolved oxygen.

The BOD value for most of the water samples were above the permissible limits (Figure 7), except that in Sukhana (winter), Naukuchiatal (winter) where BOD values were low, thus making water fit for drinking and other purposes. Samples in monsoon season have high BOD values and thus, the water was not fit for drinking. Considerably higher COD values were recorded in the monsoon season in all sites of study area, the COD ranged from 3.2 mg/L to 42.5 mg/L in all samples (Figure 8).

Discussion

In the present study, all the TVC values were found to be high in all the water samples from all the lakes. The bacterial load increased with increasing hu-

man activities during summer season, thereby indicating the direct effect of human activities on the bacterial population. Relatively very high values of TVC were observed in Dul Lake (Jammu & Kashmir), which may be accounted by the fact that here Shikaras (house boats) on the lake are very common and find a special attraction amongst large number of tourists from India and the world. The results of the present study draw support from the findings of Sood et al., (2008), (Radha & Seenayya, 2004) who have worked on the bacteriological water quality of Gangetic river system and Husainsagar lake respectively and have reported that the places with greater population influx experience a comparatively higher bacterial load.

The TC count in Dul lake in summer season was also highest; which indicates that the lake water is being contaminated form direct human activities (i.e. bathing, excreting in the house boats, small boats being used to sale eatables). During monsoon and winter period, fewer tourists visit the place, therefore less human activities results in fewer microbial counts. Surface waters may become a carrier of disease producing bacteria when it comes in contact with human and animal infective materials. These lakes are being visited by a lot of foreign and Indian tourists every year. Niewolak (2000) has also attributed the repeated increase of TVC and TC to the increase of the amount of pollution from drainage catchment in a study carried out on river water quality of Wigry national park, Poland.

As per the general observations, highest faecal coliform and faecal streptococci counts were found in summer season samples of Lake Dul, Nainital followed by Bhimtal, which is again indicative of the fact that the water sample is being contaminated from direct human activities. Lake Nainital and Bhimtal being on hill station is favorable tourist spot during summer season. Low count of FC and FS were observed in lake Naukuchiatal, this might be because of the fact that this lake is at high altitude and have low temperatures, so optimum temperature conditions are not available for the survival of these thermotolerant organisms. Geldreich (1970) has reported out that FC: FS higher than 4.0 points to pollution originating from people, but in present study the values were found to be below 2 thereby suggesting an alternative source of pollution i.e. from grazing animals.

With respect to the physicochemical parameters, in all the lake water samples the DO was found to increase with decrease in human activities during monsoon and winter seasons, during which the DO was highest. The human activities include visits of tourists,

washing, bathing, grazing of animals near the lake or in catchments area etc. In all the lake samples the BOD varied from 3.6 to 15.3 mg/mL. During monsoon the highest BOD and COD was observed in lake Dul followed by Nainital and Bhimtal and during winter BOD decreased, lowest BOD and COD was observed in lake Naukuchiatal. Earlier, Sood et al., (2008) have studied water quality of Ganga in Uttarakhand Himalayas, India and have reported a high level of BOD due to introduction of organic matter into the system as a result of anthropogenic activities. Also these values showed a proportional relation with human activities i.e. the fewer the human activities (in winter), the better the water with respect to physicochemical parameters. Higher BOD values in most of the water samples suggest that either these lakes are rich in organic matter or organic matter is being introduced in the lakes by anthropogenic activities (Tijani et al. 2005), since, BOD provides a direct measurement of state of pollution. Relationship between BOD, COD and microbial count was found inversely proportional, implying that at high organic loading rates, the ecosystem retards the growth of aerobic microorganisms and favors the growth of anaerobes; our findings draws support from Mtui & Nakamurs (2006).

The use of coliform bacteria as a measure of the faecal contamination of lakes and streams has been in practice for many years. Our study gives an indication of the extent of relation of microbial pollution and physiochemical parameters; any further addition of wastes may deteriorate the existing hygienic quality in the area. These results suggest that increase of population of coliforms in a lake environment are directly proportional to the degree of sewage and human waste pollution, which is refected by BOD and COD levels. Sah et al. (2000) have stressed on the point that the pollution in rivers and water bodies from industries may adversely affect aquatic life of water bodies' as well human health in the vicinity of rivers/lakes.

Lake Naukuchiatal was found to be safe with respect to bacteriological as well as physicochemical parameters. This can be accounted by the fact that out of all the other lakes, Lake Naukuchiatal is least visited by the tourists and is not a very famous recreation spot, but urbanization, visits of local inhabitants and grazing animals in nearby area resulted in introduction of some amount of organic matter. Tijani et al. (2005) have stated that in many developing countries, increasing agricultural activities, urbanization and industrialization leads to ever increasing contamination of streams/rivers and lakes/reservoirs, which are usually the main sources of drinking water. This clearly highlights the fact that natural stagnant water re-

sources; though find special attraction for tourism and recreation activities, this practice degrades the quality of water.

In this study, we have collected water samples from lakes of different size and depths, but in order to represent the results in a simplified way, the results of various samples of a particular lake have been presented in a composite manner. In a broad view, the lakes with higher catchments area, soil cover and land use are more polluted, owing to more anthropogenic activities. McLellan et al. (2001) stated that faecal pollution indicator organisms can be used to a number of conditions related to the health of aquatic ecosystems and to the potential for health effects among individuals using aquatic environments. The presence of such indicator organisms may provide indication of waterborne problems and is a direct threat to human and animal health. Our studies on microbial ecology and physiochemical analysis in the north Indian lakes in relation to pollution have clearly revealed that there is significant presence of bacterial indicators of faecal pollution the situation is serious and alarming. Presence of bacterial indicators of faecal contamination in lakes clearly revealed the bacteriological status of the water at that site. For this reason, monitoring of microbial contamination in lakes should be an essential component of the protection strategy in that area area. The base line data generated on bacteriological water quality of lakes may serve as biomonitoring standard and comparisons for other lakes and may be useful for all scientists, decision makers and resource managers working with environmental planning and management of such areas.

Conclusions

The rationale of this study was to evaluate the impact of season and human activities on the pollution status of seven important north Indian Lakes. This study revealed that north Indian lakes are threatened by high influx of pollutants and enteric pathogenic contamination and it can be concluded that Dul Lake is most polluted and the Lake Naukuchiatal is the least. The constant surveillance of these water bodies with respect to the bacterial indicators and physicochemical parameters provides us with the opportunity of true microbiological monitoring of the area as well as proper management actions could be applied in order to improve the quality of these lakes and consequently reduce public health risk.

Acknowledgments

The authors are grateful to the Management of Sardar Bhagwan Singh (P. G.) Institute of Bio-Medical Sciences and

Research Balawala, Dehradun, (UK), India for providing research facilities required to carry out this work.

References

APHA, AWWA, WEF. (1999): Standards for Examination of Water and Wastewater, 20th ed. American Public Health Association, Washington DC USA.

Bureau of Indian Standards (1991): Indian standard specification for drinking water. IS: 10500, Indian Standard Institute.

Cairneross, S., Carruthers, I., Curtis, D., Feachem, R., Bradley, D. & Baldwin, G. (1980): Evaluation for Village Water Supply Planning. Wiley, Chichester, p. 277.

Central Water Commission (2007): Water & Related Statistics, India.

Craun, G. F. (1986): Water Borne Disease in the United States. CRC Press, Boca Raton, FL.

Geldreich, E. E. (1970): Applying bacteriological parameters to recreational water quality. J. American Water Work Asso. V. 62, pp.113–116.

Harwood, V. J., Brownell, M., Perusek, W. & Whitelock, J. E. (2001): Vancomycin-resistant Enterococcus sp. isolated from waste water and chicken feces in the United States. Appl. Environ. Microbiol. V. 67, pp. 4930–4933.

Hodegkiss, I. J. (1988): Bacteriological monitoring of Hong Kong marine water quality. Environ. Int. V. 14, pp. 495–499.

Islam, M. S., Siddika, A., Khan, M. N. H., Goldar, M. M., Sadique, M. A., Kabir, A. N. M. H., Huq, A. & Colwell, R. R. (2001): Microbiological analysis of tube-well water in a rural area of Bangladesh. Appl. Environ. Microbiol. V. 67, pp. 3328–3330.

Kistemann, T., Claben, T., Koch, C., Dangendorf, F., Fischeder, R., Gebel, J., Vacata,V. & Exner, M. (2002): Microbial load of drinking water reservoir tributaries during extreme rainfall and runoff. Appl. Environ. Microbiol. V. 68, pp. 2188–2197.

Mtui, G. V. S. & Nakamurs, Y. (2006): Physiochemical and microbiological water quality of lake Sagara in Malagarasi wetlands. J. Eng. Appl. Sci. V. 1, No. 2, pp. 174–180.

McLellan, S. L., Daniels, A. D. & Salmore, A. K. (2001): Clonal populations of thermotolerant enterobacteriaceaes in recreational water and their potential interference with fecal Escherichia coli counts. Appl. Environ. Microbiol. V. 67, pp. 4934–4938.

Niewolak, S. (2000): Bacteriological monitoring of River water quality in North area of Wigry National Park.. Pol. J. Environ. Studies. V. 9, pp. 291–299.

Okpokwasili, G. C. & Akujobi, T. C. (1996): Bacteriological indicators of tropical water quality. Environ. Tox.. Water Qual. V. 11, pp. 77–81.

Pathak, S. P. & Gopal, K. (2001): Rapid detection of Escherichia coli as an indicator of faecal pollution in water. Indian J. Microbiol. V. 41, pp.

139–151.

Pathak, S. P., Mathur, N. & Dev, B. (1991): Effect of socio biological activities on microbial contamination of river water in different reasons. Environ. Pollu. Res. Land Water. pp 245–254.

Pipes,W. O. (1981): Bacterial indicators of pollution. CRC Press Inc., Boca Raton, FL, p. 242.

Radha, S. & Seenayya, G. (2004): Ecological aspects of highly polluted and eutrophicated Husainsagar Lake sediments and its impact on mineralization of organic matter. Asian J. Microbiol. Biotechnol. Environ. Sci. V. 6, 367–371.

Rao, S. M. & Mamatha, P. (2004): Water quality in sustainable water management. Curr. Sci. V. 87, pp. 942–946.

Sah, J. P., Sah, S. K., Acharya P., Pant D. & Lance V. A (2000): Assessment of water pollution in the Narayani River, Nepal. Int. J. Ecol. Environ. Sci. V. 26, pp. 235–252.

Sood, A., Singh, K. D., Pandey, P. & Sharma, S (2008): Assessment of bacterial indicators and physicochemical parameters to investigate pollution status of Gangetic river system of Uttarakhand (India). Ecol. Indicators. V. 8, pp. 709–717.

Tijani, M. N., Balogun, S. A. & Adeleye, M. A (2005): Chemical and microbiological assessment of water and bottom-sediments contaminations in Awba lake (U.I), Ibadan, SW-Nigeria. RMZ-Mate. & Geoenviron. V. 52 (1), pp. 123–126.

World Health Organization (1983): Guidelines for Drinking Water Quality, Vol. 3. World Health Organization, Geneva.

Use of stable nitrogen ($\delta^{15}N$) isotopes in food web of the Adriatic Sea, Croatia

Uporaba stabilnega dušikovega izotopa ($\delta^{15}N$) v prehranjevalni verigi Jadranskega morja, Hrvaška

Petra Žvab[1,*], Tadej Dolenec[1], Sonja Lojen[2], Goran Kniewald[3], Josip Vodopija[4], Živana Lambaša Belak[5], Matej Dolenec[1]

[1]University of Ljubljana, Faculty of Natural Sciences and Engineering, Aškerčeva 12, SI-1000 Ljubljana, Slovenia
[2]Jožef Stefan Institute, Jamova 39, SI-1000 Ljubljana, Slovenia
[3]Ruđer Bošković Institute, Bjienička 54, 10000 Zagreb, Croatia
[4]Dalmar d.o.o., Obala kralja Petra Krešimira IV 64, 23211 Pakoštane, Croatia
[5]Šibenik-Knin County Administration, Vladimira Nazora 1, 22000 Šibenik, Croatia

*Corresponding author. E-mail: petra.zvab@guest.arnes.si

Received: November 6, 2009 **Accepted:** December 11, 2009

Abstract: This study presents the first attempt to classify organisms in the food web of the Adriatic Sea into trophic levels using a nitrogen ($\delta^{15}N$) isotope tracer. Three main trophic levels were identified with significantly different nitrogen values, ranging from primary producers to higher consumers. TL-1 represents plankton and POM samples, TL-2 mostly benthic organisms and TL-3 fishes. The results also indicate the influence of anthropogenic pollution, which significantly increases nitrogen values.

Izvleček: Raziskava je prvi poskus klasifikacije organizmov v prehranjevalni verigi Jadranskega morja v trofične nivoje na podlagi izotopske sestave dušika $\delta^{15}N$. Organizmi so bili generalno razvrščeni v tri trofične nivoje, ki vključujejo primerke od primarnih producentov do višjih konzumentov. TL-1 pomeni plankton in POM, TL-2 večinoma bentoške organizme in TL-3 ribe. Na izotopsko sestavo dušika pomembno vpliva antropogeno onesnaževanje, neobdelane komunalne in industrijske odplake, kot tudi marikulturne dejavnosti, ki občutno povišajo vrednosti dušikovega izotopa $\delta^{15}N$.

Original scientific paper

Key words: food web, trophic levels, nitrogen ($\delta^{15}N$) isotope composition, Adriatic Sea.
Ključne besede: prehranjevalna veriga, trofični nivoji, izotopska sestava dušika, Jadransko morje

Introduction

In ecological studies, stable isotopes, mostly carbon and nitrogen, are commonly used to trace food webs and distinguish between natural and anthropogenic sources. Using stable isotopes the sources and manner of feeding in marine ecosystems can be determined. The isotopic distribution in animals reflects the isotopic composition of their food and their position in the food web. The nitrogen ($\delta^{15}N$) values in animal bodies are usually more positive than those in their food (DeNiro & Epenstein, 1981; Minagawa & Wada, 1984; Fry, 1988). Heavy isotope enrichment for nitrogen is about 1.3–5.3 ‰ per trophic level and is more useful for studying the relations between trophic levels than that for carbon, for which enrichment is estimated to be about 1 ‰ per trophic level (Minagawa & Wada, 1984 Peterson & Fry, 1987; Fry, 1988). On the basis of stable isotope ($\delta^{15}N$, $\delta^{13}C$) composition, many researchers have tried to classify organisms into groups (trophic levels) in different aquatic and terrestrial ecosystems (Corbisier et al., 2006; Fry, 1988; Hobson et al., 2001; Iken et al., 2005; Wada et al., 1993).

The stable nitrogen isotopes also reflect unusual anthropogenic food sources that can increase or decrease nitrogen values (Fry, 1988). For this reason the interpretation should consider natural and also anthropogenic factors. Stable nitrogen isotopes can be used to track untreated communal and industrial sewage as well as animal excrement. Many papers have shown the negative influences of untreated municipal and industrial sewage (Constanzo et al., 2001; Dolenec & Vokal, 2002; Dolenec et al., 2005, 2006b, 2006c, 2007; Rogan et al., 2007) and fish farm activities on marine ecosystems (Dolenec et al., 2006a, 2007; La Rosa et al., 2001; Mirto et al., 2002; Pergent et al., 1999; Rogan et al., 2007; Ruiz et al., 2001; Sara et al., 2004). In addition, variations in stable nitrogen ($\delta^{15}N$) within the same species could be the result of seasonal effects (Constanzo et al., 2001), size and age effects (Minagawa & Wada, 1984; Wada et al., 1993), or depth effects (Saino & Hatory, 1980; Muscatine & Kaplan, 1994).

The aim of this paper is to present the relationships between stable nitrogen ($\delta^{15}N$) values in organisms in the

Adriatic Sea and their nutrition and position in the food web. For this purpose selected organisms, from primary consumers to higher consumers, were studied, and on the basis of nitrogen ($\delta^{15}N$) values were classified into different trophic levels.

Materials and methods

Study area

The study area included mostly coastal areas of the Northern and Central Adriatic Sea in Croatia. Samples were collected at several locations along the coast of Piran bay and Istra Peninsula (from Savudrija to Pula), and inshore and offshore areas of Murter Sea, the semi-enclosed Pirovac Bay, and sites around the Kornati Islands and Korčula Island (Figure 1). Some sampling locations were highly polluted by human sewage and industrial effluents, especially coastal areas in the vicinity of larger cities, marinas and ports, as well as by fish farming activities that produce N-rich waste of fish excrement and uneaten food. Sampling was also carried out at relatively unaffected sites to obtain information about the natural variability of stable nitrogen ($\delta^{15}N$) isotope composition in the Adriatic Sea.

Sample collection and analysis

Several marine organisms as well as particulate organic matter (POM) were sampled for isotopic analyses. Samples were collected from spring to autumn (May to September) from 2000 to 2008, but the seasonal and annual variations are not the topic of this study.

Water for particulate organic matter (POM) was collected at about 1 m depth at different sampling sites with different amounts of anthropogenic pollution. 5 L to 10 L of water was filtered through glass fibre microfilters (GF/C, Whatman). Filters were freeze-dried in liofilizator and prepared for isotopic analyses.

Plankton samples were collected with a plankton net at 50–0 m depth and other organisms (anemones, sponges, molluscs, sea urchins, crustaceans, fishes) by scuba diving from about 25 m depth. For this study average values of soft parts of tissues were presented. All samples were stored in plastic capsules or bags and refrigerated immediately after collection. In the laboratory, samples were rinsed with deionized water and freeze-dried for at least 72 h. Dried samples were homogenized and crushed to a fine powder by grinding in an agate mortar. Powdered samples were packed into tin capsules and were preserved in desiccators at room temperature until the analyses were carried out.

Nitrogen ($\delta^{15}N$) isotopic composition was measured using a Europa 20–20 mass spectrometer with an ANCA

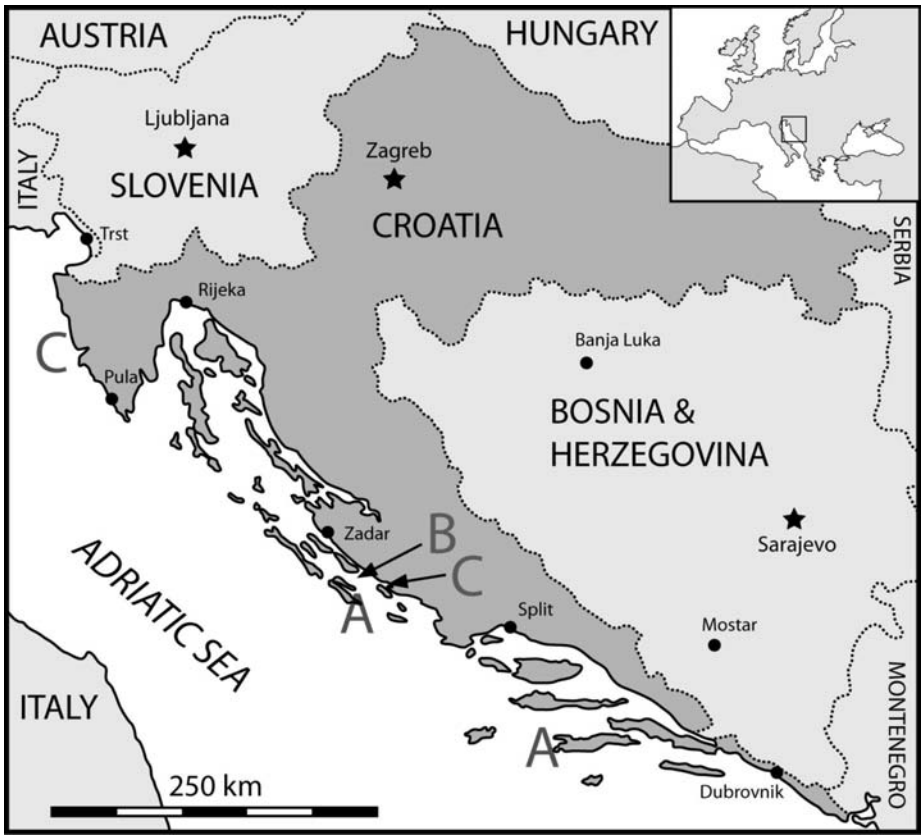

Figure 1. Map of the study area in the Adriatic Sea (Croatia) and locations of groups A, B and C with different amounts of anthropogenic pollution

SL preparation module (PDZ Europa Ltd., U. K.). The results were expressed in the standard $\delta^{15}N$ notation as parts per mille (‰) relative to the nitrogen standard (atmospheric nitrogen, $\delta^{15}N = 0$ ‰). The analytical precision (1 standard deviation) of triplicate analyses of IAEA N-1 and N-2 standards was better than ±0.16 ‰. The precision (1 standard deviation) of duplicate isotopic analyses of samples was within ±0.2 ‰.

Statistical analysis

Statistical analysis of presented data was performed by use of the statistical software program Statistica 6.0. The differences between the groups A, B, C of TL-1 and TL-2 and groups I, II, III of TL-3 were tested with t-test (Table 5).

Results and discussion

In order to understand the energy flow through the complex marine food web in the Adriatic Sea different organisms, from primary producers to upper trophic level consumers, were collected. Sampling was carried out in three areas with different amounts of anthropogenic pollution: (A) no or low anthropogenic impact around the Kornati Islands and Korčula Island, (B) inputs of fish faeces and uneaten food around fish farms near Vrgada Island and (C) municipal, industrial and agricultural inputs in coastal areas around Murter Island, the semi-enclosed Pirovac Bay and the Istra Peninsula (Figure 1).

The lowest nitrogen ($\delta^{15}N$) values were generally observed in plankton and POM samples. Plankton values in group A were between +2.5 ‰ and +4.4 ‰, and in the more polluted group C values increased up to +8.0 ‰. The mean $\delta^{15}N$ value of all plankton samples was 5.16 ‰ (Table 1, Figure 2). Similar values but with slightly higher variation were measured in POM, which generally contains a mixture of detritic material, phyto- and zooplankton, bacteria and particles from different sources. The nitrogen values varied between –1.27 ‰ and +13.79 ‰ with a mean value of 4.84 ‰ (Table 2, Figure 3). Extreme values were detected in areas that were highly influenced by human activity (group C) in the high tourist season, and low values were found in unaffected areas of group A. The relatively large variations in nitrogen ($\delta^{15}N$) values of POM and plankton samples could also be related to the rapid movement of floating material owing to the wind, current circulation and tides. Although POM and plankton samples showed notable variations in nitrogen values, they still exhibited the lowest values and were thus classified as trophic level 1 (TL-1).

The second trophic level (TL-2) contained mostly benthic organisms, including anemones (*Anemonia sulcata*), sponges (*Aplysina aerophoba*), barnacles (*Balanus perforatus*), molluscs (*Mytilus galloprovincialis, Arca neae, Patella sp., snails*), sea urchins (*Abracia lixula*) and crustaceans (*Squilla mantis, Nephrops norvegicus*). These organisms are sessile or have a very limited habitat and reflect local environmental conditions. The food for these organisms is generally from the lower trophic level TL-1 at the base of the food web. Nitrogen ($\delta^{15}N$) values varied between –1.30 ‰ up to +11.87 ‰ with a mean value of +4.74 ‰ (Table 3, Figure 4). Division into three groups regarding the amount of pollution was also evident in this group. Low values were observed in the non-affected areas (A), medium values around fish farms (B) and the highest values near the larger sources of pollution (C).

Table 1. Basic statistics for nitrogen ($\delta^{15}N$) isotopic composition of plankton in the Adriatic Sea

Group	N	Min	Max	Median	Means	SD
A	12	2.50	4.40	3.12	3.35	0.61
B	14	3.50	7.30	4.45	4.60	0.85
C	16	4.40	8.00	7.20	7.00	0.87
All groups	42	2.50	8.00	4.55	5.16	1.73

Table 2. Basic statistics for nitrogen ($\delta^{15}N$) isotopic composition of particulate organic mater (POM) in the Adriatic Sea

Group	N	Min	Max	Median	Means	SD
A	32	1.50	7.80	3.15	3.55	1.50
B	101	1.40	6.80	4.00	3.96	1.03
C	166	–1.27	13.79	5.70	5.61	1.91
All groups	299	–1.27	13.79	4.80	4.84	1.84

Table 3. Basic statistics for nitrogen ($\delta^{15}N$) isotopic composition of TL-2 in the Adriatic Sea

Group	N	Min	Max	Median	Means	SD
A	100	–1.30	10.60	2.40	2.60	2.13
B	146	1.10	8.80	4.60	4.63	1.43
C	115	0.50	11.87	6.70	6.73	2.39
All groups	361	–1.30	11.87	4.70	4.74	2.53

Table 4. Basic statistics for nitrogen ($\delta^{15}N$) isotopic composition of fishes in the Adriatic Sea

Groups	N	Min	Max	Median	Means	SD
I	8	6.50	13.45	8.12	9.16	2.48
II	14	6.90	12.70	9.67	9.93	1.79
III	31	7.80	14.70	11.20	11.22	1.90
All groups	53	6.50	14.70	10.60	10.57	2.09

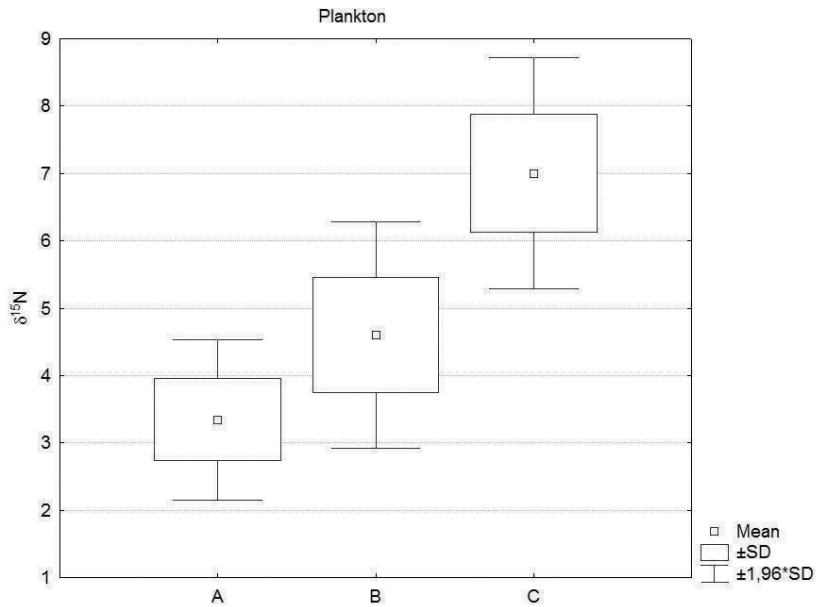

Figure 2. Whisker plots of nitrogen ($\delta^{15}N$) values of plankton in locations with different amounts of pollution

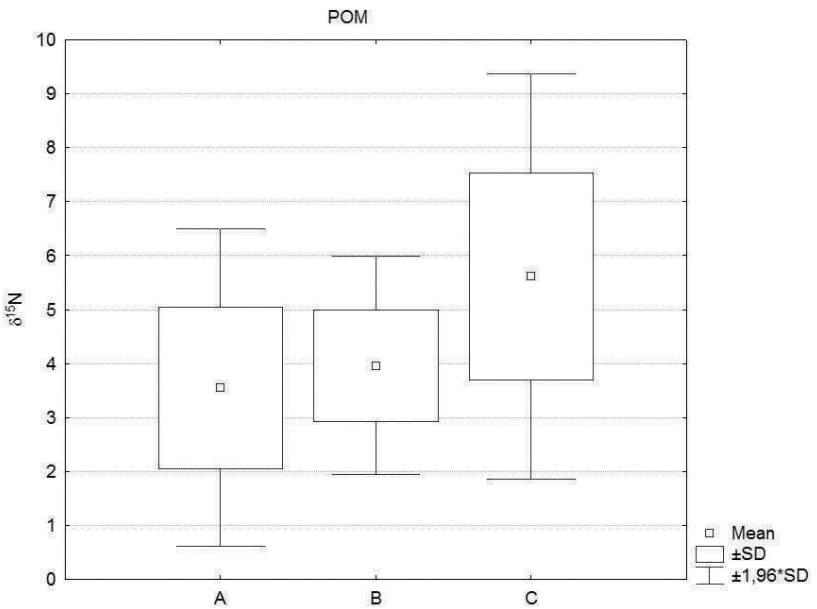

Figure 3. Whisker plots of nitrogen ($\delta^{15}N$) values of particulate organic matter (POM) in locations with different amounts of pollution

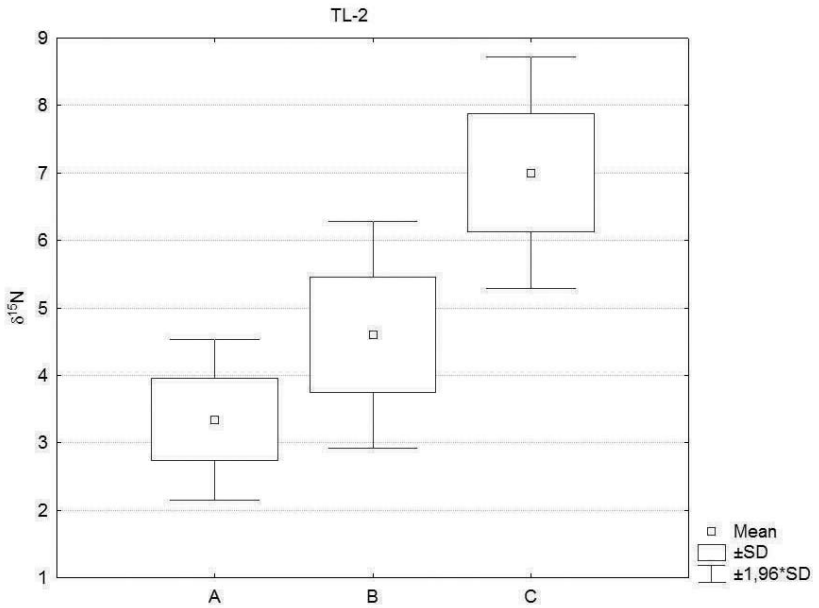

Figure 4. Whisker plots of nitrogen ($\delta^{15}N$) values of TL-2 in locations with different amounts of pollution

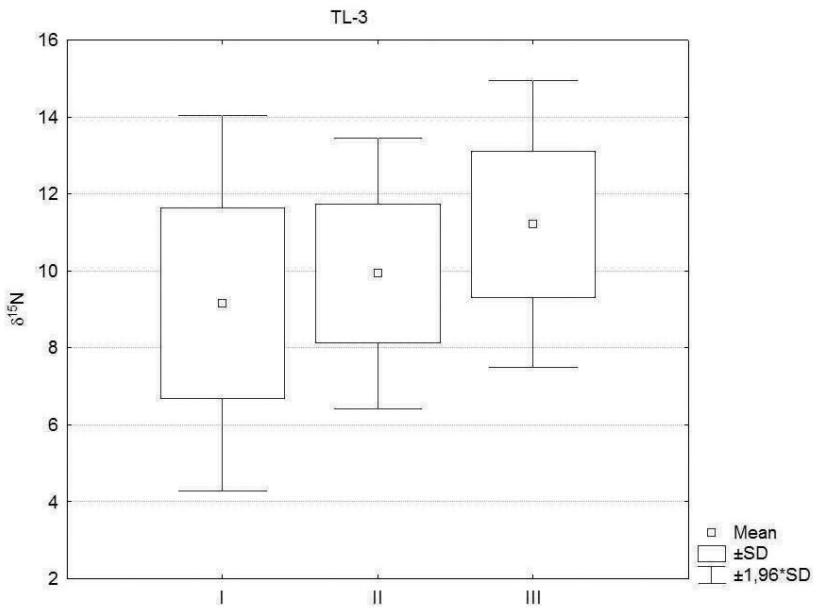

Figure 5. Whisker plots of nitrogen ($\delta^{15}N$) values of TL-3 fish tissues with different modes of nutrition

Table 5. Significance levels of the t-test to evaluate the differences between groups with different amounts of anthropogenic pollution A, B, C of TL-1 and TL-2 and groups I, II and III of TL-3 (ns = not significant, * = $p \leq 0.05$; ** = $p \leq 0.01$)

TL1	**A**	**B**	**C**
A	–	**	**
B	**	–	**
C	**	**	–
TL2	**A**	**B**	**C**
A	–	**	**
B	**	–	**
C	**	**	–
TL3	**I**	**II**	**III**
I	–	ns	*
II	ns	–	*
III	*	*	–

TL-2 is the most heterogeneous, including a large number of different species. It could probably be further divided into sublevels but the ′state of the art′ data did not allow this. Sampling was carried out in different seasons and the number of individual species varied notably (from 5 up to 150 samples). Surprisingly, some species of TL-2 showed significantly lower nitrogen values than those in TL-1, such as *Aplysina aerophoba*, which has previously been observed and studied in detail by Rogan et al. (2007). Depleted nitrogen values have been interpreted by fractionation of nitrogen isotopes during uptake and assimilation by symbiotic bacteria (Dolenec et al., 2007). Otherwise, the nitrogen ($\delta^{15}N$) values of TL-2 organisms were generally enriched compared with those of TL-1.

The highest nitrogen ($\delta^{15}N$) values were measured in fishes, which comprised the highest trophic level (TL-3) of the samples studied. Within TL-3, fish samples were divided into three sublevels according to their mode of nutrition; I. planktivores and detritivores (*Liza spp., Boops boops, etc.*), II. herbivores (*Spondyliosoma cantharus, Diplodus vulgaris,* etc.), and III. piscivores (*Merluccius merluccius, Citharus linguatula, Phycis, phycis, Muraena helena, Dicentrarchus labrax, Seriola dumerili, Conger conger,* etc.). The mean nitrogen value increased from group I to III (Figure 5); +9.16 ‰ for group I, +9.93 ‰ for group II and +11.22 ‰ for group III (Table 4, Figure 5). The isotopic composition of fish tissues depends on their ′squeamishness′ and varies within the same group. Ni-

trogen ($\delta^{15}N$) values are also the result of anthropogenic inputs, which lead to fish migration and/or adjustment to polluted water (*Liza* spp.).

The results of the t-test of groups within trophic levels are presented in Table 5. T-tests between groups with different amount of pollution A, B, C (Figure 1) of trophic levels TL-1 and TL-2 all showed significant differences at confidence level 99 % ($p < 0.01$). Slightly lower significant differences were observed between I and III as well as II and III group of TL-3 (confidence level 95 %; $p < 0.05$), while t-tests between I and II group showed no significant differences.

Conclusion

The nitrogen ($\delta^{15}N$) isotope distribution of organisms in the Adriatic Sea can be used to follow the energy flow through the food web of the ecosystem and to classify individual species within trophic levels. Enrichment of nitrogen ($\delta^{15}N$) within the whole food web was more than +10 ‰, which enabled the assessment and interpretation of feeding habits and relationships between particular organisms. Organisms in the Adriatic Sea were classified into three trophic levels: TL-1 (plankton and POM), TL-2 (mostly benthic organisms; anemones, sponges, barnacles, molluscs, sea urchins and crustaceans) and TL-3 (fishes).

Apart from demonstrating the trophic level of different organisms, this study also showed significant variation in nitrogen ($\delta^{15}N$) values within individual species. These fluctuations were related to pollution of the sampling areas. Compared to the natural background, nitrogen ($\delta^{15}N$) enrichment was observed around cities, ports and tourist facilities in the coastal regions of Murter Sea, Pirovac Bay and Istra Peninsula. These areas are exposed to untreated municipal, industrial and agricultural pollution that increases the amount of nitrogen ($\delta^{15}N$) input into the marine ecosystem. Furthermore, nitrogen ($\delta^{15}N$) enrichment could also reflect intensive aquaculture with increased input from fish faeces and uneaten food.

Acknowledgements

This research was financially supported by the Ministry of Higher Education, Science and Technology, Republic of Slovenia (Bilateral projects between Croatia and Slovenia 2001–2009) and Geoexp, d. o. o., Tržič, Slovenia.

References

Constanzo, S. D., Donohue, M. J., Dennison, W. C., Loneragan, N. R. & Thomas, M. (2001): A new approach for detecting and map-

ping sewage impacts. *Marine Pollution Bulletin*, Vol. 42, pp. 149–156.

Corbisier, T. N., Soares, L. S. H., Petti, M. A. V., Muto, E. Y., Silva, M. H. C., McClelland, J. & Valiela, I. (2006): Use of isotopic signatures to assess the food web in a tropical shallow marine ecosystem of Southeastern Brazil. *Aquatic Ecology*, Vol. 40, pp. 381–390.

Deniro, M. I. & Epstein, S. (1981): Influence of diet on the distribution of carbon isotopes in animals. *Geochimica et Cosmochimica Acta*, Vol. 45, pp. 341–351.

Dolenec, T. & Vokal, B. (2002): Isotopic composition of nitrogen and carbon in *Anemonia sulcata* as a possible indicator of anthropogenic impacts on marine costal ecosystems of the Adriatic. *Materials and Geoenvironment*, Vol. 49, No. 4, pp. 449–457.

Dolenec, T., Vokal, B. & Dolenec, M. (2005): Nitrogen - 15 signals of anthropogenic nutrient loading in *Anemonia sulcata* as a possible indicator of human sewage impacts on marine coastal ecosystem s: a case study of Pirovac Bay and the Murter Sea (Central Adriatic). *Croat. Chem. Acta*, Vol. 78, No. 4, pp. 593–600.

Dolenec, T., Lojen, S., Lambaša, Ž. & Dolenec, M. (2006a): Effects of fish farm loading on sea grass *Posidonia oceanica* at Vargada Island (Central Adriatic): a nitrogen stable isotope study. Isot. *Environ. Health Studies*, Vol. 42, No. 1, pp. 77–85.

Dolenec, T., Lojen , S., Dolenec, M., Lambasa, Ž., Dobnikar, M. & Rogan, N. (2006b): ^{15}N and ^{13}C enrichment in *Balanus perforatus* : tracers of municipal particulate waste in tha Murter Sea (Central Adriatic, Croatia). *Acta Chim. Slov.*, Vol. 53, pp. 469–476.

Dolenec, T., Lojen, S., Kniewald, G., Dolenec, M. & Rogan, N. (2006c): $\delta^{15}N$ of particulate organic matter and *Anemonia sulcata* as a tracer of sewage effluent transport in the marine costal ecosystem of Pirovac Bay and the Murter Sea (Central Adriatic). *Materials and Geoenvironment*, Vol. 53, No. 1, pp. 1–13.

Dolenec, T., Lojen, S., Kniewald, G., Dolenec, M. & Rogan, N. (2007): Nitrogen stable isotope composition as a tracer of fish farming in invertebrates *Aplysina aerophoba*, *Balanus perforatus* and *Anemonia sulcata* in central Adriatic. *Aquaculture*, Vol. 262, pp. 237–249.

Fry, B. (1988): Food web structure on Georges Bank from stable C, N, and S isotopic compositions. *Limnology and oceanography*, Vol. 33, pp. 1182–1190.

Hobson, K. A., Fisk, A., Karnovsky, N., Holst, M., Gagnon, J.-M. & Fortier, M. (2002): A stable isotope ($\delta^{13}C$, $\delta^{15}N$) model for the North Water food web: implications for evaluating trophodynamics and the flow of energy

and contaminants. *Deep-Sea Research II*, Vol. 49, pp. 5131–5150.

Iken, K., Bluhm, B.A. & Gradinger, R. (2005): Food web structure in the high Arctic Canada Basin: evidence from $\delta^{13}C$ and $\delta^{15}N$ analysis. *Polar Biol.*, Vol. 28, pp. 238–249.

La Rosa, T., Mirto, S., Mazzola, A. & Danavaro, R. (2001): Differential responses of bentic microbes and meiofauna to fish-farm disturbance in coastal sediments. *Environmental Pollution*, Vol. 112, pp. 427–434.

Miniwaga, M. & Wada, E. (1984): Stepwise enrichment of ^{15}N along food chains: Further evidence and the relation between $\delta\ ^{15}N$ and animal age. *Geochimica et Cosmochimica Acta*, Vol. 48, pp. 1135–1140.

Mirto, S., La Rosa, T., Gambi, C., Danavaro, R. & Mazzola, A. (2002): Nematode community response to fish-farm impact in the western Mediterranean. *Environmental Pollution*, Vol. 116, pp. 203–214.

Muscatine, L. & Kaplan, I. R. (1994): Resource partitioning by reef corals as determined from stable isotope composition II $\delta^{15}N$ of zooxanthellae and animal tissue versus depth. *Pac. Sci.*, Vol.48, pp.304–312.

Pergent, G., Mendez, S., Pergent-Martini, C. & Pasquali, V. (1999): Preliminary data on the impact of fish farming facilities on *Posidonia oceanica* meadows in the Mediterranean. *Oceanologica Acta*, Vol. 22, pp. 95–107.

Peterson, B. Ú‰J. & Fry, B. (1987): Stable isotopes in ecosystem studies. *Annual review ecological systems*, Vol. 18, pp. 293–320.

Rogan, N., Dolenec, T., Lojen, S., Lambaša, Ž.& Dolenec, M. (2007): ^{15}N signal of *Aplysina aerophoba* as a tracer of anthropogenic nitrogen in the Murter Sea and Pirovac bay (central Adriatic). *Materials and Geoenvironment*, Vol. 54, No. 1, pp. 63–76.

Ruiz, M., Perez, M. & Romero, J. (2001): Effects of fish farm loadings seagrass (*Posidonia oceanica*) distribution, growth and photosynthesis. Marine Pollution Bulletin, Vol. 42, pp. 749–760.

Saino, T. & Hatory, A. (1980): ^{15}N natural abundance in oceanic suspended particulate matter. *Nature*, Vol. 283, pp.752–754.

Sara, G., Scilipoti, D., Mazzola, A. & Modica, A. (2004): Effects of fish farming waste to sedimentary and particulate organic matter in a southern Mediterranean area (Gulf of Castellammare, Sicily): a multiple stable isotope study $\delta^{13}C$ and $\delta^{15}N$. *Aquaculture*, Vol. 234, pp. 199–213.

Wada, E., Kabaya, Y. & Kurihara, Y. (1993): Stable isotopic structure of aquatic ecosystems. *J. Biosci.*, Vol. 18, No. 4, pp. 483–499.

Deterioration of Lesno Brdo limestone on monuments (Ljubljana, Slovenia)

Propadanje lesnobrdskega apnenca na objektih kulturne dediščine (Ljubljana, Slovenia)

Sabina Kramar[1,*], Ana Mladenović[2], Maja Urosevic[3], Alenka Mauko[2], Helmut Pristacz[4] & Breda Mirtič[5]

[1]Institute for the Protection of Cultural Heritage of Slovenia, Conservation Centre, Restoration Centre, Poljanska 40, SI-1000 Ljubljana, Slovenia
[2]Slovenian National Building and Civil Engineering Institute - ZAG Ljubljana, Dimičeva 12, SI-1000 Ljubljana, Slovenia
[3]University of Granada, Faculty of Science, Department of Mineralogy and Petrology,
Avda. Fuentenueva s/n, 18071 Granada, Spain
[4]University of Vienna, Institute of Mineralogy and Crystallography, Althanstrasse 14, 1090 Vienna, Austria
[5]University of Ljubljana, Faculty of Natural Sciences and Engineering, Department of Geology, Aškerčeva 12, SI-1000 Ljubljana, Slovenia

*Corresponding author. E-mail: sabina.kramar@rescen.si

Received: December 14, 2009 **Accepted:** February 2, 2010

Abstract: This study deals with the characterization of Lesno Brdo limestone, widely used in the construction of Slovenian historical monuments as well as modern buildings. Samples of this limestone were subjected to a detailed investigation, using a number of different techniques: optical microscopy, scanning electron microscopy with EDS, X-ray powder diffraction, analysis by ICP-ES, porosity accessible to water under vacuum, capillary absorption, mercury intrusion porosimetry, gas sorption and ultrasonic velocity measurements. The object of these tests was to determine the mineralogical and microstructural parameters which affect the durability of the investigated stone, whose main mineral component is calcite, although quartz, dolomite and phyllosilicates are also present. Very low values of porosity were measured, as well as slow capillary

Original scientific paper

kinetics. Pore size distribution was found to be variable, and anisotropy high. The deterioration of the limestone on two monuments, one of which had been exposed to an outdoor environment, and the other to an indoor environment, was studied. The results indicated that the precipitation of soluble salts had significantly contributed to the severe observed deterioration of the limestone.

Izvleček: Prispevek obravnava lesnobrdski apnenec, ki je bil široko uporabljen pri gradnji številnih objektov kulturne dediščine in prav tako pri gradnji modernih objektov. Vzorci apnenca so bili preiskani z optično mikroskopijo, elektronsko mikroskopijo z EDS, rentgensko praškovno difrakcijo in ICP-ES. Med fizikalno-mehanskimi lastnostmi so bile merjene poroznost, vpijanje vode, plinska adsorpcija in prehod vzdolžnih ultrazvočnih valov. Z naštetimi meritvami smo želeli ugotoviti, kateri mineraloški in mikrostrukturni parametri vplivajo na obstojnost apnenca. Apnenec poleg kalcita sestavljajo še dolomit, kremen in filosilikati. Rezultati so pokazali, da ima apnenec zelo nizko poroznost in kinetiko kapilarnega dviga. Nadalje je bil predmet preiskave ugotavljanje propadanja apnencev na objektih kulturne dediščine. Ugotovljeno je bilo, da je kristalizacija v vodi topnih soli eden izmed glavnih vzrokov propadanja.

Key words: limestone, weathering response, deterioration, soluble salts, historical monuments

Kjučne besede: apnenec, obstojnost, propadanje, topne soli, kulturna dediščina

Introduction

The severity of stone deterioration depends on complex interactions between a number of environmental and intrinsic properties, as well as on the duration of exposure. In terms of mineralogy and structure, stone is an extremely complex material - a complexity that is reflected in its weathering response to the natural and the built environment. [1] Proper knowledge of the properties of stone and an understanding of deterioration factors and processes are necessary for successful maintenance, protection and suitable conservation-restoration interventions.

Since prehistoric times, limestone has been one of the most common types of building stone, with continued applications in present building works and in conservation practice as a replacement material for the reconstruction

of monuments. Although limestone consists mainly of calcite, it can show significant variations in its minor mineral composition, as well as in its structure and texture, resulting in complex and contrasting weathering behaviour. Many sedimentary rocks contain clay that can cause swelling when the stone is exposed to moisture, resulting in damage to monuments.[2, 3] Among the parameters which influence stone deterioration, moisture and the movement of water through the pore network are very important. Damage due to the soluble salt crystallization is considered to be a common risk, which plays a major role in the decay of limestone. Such salts are known to cause damage to porous materials through a variety of mechanisms, such as the production of physical stress resulting from their crystallization in the pores, differential thermal expansion, hydration pressure and enhanced wet/dry cycling caused by deliquescent salts.[4, 5] The properties, behaviour and decay of limestones have been profusely studied over the last decade by means of different approaches, especially focusing on their characterization as building materials with respect to estimates of durability[6–11] and to the assessment of limestone decay on monuments.[12–17]. However, whereas these studies have been mainly concerned with porous limestones, detailed studies of the properties of compact limestones are still rare.[18–22]

Two lithotypes of a compact limestone from the Lesno Brdo quarry, which is located approximately 10 km west of Ljubljana, were selected for a detailed study of their properties and deterioration phenomena. This limestone, known as Lesno Brdo limestone, is characterized by various colours: red, pink, and all possible nuances from light to dark grey. It has been frequently employed in the construction of Slovenian historical monuments,[23, 24, 25] as well as in modern buildings. These colours are sometimes shot through each other, whereas they are sometimes clearly separated.[23, 24] The dark grey lithotype was selected because, in recent years, due to the geological conditions, it has become easier to extract and therefore more popular for use in the construction of modern buildings. The light red lithotype was selected not only because it is very decorative, and for this reason was frequently used in historical buildings and monuments, but also because in past centuries it was the leading lithotype from this quarry. It is still available today, in smaller quantities, and is used, for example, in contemporary buildings as cladding and flooring, or as replacement material in works for the conservation and restoration of historical monuments.

Thus, the two main aims of the investigation were: firstly, to characterize the light red and dark grey lithotypes of the Lesno Brdo limestone from the min-

eralogical, chemical and petrophysical points of view, and to assess the differences between the lithotypes with respect to their durability, and, secondly, to characterize the deterioration patterns of two historical monuments, made mainly using the red lithotype, one of which had been exposed to an outdoor environment, and the other to an indoor environment.

Materials and methods

Materials

Limestone was sampled in the local active quarry of Lesno Brdo near Ljubljana (Central Slovenia). Two lithotypes of Triassic reef limestone were selected for this study: the dark grey lithotype (these samples were labelled: SLB) and the light red lithotype (these samples were labelled: PLB).

Additionally, as a part of a broader conservation - restoration projects, sampling was also carried out on two baroque monuments, located in the old part of the city of Ljubljana, Slovenia: the Fountain of the Three Carniolian Rivers, commonly known as Robba's Fountain, which is shown in Figure 1a (the samples from this monument were designated: RO), which was constructed between 1743 and 1751, and one of the side altars in the Church of St. James, in the Chapel of St. Francis Xavier, which is shown in Figure 1b (the samples from this monument were designated: JAL), and was constructed between 1709 and 1722. The elements of the fountain consist of four different types of natural stone. The architectural part of the monument consists of two different types of Slovenian limestone and a conglomerate, whereas the three statues are sculpted out of Carrara marble. The light red lithotype of Lesno Brdo limestone was used for the construction of this monument's obelisk. The side altar in the Chapel of St. James' Church is made of 18 different types of natural stone, whereas both of the above-mentioned lithotypes of Lesno Brdo limestone were used for the construction of some of the lower parts of the altar. A total of 15 samples from the two considered monuments were carefully collected, paying special attention to the sampling the different textures of the weathering forms, and the degree of damage. Detailed information about the fresh and weathered samples is provided in Table 1.

Analytical methods

Polished thin sections of six samples of the limestone from the quarry (three per lithotype) were studied by optical microscopy, using an Olympus BX-60 equipped with a digital camera (Olympus JVC3-CCD).

The samples of both unweathered and weathered limestone were examined by a Scanning Electron Microscope

Figure 1. Selected monuments and weathering forms of Lesno Brdo limestone. (a) Fountain of the Three Carniolian Rivers - the obelisk is made of Lesno Brdo limestone, and the statues of Carrara marble. (b) Side altar of the Church of St. James. Some of the stone elements of the lower parts are made of Lesno Brdo limestone. (c) The black crusts are compact aggregates of salt minerals, occurring on the surface on sheltered areas. The Figure shows a detail of the obelisk of the Fountain. (d) Fluffy efflorescence, appearing as very loosely coherent aggregates of acicular and long hair-like crystals. The Figure shows a detail of the lower part of the altar. The width of the image is about 10 cm.

Table 1. Summary of the investigated samples, showing the related weathering forms and mineralogy as determined by X-ray powder diffraction and SEM-EDS

Unweathered samples			
Limestone	*Location*	*Investigated samples*	*Primary mineralogy*
Dark grey lithotype	Lesno Brdo quarry	SLBa, SLBb, SLBc	calcite, dolomite, quartz, clinochlore, muscovite/illite
Light red lithotype	Lesno Brdo quarry	PLBa, PLBb, PLBc	calcite, dolomite, quartz, clinochlore, muscovite/illite
Samples from monuments			
Weathering type	*Location*	*Investigated samples*	*Weathering products*
black crust	fountain	RO94, RO95, RO97, RO98, RO99, RO100	gypsum
flaking	fountain	RO94, RO95, RO97, RO98, RO99	gypsum
white crust	altar	JAL173, JAL175, JAL176	gypsum
flaking	altar	JAL173, JAL182	gypsum
subflorescence	altar	JAL173, JAL182	gypsum
crumbling	altar	JAL177, JAL184	gypsum
efflorescence	altar	JAL174, JAL180, JAL181	gypsum, nitre, hexahydrite, pentahydrite

(JEOL 5600 LV), using electron backscattering. Some particular areas of the samples were analyzed for chemical composition using an Energy Dispersive X-ray Spectrometer (EDS). The excitation voltage was 20 kV, and the pressure was between 10 Pa and 20 Pa.

The mineral composition of both the unweathered limestone and the weathering products was determined by X-ray powder diffraction, using a Philips PW3710 X-ray diffractometer equipped with Cu Kα radiation, and a secondary graphite monochromator. The samples were milled in an agate mortar to a particle size of less than 50 μm. The data were collected at 40 kV and a current of 30 mA, in the range from $2\theta = (2 \text{ to } 70)^{\circ}$. Afterwards, each sample of limestone was treated in order to extract its acid-insoluble residue. About 400 mg of each sample was crushed and dissolved in 20 mL of dilute HCl (1:10)[21]. The residue was then washed with distilled water in order to remove all traces of HCl. The acid-insoluble fraction was then analyzed using X-ray powder diffraction.

All the samples of the unweathered limestone were analyzed for their major chemical composition in an accredited commercial Canadian laboratory (Acme Analytical Laboratories, Vancouver, B.C., Canada), using different analytical methods. According to the results of the reports, SiO_2, Al_2O_3, Fe_2O_3, MgO, CaO, Na_2O, K_2O, TiO_2 and P_2O_5 were measured after fusion with a mixture of lithium metaborate/tetraborate and dissolution in nitric acid by inductively coupled plasma emission spectroscopy (ICP-ES). The total carbon content was obtained by combustion in an oxygen current (LECO method) and the CO_2 and volatile contents by precision scale weighing after calcination at 1100 °C (LOI). The accuracy and precision of the sample analyses were assessed by using the reference material CCRMR SO-18 CSC.

The total porosity (N_t) of the samples of unweathered limestone (three samples of (50 × 50 × 50) mm per lithotype) was measured by water uptake under a vacuum, according to the RILEM recommendations - RILEM I.1 Norm.[26] The water absorption coefficient (A/(g m^{-2} s$^{-1/2}$) was measured according to the RILEM II.6 Norm.[26]

The pore systems of the samples of unweathered limestone (three samples per lithotype) were further characterized by means of mercury intrusion porosimetry (MIP) and gas sorption isotherms. Small blocks, of size approximately 2 cm^3, were dried in an oven for 24 h at 60 ºC, and analyzed on a Micromeritics Autopore III model 9410 porosimeter. Adsorption and desorption isotherms of argon were obtained at –196 ºC on a Micromeritics Tristar 3000 Analyzer. In rock materials several fluids can be applied as adsorbates the most commonly used being nitrogen. However, in samples with a surface area of less than 5 m^2 g^{-1}, argon adsorption measurements are more accurate than when using nitrogen, which usually yield excessively high values.[27] Prior to measurement, samples were heated at 250 °C for 8 h, and outgassed to 1.33 × 10^{-3} mbar using Micromeritics Flowprep equipment. Gas adsorption analysis in the relative pressure range of 0.05 to 0.3 was used to determine the total specific area – BET surface area of the samples.[28, 29] The BJH method was used to obtain pore size distribution curves, the pore volume and the mean pore size of the rock samples.[30]

Ultrasonic velocity measurements (USV) were applied in order to demonstrate the homogeneity of the limestone. These measurements were performed using an AU 2000 Ultrasonic Tester (CEBTP), with transmission frequency of 60 kHz. The pulse propagation velocity was measured on dry test samples (three samples per lithotype, of size: (50 × 50 × 50) mm). Three measurements were performed

in each of the three orthogonal directions. Additionally, the total structural anisotropy coefficient $\Delta M/\%$ and the relative anisotropy coefficient $\Delta m/\%$ of the stone material were obtained from the mathematical relations between the ultrasonic propagation velocities, following the equations of Guydader and Denis.[31]

Results and discussion

Characterization of samples from the quarry

Mineral and chemical composition

Petrographical analysis indicated that the limestone is very heterogeneous, being classified as mainly micritic with a transition to microsparitic (Figures 2a and 2b). Intraclasts, pellets and fragments of fossils (mainly red algae and shells) are present in both lithotypes. The light red lithotype is slightly more heterogeneous, due to the presence of numerous veins and styloliths. The styloliths are filled either with phyllosilicates (minerals of the chlorite and mica groups) and iron oxides/hydroxides or dolomite. Calcite occurs mainly as micrite, but also as sparitic crystals in veins, and as fragments of shells. Some parts of both lithotypes consist of coarse-grained dolomite crystals with sizes up to 2 mm, which are sometimes partly or completely replaced by calcite. Iron oxides/hydroxides occur in the calcitic rims of the coarse-grained dolomite. These could be clearly observed by SEM-EDS (Figure 2c), which revealed that the rims of the coarse-grained crystals of dolomite are partially replaced by calcite. The iron oxides/hydroxides occur macroscopically as a brown colour, enclosing the dolomite. The intergranular spaces of the coarse-grained dolomite and calcite are mainly filled with phyllosilicates, as was proved by SEM-EDS analysis (Figure 2c). According to the results of EDS, the chemical composition of the material in the intergranular spaces consists of K-rich alumosilicates, which are assumed to be sericite (fine grained muscovite). In some veins the intergrowing of sericite with clinochlore can be observed, as can be seen in Figure 2d. Homogenously distributed, single grains of ilmenite and apatite commonly occur in veins of phyllosilicates. Quartz occurs as autogenous or as terrigenous grains. It can also occur in veins, as polycrystallinic quartz. SEM-EDS analysis of the limestone samples also confirmed the occurrence of quartz grains, which are homogeneously distributed over the sample.

The results of the X-ray powder diffraction analysis (Table 1) of the bulk limestone indicate that calcite, as well as dolomite and quartz, are present in all the samples. Phyllosilicates such as clinochlore and muscovite/illite were detected in all three samples of the light red lithotype, but only in one sample of the dark grey lithotype (SLBa). X-ray

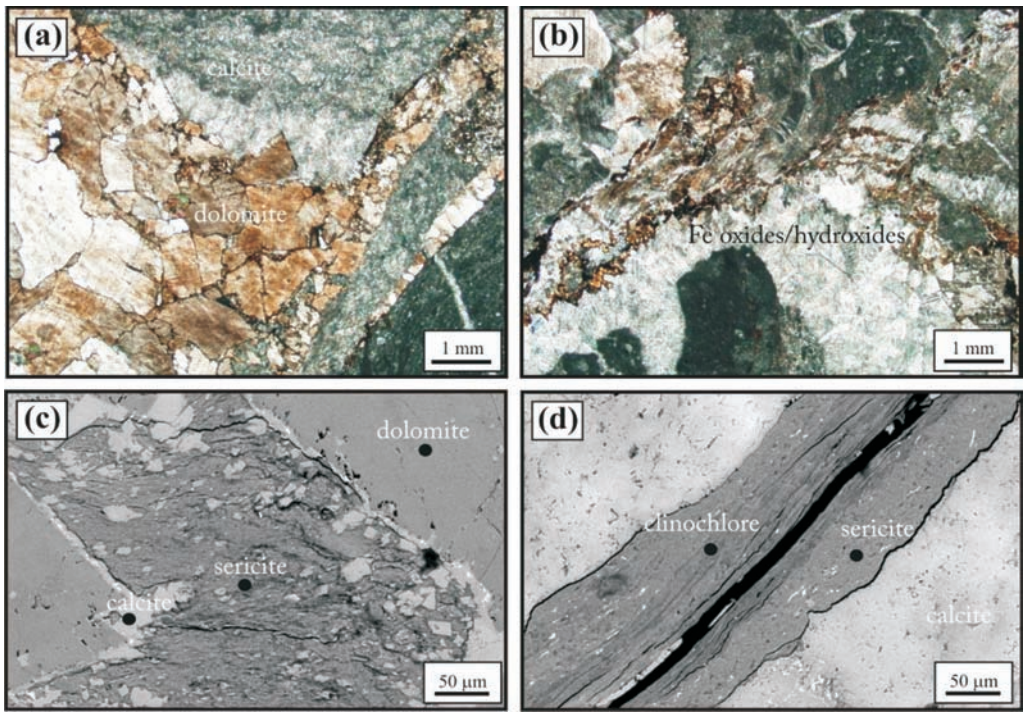

Figure 2. Microimages of Lesno Brdo limestone. (a) The dark grey lithotype. The image shows coarse-grained dolomite, surrounded by sparitic and micrite calcite. Transmitted light, parallel polars. (b) The light red lithotype. The image shows a very heterogeneous structure, with brownish veins of Fe oxides/hydroxides and clay. Transmitted light, parallel polars. (c) An SEM-BSE image of an intergranular space, filled with sericite. Fe oxides/hydroxides are present in the calcitic rims of the coarse-grained dolomite. (d) The SEM-BSE image show the intergrowing of sericite (brighter areas) with clinochlore (darker areas). The small bright areas indicate the presence of ilmenite.

Table 2. Bulk chemical composition of the limestone samples, determined by ICP-ES. All the oxides, as well as the loss on ignition - LOI and the total carbon - TOT/C, are given in mass fractions *w*/%

Samples	SiO_2	Al_2O_3	Fe_2O_3	MgO	CaO	Na_2O	K_2O	TiO_2	P_2O_5	LOI	TOT/C
SLBa	2.41	1.50	0.24	1.26	53.71	0.04	0.36	0.05	0.02	35.2	12.12
SLBb	0.92	0.35	0.05	0.59	56.27	0.02	0.08	0.01	<0.01	35.5	12.06
SLBc	0.91	0.45	0.11	3.64	50.88	0.04	0.10	0.01	<0.01	43.8	12.39
PLBa	5.73	3.41	0.79	0.90	52.47	0.06	0.80	0.10	0.02	35.7	10.92
PLBb	5.31	3.32	0.45	1.70	62.63	0.14	0.64	0.11	0.02	35.6	10.95
PLBc	2.96	1.54	0.53	2.96	51.62	0.02	0.33	0.04	0.01	36.2	12.01

powder diffraction analysis of the acid-insoluble residue likewise revealed the presence of quartz, muscovite/illite and clinochlore, as minor components. All samples of the light red lithotype consisted of muscovite/illite, clinochlore and quartz, whereas the acid-insoluble residue in the dark grey lithotype represents quartz, and only in one sample muscovite/illite and clinochlore. Due to the small quantities of ilmenite and apatite, it was not possible to detect these minerals using this method.

The results of bulk chemical analyses of all of the investigated samples are given in Table 2. They reveal high heterogeneity in the chemical and thus also mineralogical composition of the samples. In all the samples CaO is invariably the main chemical component, indicating that the limestone is mainly composed of calcite. The light red lithotype of limestone has a higher content of SiO_2, Al_2O_3, Fe_2O_3 and K_2O, thus reflecting the presence of phyllosilicates and quartz. K_2O indicates the presence of muscovite/illite, whereas the high fraction of the MgO component indicates the presence of dolomite and clinochlore. High contents of Fe_2O_3 indicate the presence of clinochlore and iron oxides/hydroxides in the veins. The contents of TiO_2 and P_2O_5 are higher in the samples of the light red lithotype, which can be attributed to the presence of ilmenite and apatite in sericite and clinochlore-rich veins.

Physical and mechanical properties

As water plays a fundamental role in stone deterioration, the properties of the stone structure and water transfer were measured. It is well known that water is one of the most important deterioration agents, and also facilitates the damaging action of other agents, such as salts. The petrophysical characteristics of the limestone are shown in Table 3. All the samples have low porosity, which is less than 1 % by mass, determined by the water vacuum method. The coefficient of capillarity is rather low, too. The average values were (0.24 ± 0.03) g m^{-2} $s^{-0.5}$ for the light red lithotype, and (0.09 ± 0.05) g m^{-2} $s^{-0.5}$ for the dark grey lithotype. The obtained values are of the same order of magnitude as for some other limestones.[18] The light red limestone exhibited slighter higher values of porosity, which is also reflected in the high water absorption coefficient. This behaviour may be explained by the presence of veins filled with clay minerals, which are more abundant in the light red lithotype.

Pore size distribution is important for understanding the movement of fluids inside the pore structure. It is well-known that different pore size can result in different behaviours relative to water.[17] Pores are classified into three types,[32] as follows: a) pores smaller than 0.1 μm, in which capillary condensation takes place; b) pores in the size range from 0.1 μm to 5.0 μm, in which

water transport mechanism is capillary suction and c) pores larger than 5.0 μm, the range of pores allowing free water to penetrate the porous material. The pore volume and pore size distribution between 0.003 μm and 100 μm (radius) were measured by mercury intrusion porosimetry. The results of two studied lithotypes are shown in Table 3. The light red lithotype of limestone is more porous than the dark grey lithotype, with open porosity values of (2.49 ± 0.97) % vs. (1.60 ± 0.76) % respectively, even though the bulk density of both lithotypes is almost the same.

When considering damage due to salt crystallization, the critical pore radius where the crystallization pressure is effective ranges below 0.05 μm.[33] The gas-physisorption method is thus suitable for investigation of this range of pore radii. Scherer[34] established that the maximum pressure that salt crystallization can achieve is highly dependent on the size of the pores, predicting that most of the damage occurs when salt-rich fluids migrate from pores of larger size to pores of smaller size, in the range between 4 nm and 50 nm. Pore size distribution thus controls the

Table 3. Physical and mechanical properties of the limestone. The pore system characteristics were determined by the water vacuum method, water absorption, Hg porosimetry and Ar sorption. Average values of ultrasound velocities, measured in three orthogonal directions (V_1, V_2, V_3), structural anisotropy (ΔM) and relative anisotropy (Δm).

Method of investigation	SLB	PLB
Porosity accessible to water (%)	0.18 ± 0.04	0.25 ± 0.03
Coefficient of capillarity (g m^{-2} $s^{-0,5}$)	0.16 ± 0.03	0.24 ± 0.03
Hg porosimetry		
Open porosity (%)	1.60 ± 0.76	2.49 ± 0.97
Apparent density (g cm^{-3})	2.74 ± 0.01	2.76 ± 0.01
Bulk density (g cm^{-3})	2.69 ± 0.03	2.68 ± 0.03
Ar adsorption		
Surface area (m^2/g)	0.0979 ± 0.0056	0.3787 ± 0.0668
Total pore volume (cm^3/g)	0.00011 ± 0.00001	0.00034 ± 0.00010
Average pore diameter (nm)	2.093 ± 0.021	2.114 ± 0.002
Ultrasound velocity measurements		
V_1/(km/s)	5.20 ± 0.17	4.95 ± 0.25
V_2/(km/s)	5.04 ± 0.09	4.76 ± 0.22
V_3/(km/s)	4.94 ± 0.14	4.41 ± 0.03
ΔM/%	3.50 ± 1.44	9.06 ± 3.72
Δm/%	3.10 ± 2.25	7.99 ± 3.85

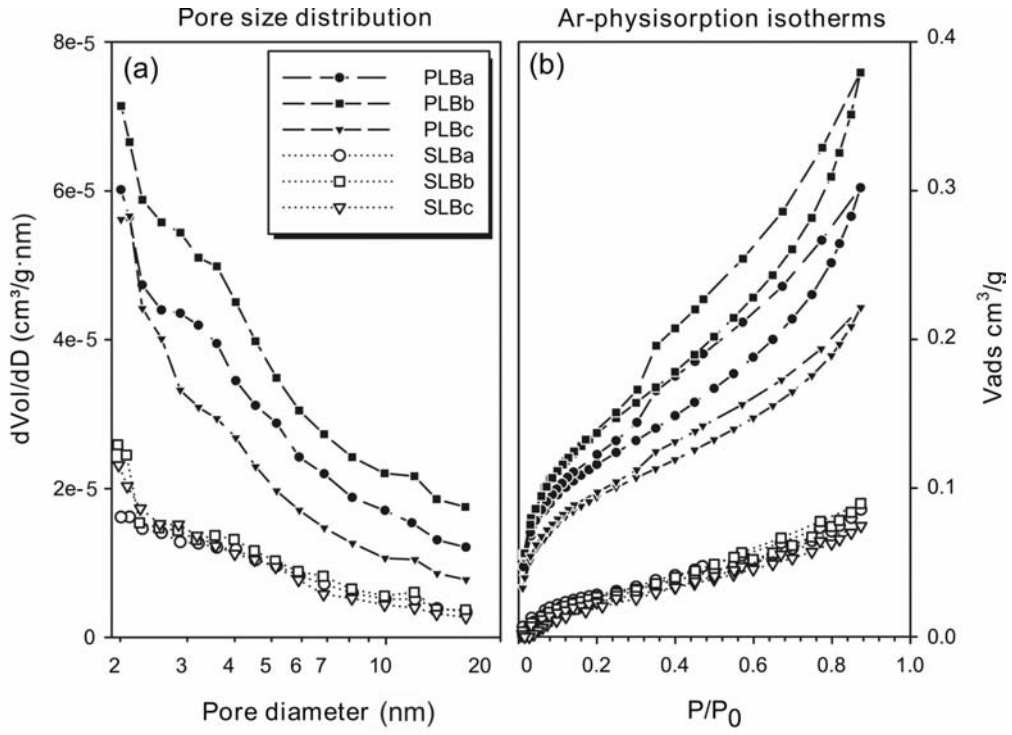

Figure 3. Results of BET measurements. (a) The volume of pores accessible to BET is significant higher for the light red lithotype than for the dark grey lithotype. (b) The Ar-physisorption isotherms for both lithotypes.

crystallization pressure. Table 3 shows that the light red lithotype has, in general, a higher BET surface area, as well as a higher average pore size, than the dark grey lithotype. The differences in pore size distribution between the two lithotypes can be seen in Figure 3a. The volume of pores accessible to gas is larger and much more variable in the case of the light red lithotype. Similarly to previous results, the higher BET surface area in the light red lithotype is the result of the presence of discontinuities filled with clay minerals. Furthermore, the Ar-physisorption isotherm is steeper, and indicates a more complex and variable pore system in the case of the samples of the light red lithotype (see Figure 3b). To the contrary, the samples of the dark grey lithotype are very homogeneous in terms of their pore size distribution (Figure 3a), as well as the complexity of the pore system network (Figure 3b). All studied samples have a physisorption isotherm of type II, which is characteristic for non-porous or macroporous materials,[27] which is confirmed by the very low surface

area in both lithotypes (Table 3). Furthermore, in the case of the samples of the light red lithotype, a H3 type of hysteresis loop can be recognised, with non-limited adsorption at high relative pressures and with forced closure of the hysteresis loop in the desorption branch around relative pressure of 0.4. Such a type of hysteresis loop is characteristic for materials with slit-shaped pores.[35]

Ultrasonic measurements can be used indirectly to define textural properties and, therefore, also physical-mechanical properties.[32] The results of the ultrasonic velocity measurements are listed in Table 3. Samples of the dark grey lithotype revealed faster ultrasonic wave propagation, indicating greater compactness and higher mechanical resistance when compared with the light red lithotype. Furthermore, the total structural anisotropy (ΔM) and relative structural anisotropy (Δm) are lower in the case of the dark grey lithotype, suggesting its higher compactness. On the contrary, the anisotropy is higher in case of the light red lithotype, as it is more heterogenous due to the more frequent appearance of discontinuities. An increase in the anisotropy of the samples is observed in case of the occurrence of bigger piles or veins of coarse-grained dolomite, calcitic veins, fissures and stylolithes in the samples. The values are in accordance with the obtained values of the porosity, as porosity decreases exponentially with velocity. Water transfer properties are directly linked to the pore network. The higher porosity and the high imbibition coefficient in the light red lithotype imply that water moves easily, and that the water transfer induces various physical-chemical reactions that eventually lead to deterioration of investigated limestone.

Limestone deterioration

Weathering forms on monuments

Within the framework of broader conservation - restoration projects, in situ investigations of the monuments by means of monument mapping was pointed out several types of deterioration phenomena. The studied limestone deteriorates extensively when subjected to either an outdoor or an indoor environment. A wide range of different weathering forms, documented according to the Fitzner classification [36] was observed. Crumbling, flaking and black crust are present on the limestone parts of the outdoor monument, whereas flaking, subflorescence, crumbling, white crust and efflorescence are present on the indoor monument. Examples of weathering forms are shown in Figure 1c and Figure 1d.

Weathering products and mechanisms

X-ray diffraction data (Table 1), supported by the results of SEM-EDS examinations, have shown that soluble salts are the main weathering products. Almost all weathering forms are re-

lated to salt crystallization, as seen in Figure 3.

The black crusts outdoor, as well the white crusts indoor, were composed of gypsum. The crusts are generally formed by less soluble salts, as gypsum.[37] The black crusts consists of gypsum crystals up to 100 μm in size, which are oriented parallel to the surface (Figures 4a, 4b and 4c). In some places individual calcite grains are enclosed in the gypsum crystals. Ba-rich (Figure 4d) or Fe-rich aerosols have been documented between the gypsum crystals of the crust, pointing to the effect of air pollutants. The boundary between the gypsum and the limestone is extremely irregular, showing progressive chemical dissolution of the calcite grains. Some of the white crusts occurring under indoor conditions (Figure 4e, with a thickness of 30 μm to 200 μm) show several alternating layers of columnar crystals. This suggests rhythmic fluctuations in the solution supply. Moreover, the salt crystals of gypsum are oriented perpendicularly to the surface of the limestone. Although the origin and growth of the sulphated crusts have been widely studied in the past,[38–43] literature data are still not uniform either the crust formation is actually a deleterious process, as rainwater arrives at the boundaries between the gypsum and the limestone where transformation of the calcite into gypsum occurs or that gypsum formation result in passivation on the surface of limestone, which might prevent further deterioration.

Salt crystallization under the surface (subflorescence) or within the pores resulted in disruption of the limestone (Figure 4f), expressed as flaking and crumbling of the limestone under both outdoor and indoor conditions. As the crystals exceed the size of the original pores, pressures strong enough to disrupt the fabric are built up by the growing crystals. These flakes are about 200 μm wide, and around 50 μm thick. The system of fissures is present 100 μm to 150 μm beneath the surface, whereas the fissures are 20 μm to 30 μm thick. Apparently, in some cases gypsum crystals nucleate in veins of clay minerals, as can be seen in Figure 4g, which are more accessible to porous flow. As salts concentrate in those parts which retain moisture longer, the swelling clay minerals enhance the salt-related breakdown. Moreover, the cyclic swelling and shrinking of clay contribute to the additional delamination of the limestone.[9, 44] Flaking of the limestone is not merely concentrated to the areas of clay-rich veins, as subflorescence in limestone occurs when the capillary flux is slower than the evaporation flux.[45] Water transfer is, due to the low porosity of the limestone, decreased, resulting in higher evaporation from the limestone surface with regard to the velocity of the capillary

flux. Thus, this zone is mechanically stressed, leading to disrupture of the limestone.

Efflorescences (Figures 4h and 4i) are composed of magnesium sulphate hydrates (hexahydrite, pentahydrite), gypsum and nitre, as proved by X-ray powder diffraction and SEM-EDS observations. Three different mineral assemblages have been observed in the efflorescences: (1) nitre and gypsum, (2) nitre, gypsum and magnesium sulphate hydrates, or (3) gypsum and

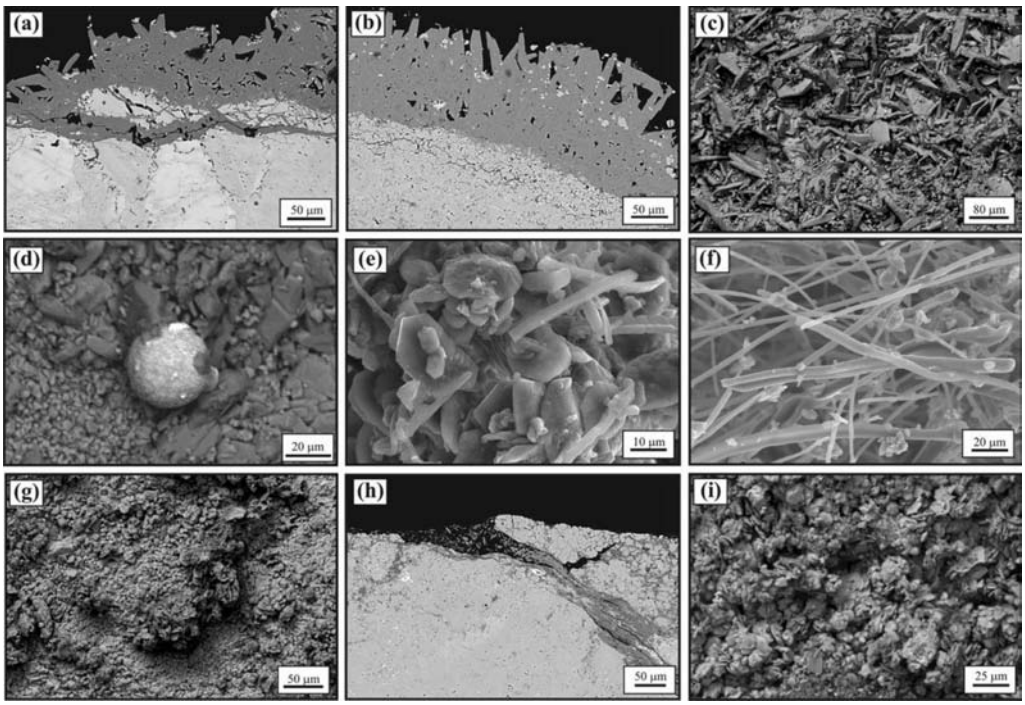

Figure 4. Microimages of deterioration patterns of the studied limestone. (a) Dissolution of calcite crystals under the gypsum crust, outdoors. On samples taken outdoors the dissolution of sparitic crystals under the gypsum crust is clearly evident. (b) Dissolution and disintegration of calcite crystals under the gypsum crust. Entrapped calcite grains in the crusts, outdoors. (c) Crystals of gypsum at the surface of the black crusts. d) A Ba-rich aerosol, entrapped between the gypsum crystals. (e) A white crust with gypsum crystals. (f) Gypsum filling the pores of the limestone leading to flaking of the limestone. (g) Gypsum crystallization in a vein of clay, which leads to flaking of the limestone, indoors. (h) Platy crystals of gypsum and elongated crystals of magnesium sulphate hydrates, indoors. (i) Fibrous crystals of nitre and platy crystals of gypsum, outdoors.

magnesium sulphate hydrates. Efflorescences appear as very loosely coherent aggregates of long hair-like needles and fibres (whisker growth), suggesting low supersaturation and a slightly humid to nearly dry surface substrate, where crystals grow on a solution film into the air.[46] Magnesium sulphates hydrates and nitre occur only on the surface of the limestone exposed to the indoor environment, due to their high solubility, whereas in the case of outdoor conditions they are not present. It has to be considered that the behaviour of multi component salt mixtures is extremely complex. It has been reported that, in normal outdoor environmental conditions, most salt remains in solution, except the rather insoluble gypsum that crystallizes out of the solution first.[4, 47] With the exception of hexahydrite–epsomite, transformations between the various species of the $MgSO_4 \times nH_2O$ series involve more than the simple removal of water: they require significant rearrangement of the crystal structure and the overcoming of activation energy barriers. Close to room temperature epsomite is the stable form in the presence of liquid water. Under dry conditions epsomite can dehydrate to form hexahydrite, and finally monohydrate kieserite.[48] The salt species that grow in efflorescences depend on the composition of the salt solution, on the properties of the substrate and on the environmental conditions during growth.[49] As joint mortars between the stone elements of the altar contain high quantities of soluble calcium and magnesium, are thus considered as potential source of these damaging salts. The contribution of nitre is significant in the samples taken from the stone elements at the bottom of the altar. The presence of nitre in those parts of the stone where there is a high capillary rise can be attributed to the solutions containing alkali potassium and nitrate that are present in the ground[50] or, alternatively, to the result of weathering due to K-bearing phyllosilicates.

Conclusions

The two lithotypes differ in their chemical composition and consequently in their mineralogy. Hence the other properties which are related to the mineral composition and their occurrence in the limestone also differ. The higher content of phyllosilicates is a remarkable feature of the light red lithotype. The porosity and values of the water transfer kinetics are very low for both lithotype, but they are slightly higher in the light red lithotype. The volume of pores accessible to gas is higher and much more variable for the light red lithotype, too. Furthermore, the Ar-physisorption isotherm is steeper and indicates a more complex and variable pore system of the light red lithotype. There were measurable differences in the USV measurements between the two lithotypes, showing higher anisotropy in the light red lithoytpe.

Limestone was found to be extensively deteriorated in both outdoor and indoor environments in the studied historical monuments, showing flaking, subflorescence, efflorescences, crumbling, and black and white crusts as deterioration phenomena. The results revealed that crystallization of soluble salts is the main weathering mechanism. Due to changeable environmental conditions, the soluble salts occurred in different varieties. Gypsum occurs as a compact crust, efflorescence and subflorescence, whereas magnesium sulphate hydrates and nitre crystallize only as efflorescence. Crystallization of gypsum under the surface resulted in flaking of the limestone. Furthermore, the presence of clay is also one of the main factors responsible for limestone deterioration, as a differential decay concentrated within the clay-rich planes resulting in the crumbling and formation of flakes.

The results presented here show that Lesno Brdo limestone, although compact, is relatively prone to deterioration. The presence of phyllosilicates indicates higher porosity and a higher imbibition coefficient than in the case of limestone not containing phyllosilicates, implying that, in the investigated limestone, water can move relatively easily, inducing physical-chemical reactions leading to its deterioration. The observed condition of the investigated historical monuments indicates that the presence of salts can be deleterious even to compact stone.

Acknowledgements

This research has been supported financially by the Slovenian Research Agency, under contract number 3211-05-000545. M. Urosevic received support in the form of a fellowship from the Spanish Ministry of Science (AP2006-036). Experimental support was provided by the Institute of Mineralogy and Crystallography, University in Vienna, and is hereby gratefully acknowledged. The authors also are grateful to Jože Drešar for performing the necessary sampling works on the selected monuments. Many thanks are due to José Alberto Padrón Navarta, for his helpful comments, and to Peter Sheppard for help with the editing of the text. The photographs shown in Figure 1a, 1b and 1 c are included by kind permission of Valentin Benedik.

References

[1] Warke, P. A., McKinley, J., Smith, B. J. (2006): Weathering of building stone: approaches to assessment, prediction and modelling. In: Kourkoulis S. K. editor. Fracture and Failure of Natural Building Stones. Springer, p. 313–327.

[2] Rodríguez-Navarro, C. E., Hansen, E., Sebastian, E., Ginell, W. S. (1997): The role of clays in the decay of ancient Egyptian limestone sculptures. *Journal of the Institute of American Conservators*, 36 (2), 151–163.

[3] Sebastián, E., Cultrone, G., Benavente, D., Linares Fernández, L., Elert, K., Rodríguez Navarro, C. (2008): Swelling damage in clay-rich sandstones used in the church of San Mateo in Tarifa (Spain). *Journal of Cultural Heritage*, 9, 66-76.

[4] Charola, E. A. (2000). Salts in the deterioration of porous materials: an overview. *Journal of the Institute of American Conservators*, 39, 327–343.

[5] Doehne, E. (2002): *Salt weathering: a selective review.* In: Siegesmund S, Weiss T, Vollbrecht A. editors. Natural stone, weathering phenomena, conservation strategies and case studies. Geological Society. London. Special Publication 205, p. 51–64.

[6] Colston, B. J, Watt, D. S, Munro, H. L.: Environmentally-induced stone decay: the cumulative effects of crystallization-hydration cycles on a Lincolnshire oopelsparite limestone. Journal of Cultural Heritage 2001; 4; 297–307.

[7] Selwitz, C., Doehne, E. (2002): The evaluation of crystallization modifiers for controlling salt damage to limestone. *Journal of Cultural Heritage*, 3, 205–216.

[8] Benavente, D., Garcià del Cura, M. A., Fort, R., Ordóñez, S. (2004): Durability estimation of porous building stones from pores structures and strength. *Engineering Geology*, 74, 113–127.

[9] Ruiz-Agudo, E., Mees, F., Jacobs, P., Rodriguez-Navarro, C. E. (2007): The role of saline solution properties on porous limestone salt weathering by magnesium and sodium sulfates. *Environmental Geology*, 52, 269–281.

[10] Cultrone, G., Russo L. G., Calabrò, C., Uroševič, M., Pezzino, A. (2008): Influence of pore system characteristics on limestone vulnerability: a laboratory study. *Environmental Geology*, 54, 1271–1281.

[11] Cardell, C., Benavente, D., Rodríguez-Gordillo, J. (2008): Weathering of limestone building material by mixed sulfate solutions. Characterization of stone microstructure, reaction products and decay forms. *Materials Characterization,* 59, 1371–1385.

[12] Tuğrul, A., Zarif, I. H.(1999): Research on limestone decay in a polluting environment, Istanbul-Turkey. *Environmental Geology,* 38, 149–158.

[13] Maravelaki-Kalaitzaki, P., Biscontin, G. (1999) Origin, characteristics and morphology of weathering crusts on Istria stone in Venice. *Atmospheric Environment*, 33, 1699–1709.

[14] Fitzner, B., Heinrichs, K., La Bouchardiere, D. (2002): Limestone weathering of historical monuments in Cairo, Egypt. In: Siegesmund S, Weiss T, Vollbrecht A, editors. Natural stone, weathering phenomena, conservation strategies and case studies. Geological Society; Special Publication 205, p. 217–239.

[15] Smith, B. J., Török, Á., McAlister, J.

J., Megarry, Y. (2003): Observations on the factors influencing stability of building stones following contour scaling: a case study of oolithic milestones from Budapest, Hungary. *Building and Environment*, 38, 1173–1183.

[16] Cardell, C., Celalieux, F., Roumpopoulos, K., Moropoulou, A., Auger, F., Van Grieken, R. (2003): Salt induced decay in calcareous stone monuments and buildings in a marine environment in SW France. *Construction and Building Materials*, 17, 165–179.

[17] Beck, K., Rozenbaum, O., Al-Mukhtar, M., Plançon, A. (2004): *Multiscale characterization of monument limestones.* In: Aires-Barros L, Zezza F, Editors. Proceedings of the 6th International Symposium on the conservation of Monuments in the Mediterranean Basin. Lisbon, p. 229–232.

[18] Sahlin, T., Malaga-Starzec, K., Stigh, J., Schouenborg, B. (2000): *Physical properties and durability of fresh and impregnated limestone and sandstone from central Sweden used for thin stone flooring and cladding.* In: Fassina V, editor. Proceedings of 9th International congress on deterioration and conservation of stone. Venice, p. 181–186.

[19] Nicholson, D. T. (2001): Pores properties as indicators of breakdown mechanisms in experimentally weathered limestones. *Earth Surface Processes and Landforms*, 26; 819–838.

[20] Török, Á. (2006): Influence of fabric on the physical properties of limestones, In: Kourkoulis S. K. editor. *Fracture and failure of Natural Building stones*, p. 487–495.

[21] Marszałek, M. (2007). *The mineralogical and chemical methods in investigations of decay of the Devonian Black »marble« from Dębnik (Southern Poland)*. In: Přikryl R, Smith B.J. editors. Building Stone Decay: From Diagnosis to Conservation. Geological Society. Special Publications 271, p. 109–115.

[22] Lindqvist, J. E., Malaga, K., Middendorf, B., Savukoski, M., Pétursson, P.: Frost resistance of Natural stone, the importance of micro- and nano-porosity, Geological Survey of Sweden External research project report, published online at: http://www.sgu.se/dokument/fou_extern/Lindqvist-et-al_2007.pdf.

[23] Mirtič, B., Mladenović, A., Ramovš, A., Senegačnik, A., Vesel, J., Vižintin, N. (1999): Slovenski naravni kamen. Geological Survey of Slovenia; Ljubljana; 1999.

[24] Ramovš, A. (2000): Podpeški in črni ter pisani lesnobrdski apnenec skozi čas. Mineral; Ljubljana.

[25] Jarc, S. (2000): Vrednotenje kemične in mineralne sestave apnencev kot naravnega kamna, Master Thesis, University of Ljubljana, Faculty of Natural Sciences and Engineering, Department of Geology, Ljubljana.

[26] RILEM, Recommended tests to measure the deterioration of stone and to assess the effectiveness of treatment

methods. Materials and Structures 1980; 14; 175–253.

[27] Sing, K. S. W., Everett, D. H., Haul, R. A. W., Moscou, L., Pierotti, R. A., Rouquérol, J., Siemieniewska, T. (1985): Reporting Physisorption Data for Gas/Solid Systems. Pure Applied Chemistry (IUPAC), 57, 603–619.

[28] Gregg, S. J., Sing, K. S. W. (1982): Adsorption Surface Area and Porosity. Academic Press; London.

[29] Adamson, A.W., Gast, A. P. (1997): Physical Chemistry of Surfaces. J.Wiley & Sons; New York.

[30] Barret, E. P., Joyner, L. G., Halenda, P. P. (1951): The Determination of Pore Volume and Area Distributions in Porous Substances. I. Computations from Nitrogen Isotherms, *Journal of the American Chemical Society*, 73, 373–380.

[31] Guydader, J., Denis, J. A. (1986): Propagation des ondes dans les roches anisotropes sous contrainte évaluation de la qualité des schistes ardoisiers. *Bulletin of the Engineering Geology*, 33, 49–55.

[32] Bourgès, A. (2006): Holistic correlation of physical and mechanical properties of selected natural stones for assessing durability and weathering. Ph. D. Thesis. München.

[33] Steiger, M. (2005): Crystal growth in porous materials II: Influence of crystal size on the crystallization pressure. *Journal of Crystal Growth*, 282, 470–481.

[34] Scherer, G. W. (1999): Crystallization in pores. *Cement and Concrete Research*, 29, 1347–1358.

[35] Lowell, S., Shields, J. E., Thomas, M. A., Thommes, M. (2004): Characterization of porous solids and powders: surface area, pore size and density. Springer.

[36] Fitzner, B., Heinrichs, K. (2002): *Damage diagnosis on stone monuments-weathering forms, damage categories and damage indices*. In: Prikryl R, Viles HA editors. Understanding and managing stone decay, Proceeding of the International Conference "Stone weathering and atmospheric pollution network (SWAPNET 2001)". Charles University in Prague. The Karolinum Press, p. 11–56.

[37] Arnold, A., Kueng, A. (1985): Crystallization and habits of salt efflorescences on walls, I., Methods of investigation and habits. In: Felix G, editor. Proceedings of the Fifth International Congress on the Deterioration and Conservation of Stone, Laussane: Presses Polytechniques Remandes, p. 255–67.

[38] Camuffo, D., Del Monte, M., Sabbioni, C. (1983): Origin and growth mechanisms of the sulphated crusts on urban limestone. *Water, Air, and Soil Pollution*, 19; 351–359.

[39] Ausset, P., Lefèvre, R. A. (2000): Early mechanisms of development of sulfated black crusts on carbonate stone. In: Fassina V, editor. Proceedings of the 9th International Congress on Deterioration and Conservation of Stone. Venice, p. 265–273.

[40] Gaviño, M., Hermosin, B., Verges-Belmin, V., Nowik, W., Saiz-Jimen-

EZ, C. C. (2004): Composition of the black crusts from the Saint Denis Basilica, France, as revealed by gas chromatographymass pectroscopy. *Journal of Separation Science*, 27; 513–523.

[41] POTGIETER-VERMAAK, S. S., GODOI, R. H. M., VAN GRIEKEN, R., POTGIETER, J. H., OUJJA, M., CATILLEJO, M. (2005): Micro-structural characterization of black crusts and laser cleaning of building stones by micro-Raman and SEM techniques. *Spectrochimica Acta. Part A*, 61, 2460–2467.

[42] VAZQUES-CALVO, C., ALVAREZ DE BUERGO, M., FORT, R., VARASS, M. J. (2007): Characterization of patinas by means of microscopic techniques. *Materials Characterization*, 58, 1119–1132.

[43] ANTILL, S. J., VILES, H. A. (2003): Examples of the use of computer simulation as a tool for stone weathering research. Building and Environment, 38, 1243–1250.

[44] RODRIGUEZ-NAVARRO, C., SEBASTIAN, E., DOEHNE, E., GINELL, W. S. (1998): The role of sepiolite-palygorskite in the decay of ancient Egyptian limestone sculptures. *Clays and Clay Minerals*, 46 (4), 414–422.

[45] LEWIN, S. Z. (1982): The Mechanism of Masonry Decay through Crystallization. In: Baer NS, editor. Conservation of Historic Stone Buildings and Monuments. National Academic Press; Washington DC, p. 120–144.

[46] ZEHNDER, K., ARNOLD, A. (1989): Crystal growth in salt efflorescence, *Journal of Crystal Growth*, 8, 513-521.

[47] CHAROLA, E. A., PÜHRINGER, J., STEIGER, M. (2007): Gypsum: a review of its role in the deterioration of building materials. Environmental Geology, 52, 339–352.

[48] JULING, H., KIRCHNER, D., BRÜGGERHOF, S., LINNOW, K., STEIGER, M., EL JARAD, A., GÜLKER, G. (2000), In: Kwiatkowski D, Löfvendahl R, editors. Proceedings of the 10th International Congress on the Deterioration and Conservation of Stone, ICOMOS, Stockholm, p. 187–194.

[49] BLÄUER BÖHM, C., KÜNG, A., ZEHNDER, K. (2001): Salt Crystal Intergrowth in Efflorescence on Historic Buildings, *Chimia 2001*, 55, 996–1001.

[50] CAMPOS-SUÑOL, M. J., DOMÍNGUEZ - VIDAL, A., AYORA-CAÑADA, M. J., DE LA TORRE-LÓPEZ, M. J. Renaissance patinas in Ubeda (Spain): mineralogic, petrographic and spectroscopic study, *Analytical and Bioanalytical Chemistry*, 391, 1039–1048.

Geological evaluation of brown coal reserves at the Hrastnik mine – RTH, Rudnik Trbovlje-Hrastnik

Geološka evalvacija zalog rjavega premoga na območju jame Hrastnik - RTH, Rudnik Trbovlje-Hrastnik

Željko Vukelič[1,*], Bojan Klenovšek[2], Ladislav Placer[1], Vladimir Malenković[3], Evgen Dervarič[1]

[1]University of Ljubljana, Faculty of Natural Sciences and Engineering, Aškerčeva 12, SI-1000 Ljubljana, Slovenia
[2]RTH, Rudnik Trbovlje – Hrastnik, d. o. o., Trg revolucije 12, SI-1420 Trbovlje, Slovenia
HTZ, I.P., d. o. o., Partizanska 78, 3320 Velenje, Slovenia

*Corresponding author. E-mail: zeljko.vukelic@ntf.uni-lj.si

Received: June 3, 2009 **Accepted:** December 14, 2009

Abstract: As provided by the Act on the gradual closing down of the coalmine Trbovlje-Hrastnik and on the development restructuring of the region, until the end of 2009 Rudnik Trbovlje-Hrastnik (RTH) will continue to supply coal to the thermal power plant Termoelektrarna Trbovlje (TET) in the planned annual volume of 0.6 million tonne. RTH continues to hold significant coal reserves of national importance to Slovenia, which might we worth exploiting at some point in the future. The management of the coalmine has made every effort to ensure continued coalmining at RTH after 2009 at the existing mines Ojstro and Trbovlje (Field III and Field Plesko), at the already closed down mine Hrastnik. This paper provides an overview of the results of the study "The Legitimacy of the Extraction of Remaining Coal Deposits at the Mines Ojstro and Trbovlje After 2009" – Stages 2 and 3, with the emphasis on the evaluation of coal deposits at the mine Hrastnik. The study was undertaken by the Faculty of Natural Sciences and Engineering, Ljubljana, in collaboration with the Economics Institute at the Faculty of Law, Ljubljana, and RTH associates.

Original scientific paper

Izvleček: Rudnik Trbovlje-Hrastnik (RTH) bo skladno z zakonom o postopnem zapiranju in razvojnem prestrukturiranju regije do vključno leta 2009 dobavljal premog Termoelektrarni Trbovlje (TET) v predvideni količini 0,6 mio. ton na leto. RTH še vedno razpolaga z znatnimi in za Slovenijo pomembnimi zalogami premoga, ki jih bo treba v prihodnje smiselno izkoristiti. Vodstvo rudnika si prizadeva, da bi eksploatacijo premoga v RTH nadaljevali tudi po letu 2009, in sicer iz že obstoječih jam Ojstro in Trbovlje (III. polje in Plesko polje) ter iz že zaprte jame Hrastnik. V tem prispevku so predstavljeni rezultati študije: »Upravičenost odkopavanja preostalih zalog premoga v jamah Ojstro in Trbovlje po letu 2009« – 2. in 3. faza, s poudarkom na evalvaciji zalog premoga v jami Hrastnik. Študijo je izdelala Naravoslovnotehniška fakulteta v Ljubljani v sodelovanju z Ekonomskim inštitutom pri Pravni fakulteti v Ljubljani in s sodelavci naročnika RTH.

Key words: brown coal, coal reserves, geological evaluation, research drilling
Ključne besede: rjavi premog, rezerve premoga, geološka evalvacija, raziskovalno vrtanje

Introduction

The geological evaluation of the remaining deposits of brown coal at Hrastnik focused on reviewing the updated brief on the categorisation, classification and calculation of the resources and deposits of brown coal in the RTH mining area as at 31st December 2002 (Mitrevski & Bravec, 2003). It includes the evaluation of the level of observance of geological exploration of the coal deposit using drill holes and the level of observance of results of structural and geological analyses of the Hrastnik coal deposit creation and development from the period of intensive geological explorations between the years 1982 and 1991. In accordance with the Act Regulating Gradual Closure of the Trbovlje-Hrastnik Mine (RTH) and Development Restructuring of the Region (2000), the closing of underground mining facilities began even before some hypotheses on geological structure and coal reserves had been verified. Considering the reassessment of the structural and geological model used in the updated brief on coal reserves as at 31st December 2002, the geological evaluation will give a general assessment of the relevance of further plans for additional geological

exploration and indicate the most optimal direction and level of further exploration, which might result in later preparation of an exploration plan for the new categorisation, classification and calculation of the resources and deposits of brown coal in the Hrastnik area and an assessment of a repeated beginning of brown coal exploitation in this traditionally mining area.

Geological exploration of the coal deposit in the Hrastnik area

Apart from the associates employed by the coalmine's geological department to monitor the preliminary works and surveys carried out at the coalmine on an ongoing basis, vital research over the past fifty years was undertaken by Kuščer (1967) with his core work Zagorje Tertiary, Gregorač (1975) who focused on the hydrogeology of the mine Hrastnik, Kuščer & Mitrevski (1979) who researched the geology of the boundary area between the mines Hrastnik and Dol, Uhan (1991) with his work on the geochemical properties of coal in the central part of the deposit, and Placer who carried out a structural-geological analysis between 1982 and 1991. In the above mentioned period Placer completed an extensive detailed geological mapping of the surface area between Moravče and Laško, and surveyed and mapped the mine facilities and the cores of exploration drill holes. Placer published the major findings of the survey and mapping of the surface area over the mines Hrastnik and Dol in 1987 in the brief "A Geological Structure Survey in the Dol-Hrastnik Area, Part II". In the three-year period (1985–1987), geologists surveyed roughly 3,200 metres of roadways, access tunnels and longwalls, and drilled eleven structural exploration drill holes in the total length of approximately 1,500 m (Uhan, 1987). The geological data obtained in the course of the above mentioned surveying and mapping of mine facilities and exploration drill holes yielded more detailed information on the structure of the "south wing" of the central part of the Hrastnik mine at and under Horizon VII. Building on the results of all previous surveys and having reviewed and processed the entire documentation held by the coalmine, Placer preformed the most comprehensive structural geological analysis until that time, and explained the tectonic development of the coal deposit. When it comes to the evaluation of remaining coal reserves in the Hrastnik area, certain structural geological questions remain unanswered; this primarily refers to the continuation of the coal seam under the hypothetical Hrastnik thrust fault. The other set of debatable questions concern the geological structure of the Eastern Underground Deposit where the continuation of the southern coal seam downwards has been established by exploratory drill holes at Brnica.

Geological structure of the Hrastnik coal deposit

The Zasavje coal-rich tertiary layers (the so-called "Trbovlje layers) sedimented on the Triassic dolomite or pseudozilian slate substrata are composed of lower clastic, predominantly clay, footwall layers, coal and upper, hanging wall marl layers.

The sedimentation of the lower segment of the coal-rich layers begins with clastic sediments in paleo-morphologic depressions. Due to filling of the paleo-relief, the thickness of these predominantly clay layers is highly variable, amounting up to 80 m. The upper parts of footwall clay are rich in organic component, and the black clay (the so-called "black footwall") gradually passes into clay coal.

The coal layer in the sedimented thickness of 20–25 m, which can be thinner or thicker due to tectonic repetitions in the form of scales and different inclinations in individual cross-sections, is characterised by the lower part containing more clay, and the upper, cleaner part containing more vitrinite substance. In the medium part, there appear centimetre- and decimetre-thick inserts of volcanic ash, clay and, most often, lime sandstone. With the increasing depth, there occurs an increasing number of decimetre-thick layers of lime sandstone or so-called carbonate inserts, which have, at the point +70 and the descending angle 45–70° southwards, achieved the total thickness even exceeding width across 15 m of the long wall at the field A between the ordinates 4550 and 4800 (Figure 1).

The lower part of coal layer was sedimented in the reduction environment and is mineralised with sulphides. The upper semiterrestic and limnic part is predominantly mineralised with carbonates, and the edge areas of paleo peat bogs passing to the hanging wall marl, it is mineralized with sulphides

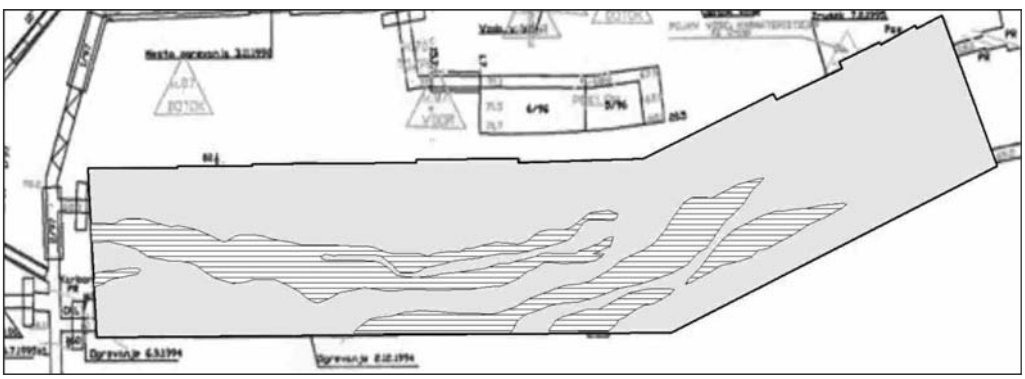

Figure 1. Carbonate layers (hatched) at point +70, Field A, mine Hrastnik

(Uhan, 1991). Depending on the type of mineralisation of final sedimentation sequence of the coal layer, its position in the former sedimentation bed could be presumed. Unfortunately, such explorations have not yet been performed for the Hrastnik coal deposit; however, some data is available on the ratio of mineralization types in the upper part of the coal layer in Trbovlje (Neža) and in the profile approximately 800 m to the east, in the Ojstro mine at the point +135, while some larger distance from the edge of the former sedimentation bed is presumed for the profile at Lopata (ordinates around 2950).

The upper border of the coal layer with the hanging wall marl is more distinctive than the lower one. Where the hanging wall marl contains abundant organic component beside coal, such layers were named "black hanging wall". In the upward direction, this brackish thin-layer marl gradually turns to brown and grey until it borders the Oligocene layers. Similarly to the footwall clay, the hanging wall marl also achieves thicknesses of approximately 80 m. In the marine environment, the Oligocene marine clay ("sivica" in Slovene) gradually sedimented above the hanging wall marl. It is characteristic for being massive, non-layered, marl-like and swellable. The average thickness of this clay sedimentation is 30 m to 50 m, or even more in some locations.

Discordantly on top of the Oligocene marine clay, the sedimentation of Laško layers composed of lithotamnic limestone, marl and sandstone begins in the area of the Hrastnik coal deposit without sandy Govce layers. The thickness of these sediments can measure 100 m or more. On top of the Laško layers, there are discordantly sedimented Sarmatian layers of various thicknesses: conglomerate, sandstone, siltstone and clay completing the sedimentation of the Zasavje tertiary bed.

The coal deposit is shows considerable tectonic deformation. The western part of the coal deposit is characteristic for relatively simple structure of the coal layer of the "southern part", but the eastern part passing into the thrust structure of the Eastern Underground Deposit is more complicated in structure.

In the western part of the coal deposit, an important factor for the estimation of reserves is the structure of the inclined, southwards leaning coal layer anticline. Its northern wing, including its core, is formed of inclined thrust scales that are often parallel to the axis plane of the fault. Tectonic deformations of such type are very rare in the southern wing of the anticline. They are presumed to be located only near the alleged Hrastnik thrust fault indicated by geological data from the drill hole Hj-2/75 and Hj-6/85 as well as the data

obtained in the course geological mapping of the western part of the drift at Horizon VII. The coal in the southern wing of the above mentioned anticline was explored, in the years 1985–87, by ten drill holes, three of which drilled through the tectonically deformed coal layer. The system of youngest tectonic deformations of the Hrastnik region, the Dinaric oriented (NW-SE) and cross-Dinaric oriented (NE-SW) faults is predominant in this area. Dinaric faults usually occur in intervals of 100 m to 150 m, occasionally less, and can be followed in the layout from the footwall to Laško and/or Sarmatian layers. Apparent strike slips along these faults can, in vertical N-S cross sections, exceed 40 m and thus strongly affect the continuity of the thickness of the coal layer under Horizon VII and VIII (Figure 2).

To the east of this location, the coal deposit structure is significantly more complicated, making the assessment of reserves a significantly more demanding task.

In relation with the passing of the Hrastnik structure into the Dol structure, tectonic deformations of the coal layer on the Blato anticline and the Dol syncline play an important role. In general, a steeper and tectonically thinner

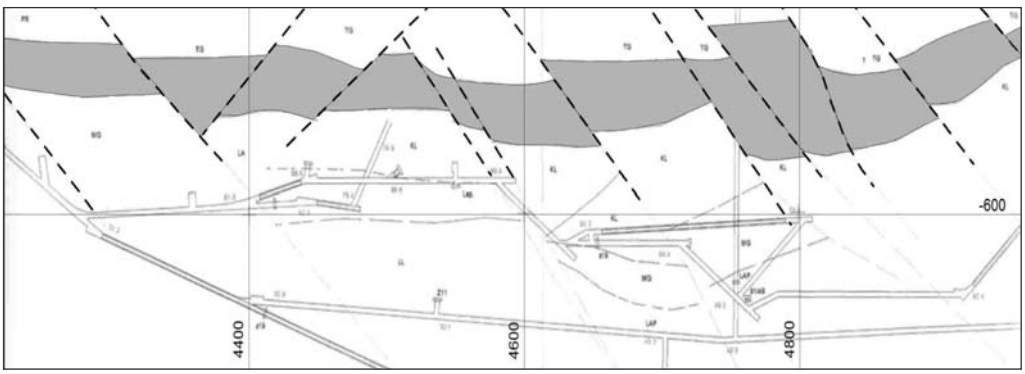

Figure 2. A structural geological prognosis of the coal seam in the southern part of the mine Hrastnik at Horizon VII

Table 1. Off-balance coal reserves at the mine Hrastnik according to the calculations provided in the updated brief on coal reserves as at 31st December 2002

Coal reserve categories	A	B	C_1	C_2	
Southern part	134 000	4 346 000	10 269 000	-	
Corner field	229 000	244 000	72 000	-	
Eastern Corner Field	77 000	455 000	2 378 000	6 272 000	
Total Hrastnik	440 000	5 045 000	12 719 000	6 272 000	24 476 000

coal layer is expected in this part of the coal deposit.

Geology-related problems in coal exploitation can be expected particularly in relation with tectonics-related thinning and discontinuities of the coal layer and increasingly thicker sedimented carbonate barren inserts in the coal layer.

Updated brief on coal reserves as at 31st December 2002

Update of the brief on the categorisation, classification and calculation of the resources and deposits of brown coal in the RTH mining area as at 31st December 2002 is based on the Brief on the coal reserves in the RTH mining area as at 31st December 1997. Changes in the assessment of reserves contained in the above mentioned update are related to the closure process based on the Act Regulating Gradual Closure of the Trbovlje-Hrastnik Mine and Development Restructuring of the Region (Official Gazette of the Republic of Slovenia, No. 61/2000). Within the framework of the 2002 update, all current coal reserves in the Hrastnik mine according to the 1997 brief were assessed as off-balance reserves in categories A, B, C_1 and C_2 (Table 1).

Based on the Rules on classifying the reserves of hard mineral substance in classes and types and on the records thereof (Official Gazette of the SFRY, No 53/79), the Hrastnik mine has been classified in the third group and second sub-group. Individual categories of reserves were calculated pursuant to the prism-method on the basis of parallel geological profiles north-south in the scale 1:2000. For the Hrastnik mine, the volume mass of 1.45 t/m^3 of coal was observed and 25-percent exploitation loss was taken over. When calculating the coal reserves in the Hrastnik mine between the ordinates 4050 and 5350, the occurrence of carbonate inserts in the coal layer, increasing with depth, was considered. The calculated coal reserves have therefore been reduced by 25 percent in this part of the mine. According to the indication in the brief as at 31st December 1997, the parameters of average quality of the reserves are the following: 20.71 percent of moist, 21.17 percent of ash, 2.38 percent of total sulphur and the calorific value of 14.78 MJ/kg of coal. In the coal samples obtained from structure drill holes during the last period of more extensive exploration drilling in the Hrastnik mining area, a slightly lower calorific value was assessed as well as ash contents higher by a few percent.

In the period from 31st December 1997 to the update of the brief on the categorisation, classification and calculation of the deposits as at 31st December 2002, 120 drill holes in total length of 3,421 m were drilled in the Hrastnik mine between the points +45 and 0; however,

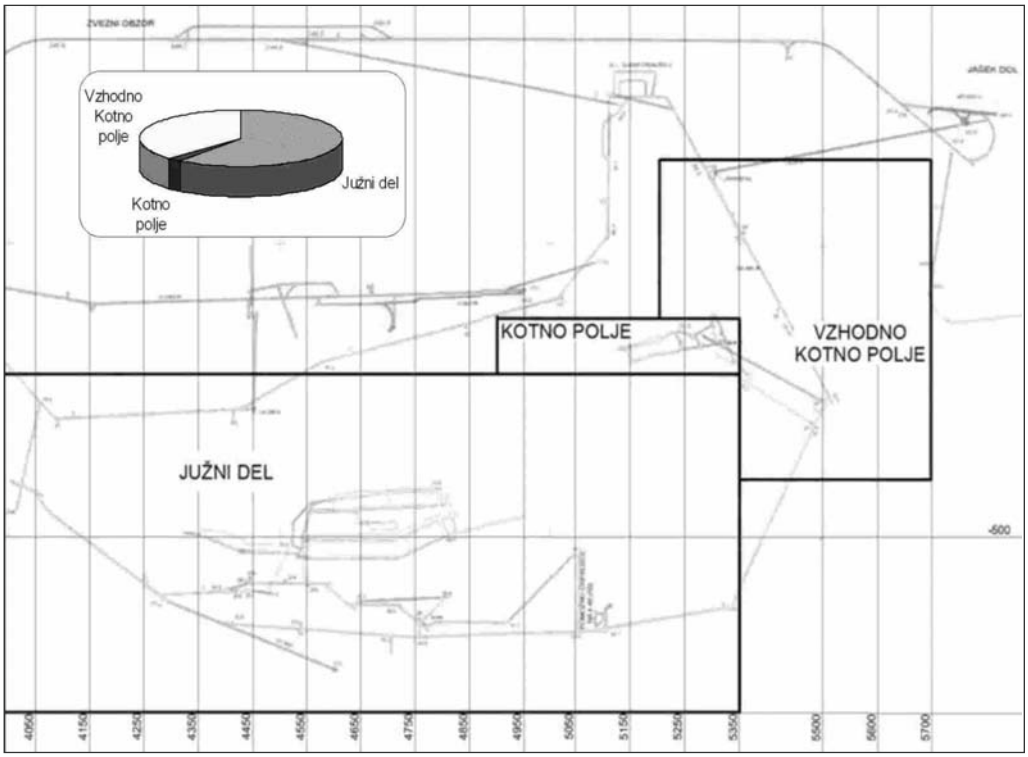

Figure 3. The main mine roadways at the coalmine Hrastnik and a sequence of geological cross-sections N-S used in the updated brief on remaining deposits (2002) for the purpose of determining actual reserves, and the share of deposits at the Southern End, Corner Field and Eastern Corner Field of the mine Hrastnik

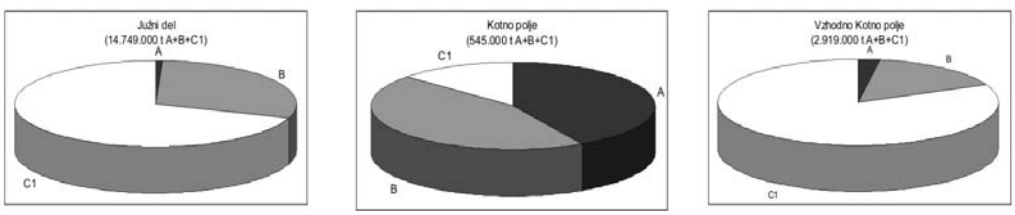

Figure 4. Coal deposits as at 31st December 2002 in the Southern End, Corner Field and Eastern Corner Field of the mine Hrastnik

the purpose of this drilling was predominantly to determine the boundary between coal and the adjacent rock mass to design exploitation levels. In the period between the years 1997 and 2002, there was no structural and geological

drilling, the results of which could influence the calculation of reserves.

The A+B+C_1 coal reserves in the Hrastnik mine (off-balance), the amount of which has not significantly changed since the end of the year 1997, represent precisely one third of the entire (both balance and off-balance) A+B+C1 coal reserves for RTH, the Trbovlje-Hrastnik mine (53,893,000 t). In addition, further sources of the C_2 category (6,272,000 t) have been recorded in the Eastern Corner Field in the mine Hrastnik (Figure 3).

The calculation of coal reserves in the Hrastnik area between the ordinates 3700 and 5350 is based predominantly on the data obtained from exploration mine drilling and mapping of mine roadways between the years 1985 and 1998 and from surface drilling holes in the Brnica area. The reliability level of this largest part of reserves in the Hrastnik mine is high. Exploration drilling for the purpose of recategorisation of C1 reserves to B reserves poses any risks here, but no significant changes in quantity are to be expected. More risk lies in exploration drilling for the purpose of determining the continuation of the coal layer beneath the alleged Hrastnik thrust fault where the cal reserves have not yet been recorded. The exploration risk is also increasing towards east where the coal reserves of the Eastern Corner Field to the ordinate 5700 have been determined on the basis of only a few drill holes and a strongly simplified structural geological model. From the ordinate 4900 towards east, the reliability of the estimation of coal reserves is considerably lower. Exploration drilling in this area could undoubtedly improve the categorisation, but due to current structural geological simplifications in the updated brief on reserves as at 31st December 2002, a reduction in quantity of currently recorded coal deposits and resources is not excluded.

Structural view on the extension of the coal seam in the Hrastnik mine beneath the exploitation level upon the closure of the mine

The opinion on the extension of the coal seam in the Hrastnik mine beneath the exploitation level upon the adoption of the act regulating a gradual beginning of closure of the mines Trbovlje and Hrastnik in the year 2000, was elaborated on the basis of the Preliminary analysis of the structure of Ojstro and Hrastnik (Placer, 1988). Additionally, it includes the data on the structure of the Laško syncline and the reconstruction of the coal deposit in Upper Oligocene (Placer, 1994) and two published articles, one on the structure of the Hrastnik coal deposit (Kuščer & Mitrevski, 1979) and one on the regional structure of the Posavje

folds (Placer, 1999). The last situation in the mine prior to its closure has been derived from the Update of the coal deposits and resources in the Hrastnik mine as at 31st December 2003 (Mitrevski & Bravec, 2003).

The Laško syncline

From the geological point of view, the Zasavje coal mines are situated in the Laško syncline, the upper part of which has been named the Laško tertiary depression with a productive coal seam. In the tectonic sense, the syncline is divided in three large structure blocks separated by the Jug and Hrastnik inclined strike slip fault. The Jug fault lies in the direction SW-NE and runs along the western edge of the coal deposit in Trbovlje and across the town. The Hrastnik fault lies in the direction NW-SE and runs through Hrastnik. The following mines are situated in individual structure blocks: Strahovlje, Loke, Kisovec, Zagorje-Kotredež and Orle in the western block, Trbovlje and Ojstro in the central block between the Jug and Hrastnik fault, and Hrastnik, Dol, Krištandol, Brezno, Huda jama and Mihael in the eastern block.

Local coordinate system

The Zasavje coal mines use the local coordinate system with the reference point at the height point 425.5 above the living quarter of Vode in Trbovlje. The productive area of the Hrastnik coal mine lies between the coordinates y = (+3500 and +5700), presumably extending to 5900 as evident form the projection in Figure 1, and x = (–700 and +200).

Structure of the Hrastnik coal deposit

The structure of the Hrastnik coal deposit is evident from the existing transverse profiles on the coordinate y (abscissa). However, there are two concepts regarding the conditions in the depth and in the eastern part where there is little or no mining activity. The first one was set by Kuščer and Mitrevski (1979) and the other one by Placer (1988). The substantial difference between them lies in three structural questions. The first one is related to the existence of the Hrastnik thrust fault introduced by Placer. According to Placer, the thrust is supposed to have cut off the coal seam, while according to Kuščer and Mitrevski, the coal seam extends in the depth direction. The second question refers to the difference in understanding the extension of the internal thrust panes towards east, and the third one is related to the interpretation of the connection between the Hrastnik and Dol structure, i.e. the relation between the Blato anticline and the Hrastnik and Dol structure.

The significance of different aspects lies in the fact that according to the concept by Kuščer & Mitrevski, the coal deposits and resources are larger than the deposits according to the concept by Plac-

er. The latter model is presented here. In the calculation of updated reserves of 31st December 2003 (Mitrevski in Bravec), the authors took into account the existence of the Hrastnik thrust, while the conditions relating to the second and third point of differences in concepts were as described by Kuščer & Mitrevski. The conditions in the border area between the Hrastnik and Dol structure are therefore strongly simplified and idealised, and probably even incorrect. The above applies to the area of profiles from y = (+5500 to +5700).

The brown coal seam in the area of the Hrastnik coal mine lies in the north-eastern wing of the Hrastnik fault which has cut through the originally uniform seam, separating it in the Ojstro and Hrastnik part. The economically most important part of the Hrastnik coal seam, the so-called main seam, with its medium-steep descent towards south and limited in the north by thrust faults in the direction W-E lying south to the Trbovlje normal fault in the same direction, representing the southern border of the Blato anticline, the core of which contains pseudozilian layers, and to its easternmost point, there lies a preserved, anticlinally sloped and heavily deformed coal seam, approximately 10 m thick and declining in the eastern direction. To the north of the Blato anticline, there lies the heavily compressed and deformed Dol syncline. The southern border of the main coal seam is formed by the Hrastnik thrust, running in the direction W-E. In the central part, the main coal seam is longitudinally cut by the internal thrust panel dividing the seam, which is uniform in the west, in two parts, the so-called "northern" seam and "southern" seam. In the economic sense, the "southern" seam is more significant. The internal thrust panel is sloped in the slip (non-flexive and unbent) anticline, with the crest descending approximately by 25 % in the eastern direction, forming at the same time the upper and the eastern boundary of the "southern" seam and, simultaneously, the lower boundary of the "northern" seam. Kuščer & Mitrevski described the sloped thrust panel as a "barren anticline". The "northern" seam is gradually reduced in the upward direction along one of the thrusts to the south of the Trbovlje fault.

The structure of the Hrastnik coalmine and the coal seam above Horizon VIII at the point +50 m is well known. At this point, coal is almost entirely excavated and the remaining part is well explored. Under this height point, the coal seam was drilled from the standing points at Horizons VII and VIII and from the surface. The level of exploration varies depending of the density of drills. It is higher in the west and lower in the east.

The presumed volume of the "southern" seam is shown in Figure 1, in the

seam projection to the vertical plane in the direction west - east, at the scale of 1 : 5,000. The surface (only in the western half of the projection) and the extension of old excavations are derived from the update of the brief on reserves (Mitrevski & Bravec, 2003). The same goes for the drill holes' drilling points. For the purpose of orientation, the level of Horizon 8 is drawn. The unexploited part of the "southern" seam can be relatively well traced from the transverse profile y = +4200 to the profile y = +5400, i.e. at the length of 1200 m and further to the profile y = +5650 where it has been established at the easternmost point by the drill hole Br. 10. This means that in the most favourable structural and lithological conditions, its length would amount to 1,460 m. In the profile y = +4200, the coal seam extends approximately from the point +90 m to approximately +60 m, and in the profile y = +5400 from approximately +60 m to approximately –220 m in the profile 5700 from approximately –110 m to approximately –290 m. Unlike the profiles y = +4100 in y = +4450, the location of the Hrastnik thrust in the profile y = +5700 has been determined according to interpolation between the drill holes Br. 13 and Br. 10, and therefore very inaccurate. A lower level of accuracy of the thrust's location also applies for the profiles y = +4950 and y = +5390. In the profile y = +5950, the drilling at the hole D 1 was halted in the hanging wall marl, therefore there is no data on the existence of a coal seam in the outermost part in the Hrastnik structure. The thickness of the "southern" seam amounts from 25 m to 40 m. The "width" of the seam on the vertical axis in the projected plane is not correct, it is actually longer by the ratio depending on the inclination of the seam. The value of the ratio to be multiplied with the measured width in the profile is indicated on the profile line for the individual profiles and amounts from 1.05 to 1.25. The western part of the profile reflects the actual situation, but in the eastern direction and in the depth direction, the accuracy level gradually falls lower. This particularly applies to the location of drill points with the coal seam and to the location of the internal thrust panel and the Hrastnik thrust.

According to interpretation as presented here, the "southern" seam is gradually reduced in the eastward direction. However, as it is evident from the following text, the conditions as predicted by Mitrevski & Bravec (2003) should also be taken into consideration.

The unexploited part of the "northern" *seam* can be traced in the mine from the profile y = +5000 to the profile y = +5500 where it has been drilled through by a drill hole from Horizon VIII. Further, towards east, it has only been extrapolated. In Figure 1, the "northern" seam is not shown, as it is

impossible to show its actual volume due to unclarified tectonics. The thickness of the seam amounts to 10 m to 15 m, only occasionally it reaches 20 m. The coal seam in the Blato anticline is not included in this presentation. The longitudinal projection in Figure 1 has been complemented by the orientation profile on the coordinate y = +5400 in Figure 2 at the scale 1 : 5,000 taken from the preliminary analysis of the structure of Ojstro and Hrastnik (Placer, 1988). It shows the structural relation between the "northern" and "southern" seam and the location of the internal thrust panel and the Hrastnik thrust.

The extension of the unexploited part of the coal seam has been determined by mapping of the Horizon VII and VIII of the Hrastnik mine and by drilling from the mine and the surface. Despite numerous data, the existence of all faults and thrusts limiting the coal seam has been determined with more or less probability, as despite everything, a different interpretation is always possible. The least data is available on the location of the Hrastnik thrust fault in the depth. All data sets except one are obtained from the surface drill holes ((Br.12, Br. 2, Br. 12, Br. 13). The only data set obtained from the mine is from the drill hole Hj 19 at Horizon VII in the profile 4350 drilling the coal and the Hrastnik thrust fault; However, this data is of high quality as it proves the coal thrust on the Laško layers, thus the Hrastnik thrust. The internal thrust panel separating the "northern" and the "southern" seam was determined according to the study of mine profiles, while its role was established according to the structural analysis of the deformation dynamics (Kuščer & Mitrevski, 1979; Placer, 1988).

The characteristics of the coal seam in the "northern" and "southern" seam differ from one another. Above all, the "northern" seam is thinner and tectonically much more affected than the "southern" one. Coal in the "northern" seam has been thrust and then horizontally shifted along vertical faults, resulting in formation of scales and thinner layer; both contacts, foot wall and hanging wall, are mostly abnormal and tectonised. The "southern" seam is considerably less damaged. It contains normally developed footwall and hanging wall contact. The barren inserts are less damaged than in the "northern" seam.

The discussion on conditions in the eastern part of the Hrastnik structure and/or on the structure model by Kuščer & Mitrevski on one side, and Placer on the other, is of great significance due to its relation with eventual planning of exploration works. The internal thrust panel occurs in the central part of the coal deposit; in the western part, the coal seam is merely flexurally

bent, and in the eastward direction, the flexure increases and is discontinued in the profile y = +5100. Further towards the east, the size of the discontinuation in the known part of the mine is increasing. The difference between both concepts lies in the prediction by Kuščer & Mitrevski for the eastward shift to gradually reduce again. Therefore, the "northern" and the "southern" seam are reunited into one seam in the profiles from y = (+5500 to +5700) (Mitrevski & Bravec, 2003). Placer allows a possibility that the eastward shift is not reducing, so the seams would remain separated. However, there is no proof to substantiate it.

The southern wing of the Blato anticline is supposed, according to Kuščer & Mitrevski, to represent a normal substrate of the main seam, i.e. the "northern" seam. At its southern side, only the internal thrust panel is supposed to be situated, and the stronger thrust panel should be located in the north. A similar thrust panel should be running into the footwall of the Dol seam. Further towards east, the conditions should be simplified even more, and the coal from the Dol syncline should pass towards south, into the Blato anticline and in its southern wing, into the main coal seam of the Hrastnik coal deposit. In this sense, the profiles from y = +5500 to y = +5700 in the upgrade of the brief on coal reserves by Mitrevski & Bravec (2003) have also been elaborated. Conditions in this part of the coal deposit are represented on the simplified diagram of the profile y = + 5700 from the updated brief. According to Placer (1988), however, conditions are more complicated. Considering the structure of Brezno, Krištandol and Dol, the Blato anticline and the Dol syncline lie in a strongly compressed thrust zone of pseudozilian and coal-rich layers. The connection between the main seam in Hrastnik and the Dol seam is therefore severely deformed by currently vertical thrusts and strike slip faults in the direction W-E.

The original coal deposit

For a complex estimation of the perspective of the coal deposits in Hrastnik, an important role is played by the ratio between the location of the original coal deposit in the time of coal silt sedimentation in the Upper Oligocene and the current location of the Laško syncline lying in the direction west-east, while the direction of the original coal deposit was WSW-ENE. Strahovlje, Loke and Kisovec therefore lie in the southern wing of the syncline, Kotredež and Orle in the southern and partially central part of the syncline, Trbovlje in the central part of the syncline, and Ojstro, Hrastnik, Dol, Brezno, Huda Jama and Mihael in the northern wing of the syncline. Accordingly, the current coal mines are located in various parts of the original Upper-Oligocene coal de-

posit, some in its central part, some at the outermost edge and some in the intermediate area. It is logical to expect the thickest seam in the central part, and the thinnest one at the borders, although the original paleogeographic shape of the swamp might have been different. The above described model is ideal, but fits reasonably well the conditions in the nature. In the central part of the syncline and the original coal deposit, where Trbovlje is situated, the coal seam and the footwall clay layer are the thickest. The coal seam is gradually becoming thinner and poorer in western and eastern direction. The thinnest and economically least important part is situated in Strahovlje in the west and in Mihael near Laško in the east, partially reaching across the Savinja river. The main coal seam in Hrastnik, i.e. the "southern" seam, is situated between the central and border region of the original coal deposit, so it can be expected to become thinner and poorer in the depth and eastern direction. Due to the inclined position of the original coal deposit against the Laško syncline, the erosion has removed a large part of it, possibly even a half of it.

The Hrastnik thrust fault is an important structural element of the Hrastnik structure. It has been proven in the western part of the coal deposit, and in the eastward direction, its existence is not at questionable as its position. Without the Hrastnik thrust, one cannot explain the structure of the southern edge of the Hrastnik structure and the depth extension of the coal seam. In the eastward direction, it is related to the proven southward oriented Kojzica thrust near Šmarjeta. Along the Hrastnik thrust, the northern wing of the Laško syncline overlapped, in the southward direction, its southern wing, with the largest shift along the Hrastnik thrust fault, causing extensive narrowing of the syncline in this area. It can thus be presumed that the cut-off part of the coal seam along the Hrastnik thrust is covered with the mine structure and shifted in the depth direction towards the north. The size if the shift can only be roughly estimated from two aspects: in the first aspect, we add the reduced thickness of the syncline in Hrastnik against its width in Laško and the size of the shift along the thrust in the Kojzica profile. The sum amounts to approximately 1000–1500 m. The shift may not be that extensive, considering the compensations due to bending. Another aspect is an assumption that the covered part of the coal deposit is situated in the prolongation of the Ojstro seam. In such case, the shift would be less extensive. However, it is a theoretical question. The explorations in this sense should be abandoned, as the missing part was situated near the edge of the original coal deposit, therefore resulting in a presumably thinner and poorer seam.

Field exploration and its costs

Given the characteristics of the Hrastnik rock strata and coal seam, and assuming that the investment is economically viable, it would be advisable for initial exploration to focus on the "southern" seam over the Hrastnik thrust, which is only –40 m deep, while the exploration of the "northern" seam should be attempted only in the case of its thickness proving economically viable. The thickness of the "northern" seam is 10–15 m and only occasionally reaches 20 m. Given what we know, any surveys of the coal deposit under the Hrastnik thrust would be pointless

Table 2: Estimated cost of three structural exploration drill holes

DRILLING WORKS **DRILL HOLE V-1** / HOLE DEPTH: 650 m

No.	Type of works	Unit	Quantity	Price (EUR)	Amount (EUR)
1.	Construction of the access road	M	50	50.00	2 500.00
2.	Construction of the platform for the drilling set	m^2	250	10.00	2 500.00
3.	Transportation of the drilling set and equipment, assembly and dismantling	lump-sum			3 000.00
4.	Drilling for the first column without core sampling and column installation	M	12	150.00	1 800.00
5.	Core drilling	M	638	230.00	146 740.00
6.	Core containers (archive)	pcs	130	60.00	7 800.00
8.	Transport of the core to the laboratory	lump-sum			2 000.00
	TOTAL				**166 340.00**

GEOLOGICAL AND LABORATORY ANALYSES **DRILL HOLE V-1**

Type of works	Quantity	Price (EUR)	Amount (EUR)
1. Geological works			13 000.00
Geological mapping of the core			
Sample collection			
Elaboration of the drill hole profile			
Elaboration of the transverse geological cross-section			
2. Laboratory analyses			8 000.00
3. Elaboration of report			3 000.00
TOTAL			**24 000.00**

DRILL HOLE V-1	Price (EUR)
Drilling works	**166 340.00**
Geological and laboratory analyses	**24 000.00**
TOTAL	**190 340.00**

at this point, primarily on account of its extreme depth and costs involved.

On the basis of comprehensive reference points of the geological evaluation of coal reserves, we propose a construction of three structural exploration drill holes from the surface with an average depth of 650 m. Upon acquisition of positive results, one drill hole will be equipped as a piezometer. Estimated costs for the drill hole construction are shown in Table 2 for each individual drill hole.

DRILLING WORKS **DRILL HOLE V-2 /** HOLE DEPTH: 650 m - PIEZOMETER

No.	Type of works	Unit	Quantity	Price (EUR)	Amount (EUR)
1.	Construction of the access road	M	50	50.00	2 500.00
2.	Construction of the platform for the drilling set	m^2	250	10.00	2 500.00
3.	Transportation of the drilling set and equipment, assembly and dismantling	lump-sum			3 000.00
4.	Drilling for the first column without core sampling and column installation	M	12	150.00	1 800.00
5.	Delivery and installation of the piezometer pipe	M	650	100.00	65 000.00
6.	Core drilling	M	638	230.00	146 740.00
7.	Core containers (archive)	pcs	130	60.00	7 800.00
8.	Transport of the core to the laboratory	lump-sum			2 000.00
	TOTAL				**231 340.00**

GEOLOGICAL AND LABORATORY ANALYSES **DRILL HOLE V-2**

Type of works	Quantity	Price (EUR)	Amount (EUR)
1. Geological works			13 000.00
Geological mapping of the core			
Sample collection			
Elaboration of the drill hole profile			
Elaboration of the transverse geological cross-section			
2. Laboratory analyses			8 000.00
3. Elaboration of report			3 000.00
Total			**24 000.00**

DRILL HOLE V-2	Price (EUR)
Drilling works	**166 340.00**
Geological and laboratory analyses	**24 000.00**
TOTAL	**255 340.00**

DRILLING WORKS **DRILL HOLE V-3** / HOLE DEPTH: 650 m

No.	Type of works	Unit	Quantity	Price (EUR)	Amount (EUR)
1.	Construction of the access road	M	50	50.00	2 500.00
2.	Construction of the platform for the drilling set	m^2	250	10.00	2 500.00
3.	Transportation of the drilling set and equipment, assembly and dismantling	lump-sum			3 000.00
4.	Drilling for the first column without core sampling and column installation	M	12	150.00	1 800.00
5.	Core drilling	M	638	230.00	146 740.00
6.	Core containers (archive)	pcs	130	60.00	7 800.00
8.	Transport of the core to the laboratory	lump-sum			2 000.00
	TOTAL				**166 340.00**

GEOLOGICAL AND LABORATORY ANALYSES **DRILL HOLE V-3**

Type of works	Quantity	Price (EUR)	Amount (EUR)
1. Geological works			13 000.00
Geological mapping of the core			
Sample collection			
Elaboration of the drill hole profile			
Elaboration of the transverse geological cross-section			
2. Laboratory analyses			8 000.00
3. Elaboration of report			3 000.00
TOTAL			**24 000.00**

DRILL HOLE V-3	Price (EUR)
Drilling works	**166 340.00**
Geological and laboratory analyses	**24 000.00**
TOTAL	**190 340.00**

TOTAL COSTS FOR THE CONSTRUCTION OF DRILL HOLES V-1, V-2 and V-3	Price (EUR)
DRILL HOLE V-1	**190 340.00**
DRILL HOLE V-2	**255 340.00**
DRILL HOLE V-3	**190 340.00**
TOTAL	**636 020.00**

During the execution of exploration drill holes, a decision on the relevance of the execution of all three drill holes and on the manner of execution of the piezometer would be made, considering the individual data collected from the drill hole V-1. The depths of the drill holes have been estimated, but should not exceed the depth of 650 m.

Conclusion

The off-balance A + B + C_1 coal reserves in the Hrastnik mine, the amount of which has not significantly changed since the end of the year 1997, represent precisely one third of the entire (both balance and off-balance) A+B+C1 coal reserves for RTH, the Trbovlje-Hrastnik mine (53,893,000 t). In addition, further sources of the C2 category (6,272,000 t) have been recorded in the Eastern Corner Field in the mine Hrastnik. The elaborated geological evaluation and the necessary scope of research surface drilling represent a good basis for coal reserve recategorisation. The results of exploration drilling will enable the final confirmation of exploitation reserves of brown coal in the Hrastnik mine.

The purpose of the study "The justifiability of the exploitation of the remaining coal reserves at the mines Ojstro and Trbovlje after the year 2009" – Phases II and III, and the evaluation of coal deposits at the mine Hrastnik was to produce an estimate and identify the necessary scope of activities that would enable the remaining reserves to be determined with a higher degree of precision and subsequently recategorised as actual reserves, and to verify the exploitable coal reserves which, once confirmed, would provide a basis of determining the economic viability of further mining at the coalmine Hrastnik.

Summary

Geological Evaluation of Brown Coal Reserves at Hrastnik Pit - RTH, Rudnik Trbovlje – Hrastnik

The geological evaluation of the remaining deposits of brown coal at Hrastnik focused on reviewing the updated brief on the categorisation, classification and calculation of the resources and deposits of brown coal in the RTH mining area as at 31 December 2002 (Mitrevski and Bravec, 2003).

Apart from the associates employed by the coalmine's geological department to monitor the preliminary works and surveys carried out at the coalmine on an ongoing basis, vital research over the past fifty years was undertaken by Kuščer (1967) with his core work *Zagorje Tertiary*, Gregorač (1975) who focused on the hydrogeology of the mine Hrastnik, Kuščer and Mitrevski (1979) who researched the geology of the bound-

ary area between the mines Hrastnik and Dol, Uhan (1991) with his work on the geochemical properties of coal in the central part of the deposit, and Placer who carried out a structural-geological analysis between 1982 and 1991. In the abovementioned period Placer completed a geological survey and mapping of the surface area between Moravče and Laško, and surveyed and mapped the mine roadways and the cores of exploration drill holes. Placer published the major findings of the survey and mapping of the surface area over the mines Hrastnik and Dol in 1987 in the brief "A Geological Structure Survey in the Dol-Hrastnik Area, Part II". In the three-year period 1985–1987 geologists surveyed roughly 3,200 m of roadways, access tunnels and longwalls, and drilled eleven structural exploration drill holes in the total length of approximately 1,500 m (Uhan, 1987). The geological data obtained in the course of the abovementioned surveying and mapping of mine roadways and exploration drill holes yielded more detailed information on the structure of the "south wing" of the central part of the coalmine Hrastnik at and under Horizon VII. Building on the results of all previous surveys and having reviewed and processed the entire documentation held by the coalmine, Placer preformed the most comprehensive structural geological analysis until that time, and explained the tectonic development of the coal deposit. When it comes to the evaluation of remaining coal reserves in the Hrastnik area, certain structural geological questions remain unanswered; this primarily refers to the continuation of the coal seam under the hypothetical Hrastnik thrust fault. The other set of debatable questions concern the geological structure of the Eastern Underground Deposit where the continuation of the southern coal seam downwards has been established by exploratory drill holes at Brnica.

Given the characteristics of the Hrastnik rock strata and coal seam, and assuming that the investment is economically viable, it would be advisable for initial exploration to focus on the "southern" seam over the Hrastnik thrust, which is only 25–40 m deep, while the exploration of the "northern" seam should be attempted only in the case of its thickness proving economically viable. The thickness of the "northern" seam is 10 m to 15 m and only occasionally reaches 20 m. Given what we know, any surveys of the coal deposit under the Hrastnik thrust would be pointless at this point, primarily on account of its extreme depth and costs involved.

The western end of the "southern" seam has been comparatively well surveyed. However, more detailed surveys of the eastern end should be carried out; this applies in particular to the layout of the Hrastnik thrust.

The question of a direct connection between the "southern" and "northern"

coal seams at the far eastern end of the coal deposit at Hrastnik remains open, as there is always a possibility that the shift along the internal thrust layer in that direction may be diminishing. Should the opening of the "southern" seam be deemed economically viable, however, that possibility should also be explored.

Suitable drilling sites have been identified both on the surface and in the mine. At Horizon 8 (+50 m) the relevant tunnel reaches up to coordinate y = +5350. Access to Level 0 is provided from Horizon 7 (+85 m) downwards. Point 0 is located at cross-section y = +4900. Horizon 8 is more suitable for drilling; the required access tunnel to the far end of the "southern" seam would be at least 600–700 m long and possibly longer with drill holes reaching 200 m to 300 m deep, depending on the layout of the proposed tunnel. The "southern" seam can also be accessed from the surface. The average depth of the proposed drill holes would be about 600 m i.e. between 500 m to 700 m. The cost/benefit analysis would indicate which part should be explored from the mine and which part from the surface.

The most promising point at which the connection between the "southern" and "northern" seams at the eastern end of the coal deposit should be explored would be at cross-section y = +5650 at the location of the existing drill hole Br.10.

Access for the purpose of surveying the "northern" seam from the surface is less favourable.

The far eastern boundary of the Hrastnik coalmine deposit has not been determined. Known findings about the position of the originally identified deposit relative to the Laško synclinal lead us to believe that the uniform or divided main seam is leaning at an angle onto the thrust zone along the northern perimeter of the Laško synclinal. Since we are approaching the outermost boundary of the originally identified deposit in the eastern direction, the potential of this area is limited by that boundary, which translates into a gradual diminishing and thinning of the coal seam.

The proposed surveys at the Hrastnik coalmine deposit should facilitate a recategorisation of reserves and resources, and should focus primarily on the eastern end of the mine. The proposed exploration involves three drill holes to the depth exceeding 650 m. The total cost of drilling would amount to EUR 636,000.

Total actual deposits are expected to be below the figure suggested in the reassessment of resources and reserves carried out in 2003 (Mitrevski and Bravec). The proposed downgrading of reserves applies to the "northern" seam and the transitional area between the Hrastnik

and Dol mines due to the tectonic thrust and shifting tectonic plates, which thinned the original seam and broke it up into individual lens. Due to the lack of field data, the figures presented in the reassessed resources and reserves brief are somewhat idealised.

The purpose of the study "The Legitimacy of the Extraction of Remaining Coal Deposits at the Mines Ojstro and Trbovlje After 2009" – Stages 2 and 3, and the evaluation of coal deposits at the mine Hrastnik was to produce an estimate and identify the necessary scope of activities that would enable the remaining reserves to be determined with a higher degree of precision and subsequently recategorised as actual reserves, and a verification of exploitable coal reserves which, once confirmed, would provide a basis of determining the economic viability of further mining at the coalmine Hrastnik.

References

Dervarič et al. (2008): Upravičenost odkopavanja preostalih zalog premoga v jamah Ojstro in Trbovlje po letu 2009 in zaprtega dela jame Hrastnik – I. faza (*Justifiability of exploitation of the remaining coal reserves in the mines Ojstro and Trbovlje after the year 2009 and the closed-down section of the Hrastnik mine - Phase I*). UL NTF OGTR, September 2008.

Dervarič et al. (2009): Upravičenost odkopavanja preostalih zalog premoga v jamah Ojstro in Trbovlje po letu 2009 in zaprtega dela jame Hrastnik – II. in III. faza (*Justifiability of exploitation of the remaining coal reserves in the mines Ojstro and Trbovlje after the year 2009 and the closed-down section of the Hrastnik mine - Phase II and III*). UL NTF OGTR, March 2009.

Kuščer, D. & Mitrevski, G. (1979): Geologija mejnega območja med jamama Hrastnik in Dol (*Geology of the border area between the mines Hrastnik and Dol*). *Rudarsko-metalurški zbornik 26/2–3*, 167–178, Ljubljana.

Placer, L. (1988): Preliminarna analiza strukture Ojstrega in Hrastnika (*Preliminary analysis of the structure of Ojstro and Hrastnik*). RTH Archive.

Placer, L. et al. (1994): Stratigrafski in tektonski razvoj Laške sinclinale (*Stratigraphic and tectonic development of the Laško synclinal*). RTH Archive.

Placer, L. 1999 (1998): Structural meaning of the Sava folds. *Geologija 41*, 191–221, Ljubljana.

Mitrevski, G. & Bravec, B. (2003): Renovelacija elaborata o kategorizaciji in klasifikaciji izračunanih zalog in virov rjavega premoga na območju pridobivalnega prostora Rudnika Trbovlje-Hrastnik (RTH) s stanjem 31. 12. 2003 (*Update of the brief on the categorisation, classification and calculation of the resources and deposits of brown coal in the RTH mining area as at 31st December 2003*).

RTH Archive.

Influence of movements in tectonic fault on stress-strain state of the pipeline ČHE Kozjak

Vpliv premikov v prelomni coni na napetostno deformacijsko stanje cevovoda ČHE Kozjak

Bojan Žlender[1,] *, Borut Macuh[1]

[1]University of Maribor, Faculty of Civil Engineering,
Smetanova ulica 17, SI-2000 Maribor, Slovenia

*Corresponding author. E-mail: bojan.zlender@uni-mb.si

Received: February 18, 2009 **Accepted:** July 1, 2009

Abstract: In the frame of pumping hydroelectric station Kozjak the construction of pipeline's tunnel in length of 2400 m that overcomes 710 m of see level difference between machine house and reservoir hydraulic drop is foreseen. The pipeline layout is mostly in layers of compact rock, and it overcome eleven tectonic faults. Material in these faults is remolded and weathered due to water presence, and according to the preliminary estimation the width of tectonic faults is between 25 m and 80 m. The analysis considers deformations and stresses in pumping pipeline due to movements in tectonic fault. To estimate this stress-strain response mathematical model in form of differential equation was made.

The variables in analysis were relative movement in tectonic fault, width of tectonic fault, area of pipeline cross-section, pipeline strength, compact rock strength and remolded rock strength. Inner forces or stresses and strains in pipeline cross-section were determined through analysis. It was found out that the width of tectonic fault essentially influence their distribution along tectonic fault width. The analytical solutions were compared with solution obtained according to the finite element method.

Izvleček: V sklopu graditve črpalne hidroelektrarne Kozjak je predvidena gradnja tlačnega cevovoda dolžine 2400 m, ki bo premagoval skupni padec 710 m. Trasa cevovoda poteka pretežno v slojih kom-

Original scientific paper

paktnih kamnin. Problem je, da vzdolžno prečka enajst prelomnih con. Na teh mestih je hribina razdrobljena in zaradi dotokov vode preperela. Po prognoznih podatkih je širina takih con med 25 m in 80 m. Analiza obravnava deformacije in napetosti tlačnega cevovoda zaradi premikov v prelomni coni. Za določitev napetostno deformacijskega odziva zaradi pomikov v prelomni coni je bil izdelan matematični model v obliki diferencialnih enačb.

V analizi so bile spremenljivke velikost relativnega pomika v prelomni coni: širina prelomne cone, prerez cevovoda, trdnost cevovoda, trdnost kompaktne hribine in trdnost pregnetene hribine. Določale pa so se notranje statične količine oz. napetosti in deformacije v prerezu cevovoda. Ugotovljeno je bilo, da je bistvenega pomena za njihovo razporeditev širina prelomne cone. Analitične rešitve so bile primerjane z rešitvami, dobljenimi po metodi končnih elementov.

Key words: tectonic fault, tunnel, tunnel deformation, rock stiffness
Ključne besede: prelomna cona, predor, deformacija predora, togost kamnine

Introduction

The construction of pipeline's tunnel of pumping hydroelectric station Kozjak is foreseen. It is composed of three main parts: engine house, accumulation lake, and the pipeline that connects engine house and reservoir. The engine house is located near river Drava, reservoir is on the 700 m higher plateau of Kozjak, and the pipeline is few ten meters under its eastern slope.

The geological characteristics were preliminary investigated in 1979 and 1980. The further activities of the project were stopped, until it was anew activated in year 2004. The project is in the outline scheme phase.

The paper considers only the problem of tunnel's deformations and stresses due to the movements in tectonic faults. The main questions that arise are:

- deformation of the tunnel's structure,
- distribution of normal and shear stresses in the tunnel's cross-section,
- bending moments and shear forces in the tunnel's cross-section,
- influence of the movement in tectonic fault, the tectonic fault's width, and the ratio of stiffness in compact rock and tectonic fault.

In order to answer the questions that arise, mathematical model of the problem was made. The model encounters morphological and geomechanical properties of the ground, geometry of the planned pipeline, and technological conditions of the pipeline erection. Model is given in the form of differential equations together with assumed boundary conditions that follows geometry and technology of the construction. The solutions of the equations are functions of deflection, slope, bending moment, shear force, and resistance intensity.

The analytical solutions were compared with solutions obtained according to finite element method (FEM) and using program code Plaxis 3D Tunnel.

Geology

The geological characteristics given in geological reports were determined using field geological reconnaissance, photo-geological analyses, and hydro-geological, geophysical and sounding investigations. The results of investigations are given in geological-geotechnical reports [1], [2] that give: geomorphologic description, geologic structure, hydrogeological conditions and tectonics. In 2004 the additional investigations and supplement geotechnical report was done [3] that present review of established geological characteristics of preliminary reports, geotechnical analyses and proposal of supplementary investigations for the realization of planned project. The longitudinal section through pipeline with geology is on Figure 1.

Geomorphologic description

The pipeline's tunnel is designed deep in the slope of eastern Kozjak between Drava River and Kolar's peak. The agitated formed terrain is characteristic, that is the result of geological structure, tectonic, precipitation conditions and the formation history of the ground. The valleys and ravines are bounded mostly on older and bigger tectonic faults where the erosion is more intensive due to crumbled rocks. The crests are connected with very steep slopes appears where compact and more subsistence rocks. On the peaks of the ascents where the activity of surface waters is less distinctive thicker decaying cover and distinctive dome-shaped peaks rise.

Geological structure

The major part of the investigated region belongs to the metamorphic rock complex characteristic for the whole region of central Alps. The metamorphic rocks originated mainly at regional metamorphosis bounded on extensive orogenic zones.

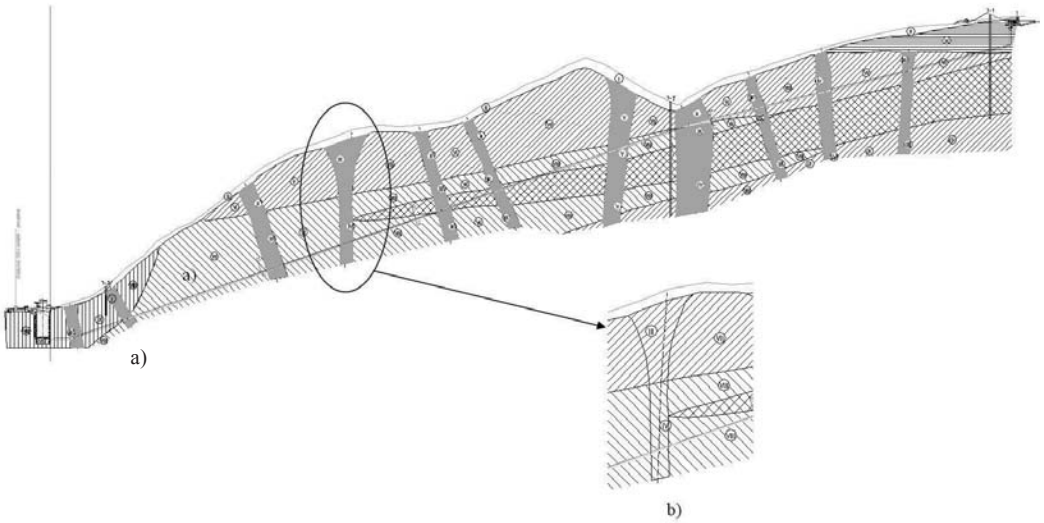

Figure 1. Geology with pipeline: a) longitudinal cross-section, b) enlargement of the tectonic fault

The most widened rocks of the investigated region comprise blestnik and gneisses that are irregular interchange in thinner and thicker layers. On the slope peaks of the investigated region presents those rocks basis of diaphtorite and diaphtorite schists. The described rocks appear on the surface on the steep slopes in direction of pipeline line, they can be tracked also down to the foothill of the slope.

The upper part of the upper half of the tunnel alignment is mainly composed of blestnik and the lower portion mainly of gneiss. Both series are intercalated by amphibolites and biotite-epidote schists. The occurrence of amphibolites is rather rare at higher elevations. The amphibolites may grade into the schists in places.

The next series in flow direction is composed of marble, calcite bearing blestnik, dolomite, and calcitic schists in irregular sequences. The calcitic schist forms the transition between marble, carbonaceous schist and biotite-muscovite, blestnik or

gneiss, respectively. All layers are dipping steeply to vertical, i.e. between 60° and 90° towards south or north due to intense folding. Further downstream the inclination flattens to 30° to 60° with decreasing intensity of folding.

The slopes are mainly covered by in-situ weathered materials from the underlying bedrock. The overburden is composed of sand and angular fragments of rock in different degrees of weathering. The thickness depends on the steepness of the slope as follows: steep slope (0.5–1.5 m), moderate slope (1.0–2.0 m), and flat slope (2.0–5.0 m).

Tectonic

The project area is composed of Cambrian sediments, which have undergone orogenic deformations and metamorphosis. It is deemed that the metamorphosis occurred in several sequences and the final stage resulted in a retrograde metamorphosis, in which the minerals were adjusted to lower temperatures and pressures. Lateral pressures have lead to intense folding and in a second phase to foliation. Dilatation movements resulted in a more or less regular pattern of fractures forming blocks of different size.

The tectonic systems of wide considered region were defined on basis of field recognition, photo-geological analyses and geophysical investigations. Three tectonic systems were stated, namely in directions SW-NE, W-E and N-S to NW-SE.

At tectonic zones mainly vertical movements appear. The width of cracked zones is 5–80 m, water inflows are possible in this places 0.5–5 L/s. The widest tectonic zones, the highest water inflows and higher seismic activities at tectonic zones of the systems N-S to NW-SE.

Hydro-geological conditions

The hydro-geological situation was investigated by surface mapping and drilling works (inflow and rising head test, and water level measurements in boreholes).

In principle two different aquifers were encountered. The first type is confined to the open joints in the bedrock, and the second type to the pores of the alluvial gravel. The area between the valley and the upper reservoir is governed by the first type of aquifer. The permeability depends on the frequency and openness of the joints. The permeability was tested by water pressure tests. The medium cracked rocks have the coefficients of permeability between 5×10^{-6} and 1×10^{-9} m/s. In tectonic zones with strongly crumbled rock material the coefficients of permeabil-

ity are essentially higher. The measurements in rocks with equal RQD showed that the values vary between 5×10^{-4} and 5×10^{-7} m/s.

In the region of the pipeline's line no continuous ground water level is presented. The filtrated water appears in cracks and tectonic crumbled or weathered zones.

Engineering geological and geotechnical characteristics

Regards to the degree of rock crackness in the region of the pipeline are classified in ten categories. First five categories present weathered and strongly tectonic cracked rocks, that have $RQD < 30$ and $Q < 1$. In higher categories belongs partly cracked to compact rocks.

The line of the pipeline course mostly in rock layers of category VII to IX; however it crosses eleven tectonic faults of system N-S and NW-SE. On these places the rock is crumbled and due to the water inflow also decaying. According to the prognosis can be classified in categories I to V, the width of such zones is between 25 m and 80 m. The foreseen properties of the rock in the course of pipeline are given in Table 1.

Project data

The inner diameter of the pipeline is 3.0 m, the wall is of reinforced concrete (RC), width of 50 cm. The pressure tunnel of length 2400 m overcomes total fall of 710 m. In up-

Table 1. Properties of rocks in pipeline region

properties / rock	RMR[(1)]	Q[(2)]	category[(3)]	k[(4)]/ (m/s)	water flow[(5)] (L/s)
cracked and weathered (17 %)	25–45	0.07–1.0	I–V	5×10^{-4}–5×10^{-7}	≥ 1, smaller water invasion
partially cracked to compact (83 %)	60–72	5–24	VI–X	5×10^{-6}–1×10^{-9}	wet, light to strong dropping

(1) Bieniawski
(2) Barton et al.
(3) Categorization regarding to degree of rock crack ness
(4) Coefficient of water permeability, filling test in boreholes T-1, T-2 and T-3
(5) Expected water flow regarding to degree of rock crack ness

per part firstly drops vertical 40 m, then course in slope about 31 %. In front of the powerhouse shaft course pipeline in length of 60 m horizontal, and then split into two legs, that leads in underground shaft of the powerhouse.

The pipeline crosses eleven tectonic zones. The rocks in tectonic zones are remolded, their strength is instantly lower than in compact rocks.

The geotechnical conditions of pumping tunnel construction are given in geological-geotechnical documentation. [3], [4] The technology is not defined yet.

The pressure tunnel will be loaded with constant and repeated loading. The constant load present outer soil pressure and pipeline own weight. The constant load is equal:

$\sigma_v = 0.8–1$ MPa
$\sigma_h < \sigma_v$

The stress in the structure and expected movements due to constant load are:

$\sigma_r = 0.8–1$ MPa (compression)
$\sigma_\varphi = 3.6–4.5$ MPa (compression)
$u_r \cong 0.2$ mm

The repeated load presents the change of the inner pressure:
$p = 0–7$ MPa
$p_{max} = 11$ MPa

The stress in the structure and expected movements due to repeated load are:

$\sigma_r = 8–11$ MPa (compression)
$\sigma_\varphi = 25–39$ MPa (tension)
$u_r \cong 1–2$ mm

Due to the possible movements in tectonic tones the additional load can appear as relative movement of the ground at the contact in tectonic zone. The magnitude of the movement in analysis is supposed at $u_{rel} = 1–10$ mm.

Mathematical model

The pipeline is axis-symmetrical with r, ϑ, x coordinates, where x-axis corresponds with the pipeline axis. The pipeline is erected in the ground, described in the space by x, y, z coordinates, where x-axis corresponds with the pipeline axis, while y-axis is vertical.

The geometrical and mechanical characteristics of the pipeline and surrounding rock are given in Table 2.

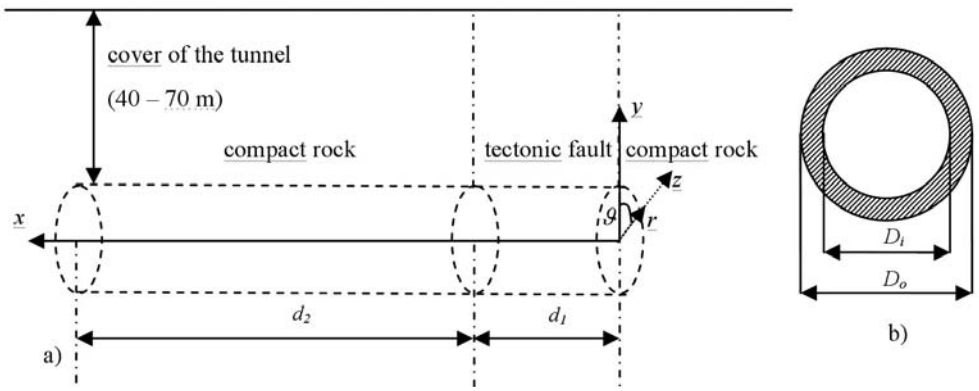

Figure 2. Mathematical model: a) longitudinal cross-section, b) pipeline cross-section.

Table 2. Geometrical and mechanical properties of pipeline and rock

$d_1 = 25–80$	m	width of tectonic fault in the pipeline axis
$d_2 = 80–200$	m	width of compact rock in the pipeline axis
$D_i = 3.0$	m	inner tube diameter
$D_o = 4.0$	m	outer tube diameter
$E = 30 \times 10^6$	kPa	elasticity modulus of the tube
$I = 8.6$	m^4	inertia moment of the tube
$u_0 = 0–10$	mm	movement in tectonic fault
$E_1 = 0–1$	GPa	elasticity modulus of tectonic fault
$E_2 = 20–30$	GPa	elasticity modulus of compact rock

The pipeline is subjected to the permanent stresses of the surrounding rock (0.3–2 MPa), repeated water pressure (7–10 MPa), and eventual movements in tectonic fault (few millimeters). The presented stress-strain analysis considers only eventual movements in tectonic fault.

- k_1 stiffness of tectonic fault
- k_2 stiffness of compact rock
- EI flexural stiffness of tunnel (pipeline)
- $y(x)$ deflection line
- $y'(x)$ slope line
- $EIy''(x)$ bending moment line
- $EIy'''(x)$ shearing force line
- $q(x)$ resistance of rock in tectonic fault

The general differential equation for footing on elastic subsoil is given:

$$EI\frac{d^4y(x)}{dx^4}=q(x) \tag{1}$$

where the resistance of rock in tectonic fault can be expressed with function:

$$q(x)=k_1\cdot y(x) \tag{2}$$

then Eq. (1) gets the following form:

$$EI\frac{d^4y(x)}{dx^4}-k_1\cdot y(x)=0 \tag{3}$$

The general solution according to [5] is:

$$y(x)=C_1\cdot e^{-x\cdot\sqrt[4]{\frac{-k_1}{EI}}x}+C_2\cdot e^{x\cdot\sqrt[4]{\frac{-k_1}{EI}}x}+ \\ +C_3\cdot e^{-x\cdot\sqrt[4]{\frac{(-1)^3\cdot k_1}{EI}}x}+C_4\cdot e^{x\cdot\sqrt[4]{\frac{(-1)^3\cdot k_1}{EI}}x} \tag{4}$$

We can introduce the following assumptions:

- the pipeline is within elastic domain,
- the pipeline is subjected to the displacement at the contact between compact rock and rock in tectonic fault [$y(x = 0) = u_0$],
- the stiffness of compact rock k_2 is very high comparing to the stiffness of rock in tectonic fault k_1 [20 $\times k_1 < k_2$],
- displacement on the other contact between compact rock and rock in tectonic fault is assumed to be equal zero [$y(x = d_1) = 0$],
- rotations on both contacts between compact rock and rock in tectonic fault are assumed to be equal zero [$y'(x = 0) = y'(x = d_1) = 0$; $y''(x = d_1/2) = 0$].

The function of rock's resistance in tectonic fault $q(x)$ has to be in accordance with deflection line $y(x)$, then we can approximate the rock's resistance line with adequate function, for example:

$$q(x)=q_0\cdot\left(1+\cos\left(\pi\frac{x}{d_1}\right)\right)= \\ =k_1\cdot y_0\cdot\left(1+\cos\left(\pi\frac{x}{d_1}\right)\right) \tag{5}$$

where, $q_0 = k_1 \times y_0$ is resistance in the middle of the tectonic fault at $x = d_1/2$, and y_0 is about half of tectonic movement u_0. Then Eq. (3) gets the form:

$$EI\frac{d^4y(x)}{dx^4}=q_0\cdot\left(1+\cos\left(\pi\frac{x}{d_1}\right)\right) \tag{6}$$

this leads using above boundary conditions (given in assumptions) to the solution:

$$y(x)=u_0\left[2\left(\frac{x}{d_1}\right)^3-3\left(\frac{x}{d_1}\right)^2+1\right]+\frac{q\cdot d_1^4}{24\cdot\pi^4\cdot EI}\left[-24+\pi^4\cdot\left(\frac{x}{d_1}\right)^2+144\cdot\left(\frac{x}{d_1}\right)^2\right.$$
$$\left.-2\cdot\pi^4\cdot\left(\frac{x}{d_1}\right)^3-96\cdot\left(\frac{x}{d_1}\right)^3+\pi^4\cdot\left(\frac{x}{d_1}\right)^4+24\cdot\cos\left(\pi\cdot\frac{x}{d_1}\right)\right] \tag{7a}$$

$$y'(x)=\frac{u_0}{d_1}\left[6\left(\frac{x}{d_1}\right)^2-6\left(\frac{x}{d_1}\right)\right]+\frac{q\cdot d_1^3}{12\cdot\pi^4\cdot EI}\left[\pi^4\cdot\left(\frac{x}{d_1}\right)+144\cdot\left(\frac{x}{d_1}\right)\right.$$
$$\left.-3\cdot\pi^4\cdot\left(\frac{x}{d_1}\right)^2-144\cdot\left(\frac{x}{d_1}\right)^2+2\cdot\pi^4\cdot\left(\frac{x}{d_1}\right)^3-12\cdot\pi\cdot\sin\left(\pi\cdot\frac{x}{d_1}\right)\right] \tag{7b}$$

$$M(x)=EI\cdot y''(x)=EI\cdot\frac{u_0}{d_1^2}\left[12\left(\frac{x}{d_1}\right)-6\right]+\frac{q\cdot d_1^2}{12\cdot\pi^4}\left[\pi^4+144-6\cdot\pi^4\cdot\left(\frac{x}{d_1}\right)\right.$$
$$\left.-288\cdot\left(\frac{x}{d_1}\right)+6\cdot\pi^4\cdot\left(\frac{x}{d_1}\right)^2-12\cdot\pi^2\cdot\cos\left(\pi\cdot\frac{x}{d_1}\right)\right] \tag{7c}$$

$$Q(x)=EI\cdot y'''(x)=12\cdot EI\cdot\frac{u_0}{d_1^3}+\frac{q\cdot d_1}{2\cdot\pi^4}\left[-\pi^4-48+2\cdot\pi^4\cdot\left(\frac{x}{d_1}\right)+\right.$$
$$\left.+2\cdot\pi^3\cdot\sin\left(\pi\cdot\frac{x}{d_1}\right)\right] \tag{7d}$$

Above solutions are given as functions of $q_0 = k_1 \times y_0$, that can be theoretically, in the case when k_1/k_2 approaches very small values, even zero. In the latter case the Eqs. (7) get the following form:

$$y(x)=u_0\left[2\left(\frac{x}{d_1}\right)^3-3\left(\frac{x}{d_1}\right)^2+1\right] \tag{8a}$$

$$y'(x)=\frac{u_0}{d_1}\left[6\left(\frac{x}{d_1}\right)^2-6\left(\frac{x}{d_1}\right)\right] \tag{8b}$$

$$M(x) = EI \cdot y''(x) = \\ = EI \cdot \frac{u_0}{d_1^{\,2}} \left[12 \left(\frac{x}{d_1} \right) - 6 \right] \qquad (8c)$$

$$Q(x) = EI \cdot y'''(x) = 12 \cdot EI \cdot \frac{u_0}{d_1^{\,3}} \qquad (8d)$$

This is well known solution that can be obtained using mechanics theory of elastic liner structures.

It can be realized, that results are influenced by the following factors:

- cross-section of the tube
- strength of the tube
- strength of the compact rock
- strength of the rock in tectonic zone
- quantity of the relative movement in tectonic zone
- width of the tectonic zone

The cross-section and the strength of the pressure tunnel do not influence deformations and inner forces in the structure, but they are important for stress state in tunnel structure. Increasing cross-section and strength of the tunnel structure lead to inversely proportional lower stresses in the cross-section of the tunnel.

The strength of the compact rock and strength of the remolded rock do not influence the magnitude and distribution of the movement and rotation of the tunnel structure (Figure 3), but they influence on the magnitude and distribution of inner forces of the tunnel structure. The distribution of inner forces is influenced also by ratio between strength of compact and remolded rock (Figure 4).

The inner forces, respectively stresses and deformations (movements, rotations) linearly depend on magnitude or the relative movement in tectonic zone (Figures 3, 4).

The width of the tectonic zone is essential for the distribution of deformations and inner forces across tunnel cross-section. Lowering tectonic zone width leads to non linear increasing of inner forces. Figure 5 presents inner forces at the edge of the tectonic zone for movement in tectonic zone equal u = 1 mm.

The analysis of stress distribution across tunnel cross-section shows, that the supposed properties of the pressure tunnel and rock significantly increase inner forces when the with of the tectonic zone is lower than 30 m. The with above 30 m is problematic concerning magnitude of inner forces also at supposed higher movements in tectonic zone, therefore deviation of the results in this region are not important.

The analytical solutions were compared with solutions obtained according to the finite element method (FEM). The results of analyses are presented in Figure 7 and are comparable to the results of analytical solutions.

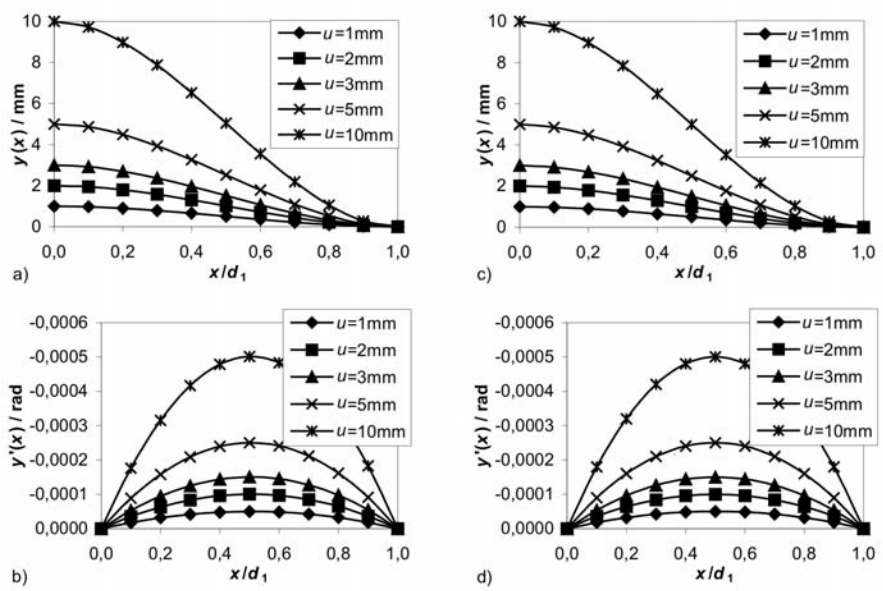

Figure 3. Results for different movements u in joint for d_1 = 30 m and k_1 = 10 MPa/m: a) movement, b) rotation; and for d_1 = 30 m and k_1 = 0: c) movement, d) rotation

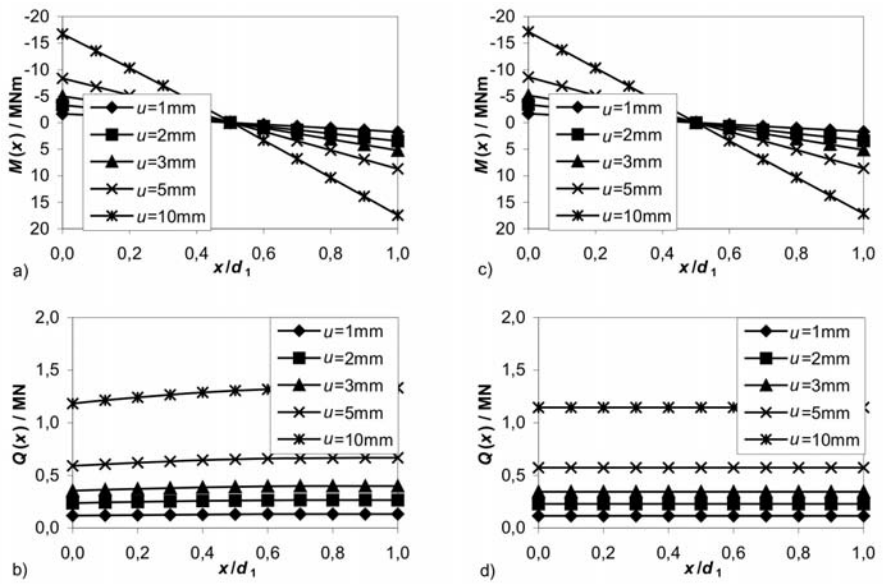

Figure 4. Results for different movements u in joint for d_1 = 30 m in k_1 = 10 MPa/m: a) bending moment; b) shear force; and for d_1 = 30 m in k_1 = 0: c) bending moment; d) shear force

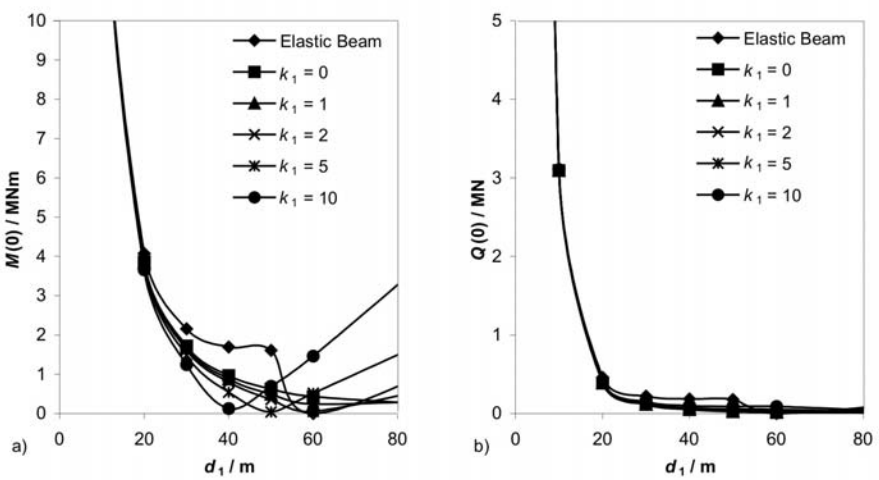

Figure 5. Inner forces as function of tectonic fault width: a) bending moment, b) shear force.

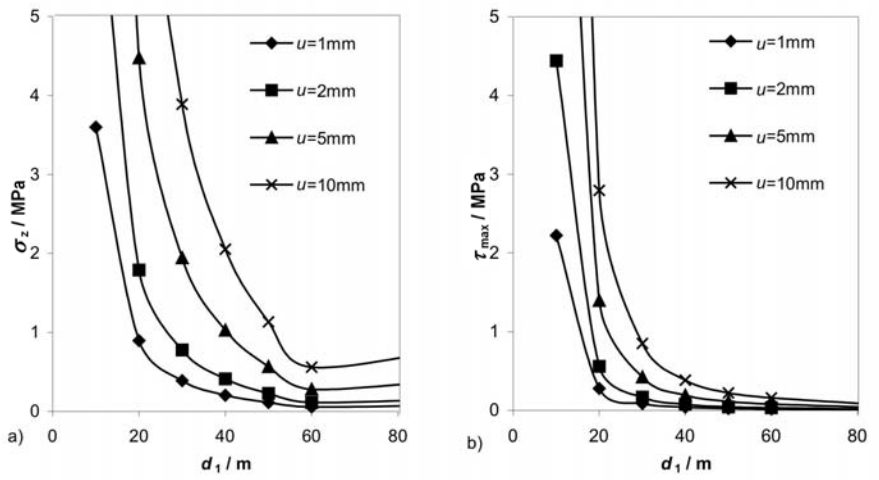

Figure 6. Stress for different movement u as function of tectonic fault width for d_1 = 1 MPa/m: a) normal stress, b) shear stress.

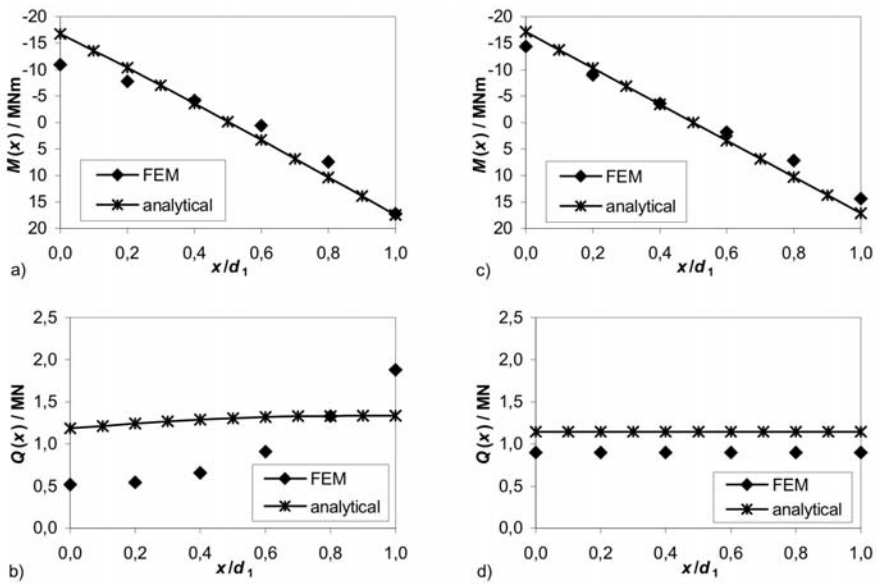

Figure 7. Results of analytical solutions and values obtained using FEM for movement u = 10 mm in joint for d_1 = 30 m in k_1 = 10 MPa/m: a) bending moment; b) shear force; and for d_1 = 30 m in k_1 = 0: c) bending moment; d) shear force.

CONCLUSIONS

To find the stress-strain response due to the movement in tectonic fault, the mathematical model was made in the form of differential equations. The general solution of the problem is given which is not in the closed form. Introducing assumed shape of the deflection line that is in accordance with the resistance line of the rock in tectonic fault, we obtain the simple solution in a closed form.

The solutions of the equations are functions of deflection, slope, bending moment, shear force, and resistance intensity.

The analysis shows, that the magnitude of the movement in tectonic fault, width of tectonic fault, cross-section and strength of the tunnel, and stiffness of tectonic fault and compact rock essentially influence the magnitude of the stresses and deformations of the tunnel structure.

The inner forces, respectively stresses and deformations linearly depend on the magnitude of the relative movement in tectonic cone.

The cross-section and the strength of the pressure tunnel do not influence magnitudes of the movement and rotation of

the tunnel. Increasing cross-section and strength of the tunnel structure lead to inversely proportional lower stresses in the cross-section of the tunnel.

The strength of the compact rock and strength of the remolded rock do not influence the magnitude and distribution of the movement and rotation of the tunnel structure. However, they influence on the magnitude and distribution of inner forces of the tunnel structure. The distribution of inner forces is influenced also by ratio between strength of compact and remolded rock (Figure 4). The width of the tectonic zone is essential for the distribution of deformations and inner forces across tunnel cross-section. Lowering tectonic zone width leads to non linear increasing of inner forces.

The analysis of stress distribution across tunnel cross-section shows, that the supposed properties of the pressure tunnel and surrounding the critical width of the tectonic zone is between 20 m and 30 m. For width above 30 m the magnitudes of inner forces exceedingly fall also at supposed higher movements in tectonic zone.

The results of analytical solutions are comparable with results obtained according to FEM.

The advantage of the analytical solutions is in presentation of the results in form of function, while the calculation according to FEM gives the results for certain chosen geometrical and material data.

Acknowledgments

The financial support of the Ministry of High Education, Science and Technology of the Republic of Slovenia is gratefully acknowledged.

References

[1] ČRPALNA ELEKTRARNA KOZJAK - Geološko geotehnično poročilo za potrebe projekta Črpalne elektrarne Kozjak, Mapa I, Mapa II, Mapa III, GZL, Opr. št. pov.: 263/1-1980, 1980.

[2] Poročilo o geološko geotehničnih raziskavah za ČE Pohorje – varianta Kolarjev vrh, Mapa I, Mapa II, Mapa III, Opr. Št. Pov.:207/1-1979, 1979.

[3] Študija geotehničnih pogojev za potrebe projektiranja ČHE Kozjak, Univerza v Mariboru, Fakulteta za gradbeništvo, Maribor, 2004.

[4] Študija ČHE KOZJAK, IBE d.d., svetovanje, projektiranje in inženiring, Ljubljana, štev.proj. IBKO-A301/112A, december 2003.

[5] Oden, J. T. (1967): Mechanics of Elastic Structures, McGraw-Hill, New York, 1967.

Possibilities of coal conversion into gas fuel from the aspect of greater valorization of available energy resources in Serbia by implementing UCG

Možnosti uplinjanja premoga z vidika večje uporabnosti energetskih virov v Srbiji z uporabo podzemnega uplinjanja premoga (PPP)

David Petrović[1], Duško Đukanović[2], Miodrag Denić[3,*]

[1]4D KONSALTING, Beograd, Srbija
[2]PEU Resavica, Biro za projektovanje Beograd, Makedonska 33, Beograd, Srbija
[3]JP PEU Resavica, Petra Žalca 2, Resavica, Srbija

*Corresponding author. E-mail: miodrag.denic@yahoo.com

Received: May 25, 2009 **Accepted:** November 4, 2009

Abstract: Taking into account the quantity and quality of energy resources which are available, especially the growing need for more cost-effective use of primary energy resources (therefore, not only of secondary), we are now in the position to conquer the technology of exploitation of out-of-balance reserves, as well as of mining residues from the balance reserves. The method without alternative for such coal reserves is underground coal gasification (UCG).
In opting for activities in that respect the most important thing is the approach to the most possible reasonable choice of optimal location for UCG. Apart from that, it is necessary to envisage the quantities of coal which could be gasified and thereby to define the amount of total gas produced from UCG.

Izvleček: Ob upoštevanju kvantitete in kvalitete energetskih virov, ki so nam na voljo, posebej še, ob upoštevanju naraščajočih potreb po bolj cenovno uspešnem izkoriščanju primarnih virov energije (torej, ne samo sekundarnih), smo sedaj v stanju, da uporabimo tehnologijo pridobivanja zunaj bilančnih rezerv, kakor tudi ostankov rudniških bilančnih rezerv. Metoda, ki v primeru premoških rezerv nima alternative, je podzemno uplinjanje premoga (PPP).

Original scientific paper

Pri izbiri aktivnosti v tej smeri je najpomembnejše določiti optimalno lokacijo za uporabo metode (PPP). Ne glede na to, je neobhodno oceniti količino premoga, ki bi lahko bil uplinjen in s tem oceniti skupno količino proizvedenega plina z metodo (PPP).

Key words: energy resources, underground coal gasification (UCG)
Ključne besede: energetski viri, podzemno uplinjanje premoga (PPP)

Introduction

Having in mind that according to researches conducted so far, our country posesses very small amount of oil and natural gas as compared to its need, the necessity of continuous study and development of more complex technologies of coal usage, on order for our industry to be less dependant on imports of energy and energetic raw materials. Since better quality coal is located deeper under the ground, and is therefore more suitable for underground exploitation, it is logical that certain cases should be treated with corresponding methods, although any form of exploitation would eventually yield 30–40 % of coal.[5]

Along with other difficulties that underground coal mines have to face, these methods prove themselves non-profitable more than often, and the mine would simply be put out of comission. Does it always have to be this way? These significant amounts of coal (60–70 %) that are being left behind, with some layers of coal that have not even been treated, don't seem to have any significance to anyone. That could be well understood in case that energetic resources are abundant, so there would be no concern for the future and its generations.[3]

This could also be acceptable if there were no alternatives for coal exploitation. These alternatives have been an interesting subject of study from time to time, but a broader social and expert interest for realisation of these ideas, which were a subject of many studies, was not present.

If suitable comparative parameters of conventional underground exploitation related to possible underground gassification of certain coal site [1] are to be examined, and especially if the site in question is an unprofitable one, the preference would be more than obvious. Also, on of the alternatives is, in some cases, gassification and retorting of shale, which has already been written and discussed, but all activity has ended there.

Why UCG?

Considering significant non-balance reserves and spoil debris of balance reserves in Serbia, a question stands for a long time about our energetic tomorrow. With such intensity of reserve spending and with a very poor employment of coal layers, the possibility of exploitation of such reserves poses itself as an inevitability.[4]

The fundamental energetic resource of Serbia is coal: lignite with favorable characteristics for surface exploitation and brown and stone coal deeper underground, whose exploitation is only possible in pits. The non-balance of significant amount of reserves has mostly been determined because of technological and economic unduliness of existing unconventional exploitation.

From our industrial and strategic point of view, it is very important for these reserves to be valorized, seeing that they are very significant. That would improve the country's situation concerning energy and lower import dependency. Thus, the technology of conversion of coal into gas fuels using the UCG is an achievement that opens the door not only to cheaper production of energy, but also to partial substitution of natural gas and fuel oil imports. From the perspective of country's energy strategies, by converting coal into gas fuels and by rationalizing energy consumption, this is the fastest and surest way of solving current energetic problems in the country.

Therefore, it is time to treat the problem of poor rationalization of coal production (i.e. taking the energy resources away from nature) in this manner, and not only the problem of rational use of energy created by coal treatment (e.g. electric energy).

The parameters by which determining whether or not a certain coal site is suitable for underground gasification are influenced, are, among many, the following: coal reserves (non-balanced and spoil debris of balanced reserves), maximum depth, thickness, angle of repose as well as ash, humidity and coal particles.

From this point of view, some general assumptions are important, such as:[2, 7, 8]

- With mines with sufficient reserves, facilities and tradition, it is important to determine is the underground gasification planned.
- Mines that can develop normally, as in the previous case, with a difference that their raw material basis demands additional investigation, based on which a decision could be made for their further development.
- Mines whose raw material basis is limited, and a limitation for coal marketing, must reorient their production and cease their previous

activities, as soon as reserves are depleted.
- Mines without larger perspective and mosty of local importance – the factors of exploitation are such that underground exploitation does not give assurance concerning profitability and work safety, and does not offer anything new technology-wise, although their coal reserves may be very significant.

UCG has a range of advantages over convntional underground exploitation:
- Lesser cost of building of an UCG station than a conventional pit
- Productivity is increased several times
- The price of final product per unit is lesser than the same unit made by pit exploitation
- UCG does not involve hard and dangerous work like conventional exploitation does
- Transport, loading and unloading of coal and other materials are not present as with conventional exploitation
- Ash and slag remain underground so there is no transport and therefore no environment and atmosphere pollution
- The UCG method is suitable for sites with difficult geological conditions, which are not suitable neither for underground nor surface exploitation.

Identification of JP PEU coal sites from the aspect of possible implementation of UCG

Balanced reserves of all types of coal on sites that are not being actively exploited and all coal types could be exploited by UCG, are shown in the following tables and diagrames.[4]

Comparative analysis of technical, physical and mechanical characteristics of coal on treated sites

The analysis is related to specific technical, physical and mechanical parameters of coal types in question such as:
- Reserve category (A,B,C)
- thickness
- max depth
- coal humidity
- ash level
- vaporizing materials
- lower heat power of coal (DTE/H_d).

This analysis is made by using the data from table 4, while table 5 will address:
- tectonics
- gas surface protruding protection
- hydrogeological properties
- site status (SAE / VE)
- necessity of land purchase
- number of gas consumers.

Table 1. UCG applicable stone coal reserves

Basin-pit	Balanced (10^3 t)	Non-balanced (10^3 t)	Total (10^3 t)	Rank
Vrška Čuka	2.361,230	350,000	3.711,230	4
Rtanjski Basen	1.598,000	-	1.598,000	5
Ibarski Basen	2.632,540	1.223,980	3.856,520	3
Mlavsko Pečki	-	6.100,000	6.100,000	2
Nova Jerma	12.290,000	-	12.290,000	1
Dobra Sreća	-	500,000	500,000	-
Podvis	-	500,000	500,000	-

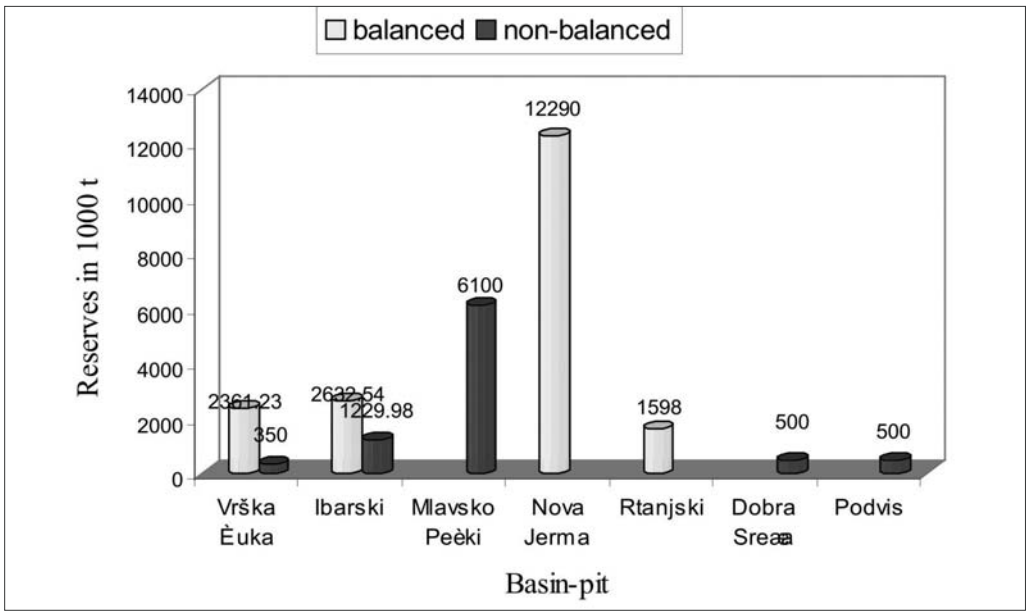

Figure 1. UCG applicable stone coal reserves

Tabela 2. UCG applicable brown reserves

	Basin-pit	Balanced 10^3 t	Non-balanced 10^3 t	Total 10^3 t	Rank
SAE	Rembas	12.207,33	540,06	12.747,39	3
	Bogovina	2.058,26	1.897,19	3.955,45	6
	Sokobanja	58.127,96	2.763,27	60.891,23	1
VE	Aleksinac	12.320,19	15.195,43	27.515,62	2
	Jankova Klisura	3.795,00	2.416,00	6.211,00	4
	Nova Manasija	3.351,00	934,00	4.285,00	5
	Jelašnica	-	1.800,00	1.800,00	-
	Vrdnik	-	588,00	588,00	-
Total (SAE+VE)		91.859,74	26.133,95	117.993,69	-

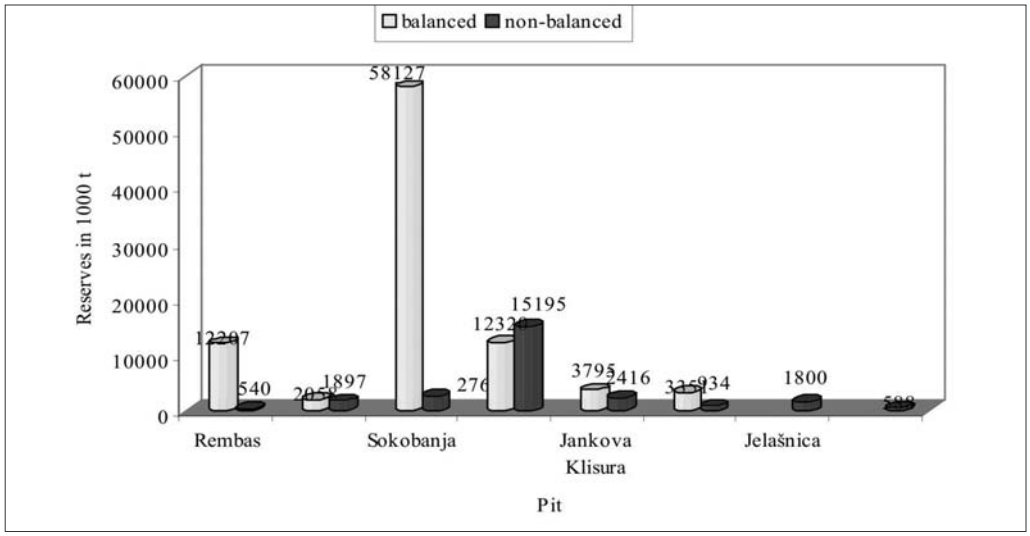

Figure 2. UCG applicable brown reserves

Table 3. UCG applicable brown-lignite reserves

	Basin - pit	Balanced 10^3t	Non-balanced 10^3t	Total 10^3t	Rank
SAE	Lubnica basin	13.591,190	2.319,630	15.910,820	4
	Sjenica basin	187.086,180	7.709,550	194.795,730	1
VE	Despotovac basin	27.956,970	684,480	28.641,450	3
	Melnica	39.537,400	-	39.537,400	2
Total (SAE + VE)		268.171,740	10.713,660	278.885,400	-

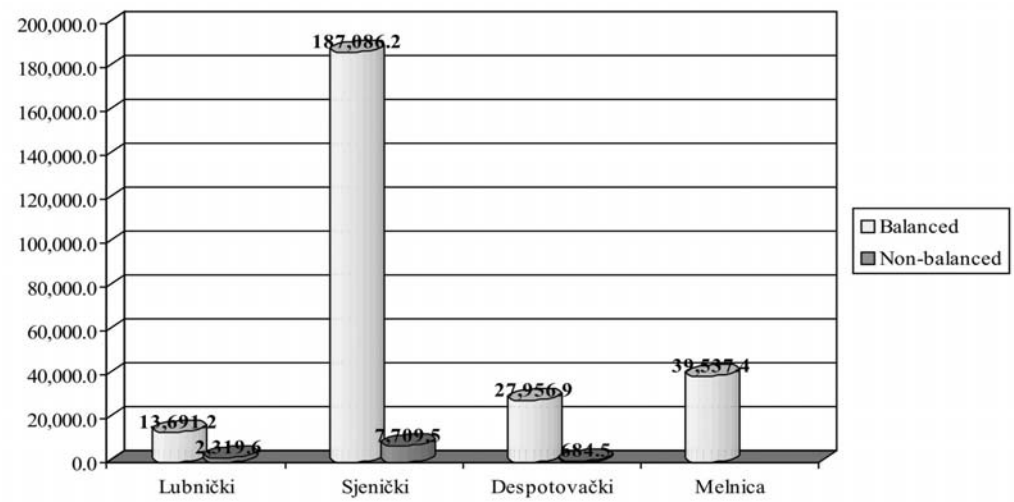

Figure 3. Reserves of brown-lignite coal for UCG

Table 4. Comparative analysis of internal technica, physical and mechanical parameters

Site/ Basin / Parameters	NOVA JERMA **(SC-VE)**	MLAVSKO-PEČKI **(SC-VE)**	IBARSKI BASEN **(SC-SAE)**	VRŠKA ČUKA **(SC-SAE)**	SOKOBANJSKI BASEN **(BC-SAE)**	ALEKSINAČKI BASEN **(BC-VE)**	REMBAS **(BC-SAE)**	JANKOVA KLISURA **(BC-VE)**	SJENIČKI BASEN **(B/LC-SAE)**	MELNICA **(B/LC-VE)**	DESPOTOVAČKI BASEN **(B/LC-VE)**	LUBNICA **(B/LC-SAE)**
Reserves (B+VB+POT.) 10^3 t	**12.290**	**6.100**	**3.856,52**	**8.717,23**	**60.891,23**	**37.515,62**	**27.747,39**	**6.211**	**244.795,73**	**49.537,40**	**48.641,45**	**15.910,19**
Thickness m	**2÷8** +	**2÷5** +	**1,2÷20** +	**>0,5-5** +	**20÷30** +	**5÷7** +	**1÷20** +	**2÷9** +	**10÷14** +	**5÷7** +	**2÷8** +	**4÷10** +
Max depth m	**300÷700** +	**300** +	**100÷900** +	**300÷600** +	**400÷700** +	**500÷700** +	**150÷400** +	**150÷300** +	**150÷300** +	**50÷360** +	**80÷250** +	**150÷300** +
Coal humidity W %	**4,90** +	**3,87** +	**0,6÷6,35** +	**0,96** +	**19,22** +	**10,01** +	**6,20÷21,35** +	**22,50** +	**30,85** +	**26,8÷31,4** +	**24,08** +	**26,43** +
Ash quantity p %	**35** +	**35** +	**16÷59** -	**13,19** +	**11,83** +	**23,16** +	**9,12÷13,72** +	**24,00** +	**11,90** +	**17,6÷25,4** +	**13,82** +	**16,34** +
Vaporizing mat. %	**14,25** +	**26,7** +	**16÷30** +	**8,82** +	**36,52** +	**42,79** +	**32,19÷36,52** +	**27,20** +	**32,31** +	**26,82** +	**25,69** +	**33,94** +
DTE/H_d kJ/kg	**22.500** +	**21.000** +	**18.000÷ 24.000** +	**29,73** +	**18.964** +	**19.974** +	**18.490÷ 19.473** +	**19.200** +	**14.134** +	**11.637** +	**11.858** +	**14.681** +
Angle of repose °	**10÷40** +	**15÷22** +	**10÷40** +	**20÷45** +	**40÷50** +	**10÷30** +	**5÷30** +	**15÷30** +	**5÷20** +	**15÷30** +	**12÷25** +	**10÷20** +

Note: Plus sign marks every data that is within favourable limits for UCG implementation; minus sign marks data that are out of such limits

Table 5. Comparative analysis of external influences

	Reserves points (1÷4)	**Tectonics** points (1÷2)	**Hydrogeol.** points (1÷3)	**Natural gas protection** points (1÷3)	**Land Purchase** YES NO -2 +2 (points)	**Gas consumers** existing potential (3) (1÷2)	**Total** points
NOVA JERMA (SC-VE)	4	1	2	2	-2	1	8
MLAVSKO-PEČKI (SC-VE)	3	1	2	2	-2	1	7
IBAR BASIN (SC-SAE)	2	2	2	2	+2	2	12
VRŠKA ČUKA (SC-SAE)	1	1	3	1	+2	1	9
SOKOBANJA BASIN (BC-SAE)	4	1	2	2	+2	1	12
ALEKSIN. BASEN (BC-VE)	3	2	3	2	+2	2	14
REMBAS (BC-SAE)	2	2	3	2	+2	2	13
JANKOVA KLIS. (BC-VE)	1	2	2	2	-2	1	6
SJENICA BASIN (B/LC-SAE)	4	2	1	2	+2	1	12
MELNICA (B/LC-VE)	3	1	3	2	-2	2	9
DESPOTOV. BASEN (B/LC-VE)	2	2	3	2	-2	2	9
LUBNICA (B/LC-SAE)	1	2	3	3	+2	1	12

By analysing this data, one comes to a concslusion that selected mines meet the criteria for implementation of UCG, with the exception of Ibar stone coal mines which have 50 % larger quantities of ash that the allowed bottom level. But, this information (59 % of ash) does not relate to all sites, but

only the Progorelica site, while Jarando, Tadenje and Ušće meet the above criteria.

It is imperative to emphasize that data from this table is different in three cases from those in tables 1 and 2, because in this table, potential coal reserves data for Vrška Čuka, Soko Banja, Aleksinac, Rembas, Sjenica, Melnica and Despotovac basins has been added, based on reserve situation data of PE PEU from the beggining of 2007.

As far as coal thickness is concerned, values are also favourable (it is profitable to gasify layers from 0.6 m thickness onward), as well as for coal humidity, and especially angles of repose.

Based on knowledge of problems concerning UCG and based on values of these parameters, a preliminary ranking list of UCG suitability has been made, but only taking into consideration the data from this table (a final list is given in section 3.3, after table 6).

As far as the status of treated sites for UCG implementation goes, a point system has been made based on tectonic influences, hydro geology etc. Such system is also being used worldwide (it is necessary to emphasize that in cases where land property purchase is necessary, negative points have been given because of increase of investment costs).

Based on the data from these two tables, a final list can be made for possible implementation of UCG on certain coal sites.

Available energetic potential of certain sites in relation to possible UCG implementation

If by available reserves we mean the quantities in current balanced reserves and complete non-balanced reserves, by taking experiences from all over the world into consideration, where 'endangered' quantities have been used between 72 % and 96 %, we can assume that 80 % is a reasonable average, and can therefore determine available energetic potentials for the mines in question (RASENPOT).

Of course, SAE (with active exploitation) and VE (without exploitation) mines will also be considered with their balanced and non-balanced reserves, i.e. 80 % out of those (it is clear that all available energetic potentials for UCG would be even larger if potential reserves should be brought into consideration, but not for now).

RANKING OF SUBTERRANEAN EXPLOITATION BASED ON UCG SUITABILITY CRITERIA

In table 6, in each of 4 SC trestles points from 1 through 4 have been assigned based on given RASENPOT; it is similar for dark and lignite coal (therefore, each group has been assigned points 1 through 4).

Based on table 5 and data from table 6, a final ranking of suitability of treated trestles can be made. Table 7, which follows,

Table 6. Available energetic potentials of some sites in PE

Basin/site	80 % (BIL+VB) t	Heat power H_d/(kJ/kg)	Available en. pot. RASENPOT, GJ	teu	mld kW h	Rank
SC-VE **NOVA JERMA**	9.832.000	22.500	221.220.000	7.547.595	61,45	8.
SC-VE **MLAVSKO-PEČKI**	4.880.000	21.200	103.456.000	3.529.717	28,74	10.
SC-SAE **IBAR**	3.085.216	21.000	64.789.000	2.210.474	18,00	5.
SC-SAE **VRŠKA ČUKA**	2.168.984	29.730	64.484.000	2.200.068	17,91	11.
BC-SAE **SOKOBANJA**	48.712.984	18.904	920.870.000	31.418.287	255,81	2.
BC-VE **ALEKSINAC**	22.012.496	19.974	439.678.000	15.000.955	122,14	1.
BC-SAE **REMBAS**	10.197.912	19.000	193.760.000	6.610.713	53,82	4.
BC-VE **JANKOVA KLISURA**	4.968.800	17.500	86.954.000	2.966.700	24,15	12.
B/LC-SAE **SJENICA (ŠTAVALJ)**	155.836.584	15.000	2.337.549.000	79.752.610	649,35	3.
B/LC -VE **MELNICA**	31.629.920	11.637	368.077.000	12.558.069	102,25	7.
B/LC -VE **DESPOTOVAC**	22.913.160	12.000	274.958.000	9.381.030	73,38	9.
B/LC -SAE **LUBNICA**	12.728.656	15.000	190.930.000	6.514.159	553,04	6.

1teu = 2,931 × 10^{10} J =29,31 × 10^{9} J =29,31 GJ = 8,142 × 10^{3} kW h = 8,142 MW h

quantities of gas at normal conditions (m^3) that could be obtained from available coal for UCG (column 1, table 6).

World experiences point that quantity of gas yielded from 1kg of coal depends on its heat power and varies

Table 7. Ranking of trestles according to UCG suitability

Rank	Basin/trestle	Points (tab.5+6)	RASENPOT mil. GJ		mld. kW h		Quantity of gas mld. m^3	
			SAE	VE	SAE	VE	SAE	VE
1.	ALEKSINAC (BC-VE)	14 + 3 = **17**		439,68		122,14		38,5
2.	SOKOBANJA (BC-SAE)	12 + 4 = **16**	920,87		255,81		85,5	
3.	SJENICA (B/LC -SAE)	12 + 4 = **16**	2.337,55		649,35		152	
4.	REMBAS (BC-SAE)	13 + 2 = **15**	193,76		53,82		18	
5.	IBARSKI (SC-SAE)	12 + 2 = **14**	64,79		18,00		8	
6.	LUBNICA (B/LC -SAE)	12 + 1 = **13**	190,93		53,04		12,5	
7.	MELNICA (B/LC -VE)	9 + 3 = **12**		368,08		102,25		31
8.	NOVA JERMA (SC-VE)	8 + 4 = **12**		221,22		61,45		24
9.	DESPOTOVAC (B/LC -VE)	9 + 2 = **11**		274,96		73,38		22
10.	MLAVSKO-PEČKI (SC-VE)	7 + 3 = **10**		103,46		28,74		12
11.	VRŠKA ČUKA (SC-SAE)	9 + 1 = **10**	64,48		17,91		5,5	
12.	JANKOVA KLIS. (BC-VE)	6 + 1 = **7**		86,95		24,15		9
TOTAL		**SAE**	**3772,38**		**1047,93**		**281,5**	
		VE		**1494,35**		**412,11**		**136,5**

Legend (marks): JPPEU-Public enterprise for underground coal exploitation; B/L-brown-lignite coal, SC-VE- stoun coal-withoau exploitation; SC-SAE- stoun coal-with active exploitation; BC-VE- brown coal without exploitation; BC-SAE- brown coal-with active exploitation; B/LC-VE- brown-lignite coal without exploitation; B/LC-SAE-brown-lignite coal-with active exploitation; RASENPOT- available energetic potentials.

from 1.5–5.5 m^3/kg. For stone coal this value is 3.5–5.5 (let's say 3.80), for lignite 2.5–4 (let's say 2.70), and for dark lignite 1.5–2.5 (let's say 1.5 m^3/kg). If gas usage ratio (on conversion of coal to gas) is 65 %, then (for example, Aleksinac lignite):

$m_g = 22 \times 10^{-3}$ mld t × 2700 m^3/t × 0.65 = 38.5 mld. m^3 of gas at normal conditions.

CONCLUSION

When overwieving the data from previous tables one can conclude that Ibar mines, although suitable for UCG, couldn't be of special interest fot UCG because of small amounts of gas expected with applyng the UCG. The quantities of coal that would be gasified are not very significant. Their status would therefore remain unchanged.

Other mines named in the table could yield billions of m^3 of gas - SAE as well as VE. Aleksinac is of special interest, because of the following:

- It has been VE for years, almost forgotten
- Large quantities of high-quality coal (38.5 billion m^3) would be an embarassment if neglected.

In addition to this information, cogenerator power plant Sokolov in the Czech Republic produces one billion m^3 of gas out of 400 MW (electr.) a year in a surface gas generator (surface gasification is more expensive than subterranean). Ten percent of natural gas is also being used for 'straightening out' encumberance.

Mines with underground exploitation are short-lived. A period of a few decades passes quickly. At that point, there is no use to wondering about solutions.

Direkcion next activities connected for Aleksinac mine (as first ranking-table 7.) are show through:

- By re-activating the mine, significant quantities of abandoned coal could be used, with all well known energetic, ecological and economic effects and advantages
- It would be a massive opportunity for employment and the city of Aleksinac would be moved away from idleness that has been going on since the last tragic accident at the end of 1980s
- Other mines, that have been closed because of non profitable underground exploitation, could follow suit
- Gas obtained in this way could be used for power plants (existing, as well as purposely built) and therefore lower the dependancy on imported energy resources
- It the case of Aleksinac mine, the

gas could be used to heat the city itself, but also Niš and Kragujevac. It could used as well as a technological gas, and the building of a special gas powered power plant would be justifiable, and eventually a co-generated power plant (this is justified by enormous amounts of UCG yielded gas, which has been presented earlier).

After realized results in Aleksinac mine, similar activites it could be expected and developing in other deposits.

References

[1] Dunajewski, J. (1984): *Przeplyw ciepla i masy u procesie podziemnego zgazowania wegla*, Gliwice, str.1–8.

[2] Krejnin, E. V.(1982): *Podzemna gasifikacija ugljenih slojeva*, ''Nedra'', Moskva, 250 p

[3] Medved, M., Dervarič, E., Skubin, G. (2008): Premog in njegova vloga v EU ter na področju JV Evrope. V: *Prihodnost energije : nafta - vpliv cen na energetsko politiko in gospodarstvo : ali bomo zaslužili ali plačali: (16. septembra 2008)*. Ljubljana: Planet GV, 2008, str. 28–39.

[4] Palarski, J. (1986): *Gas and heat transport in the underground coal gasification*, Symposium UCG, Saarbricken, 6 p.

[5] Petrović, D. (1988): *Izučavanje primjene PGU kod vanbilansnih rezervi uglja na području SB ugljenog basena*, Disertacija, Tuzla.

[6] Petrović D., Ivković M., Denić M., Dragosavljević Z. (2008): *Studija identifikacije i klasifikacije podzemnih ležišta uglja u Srbiji sa aspekta moguće primene PGU*, "4D KONSALTING" Bg i JP PEU Resavica. 140 p.

[7] Vižintin, G. et al. (2008): Advance 3D finite elements modelling of groundwater drawdown in Velenje coal-mine=Napredno 3D modeliranje odvodnjavanja spuštanjem nivoa podzemnih voda-primenom metode konačnih elementa u rudniku uglja Velenje. V: VIDANOVIĆ, Nebojša (ur.), TOKALIĆ, Rade (ur.). Zbornik referatov. Beograd: Univerzitet u Beogradu, Rudarsko-geološki fakultet, str. 21–27.

[8] Vižintin, G. et al. (2008): Using virtual tools for 3D oil and gas presentations= upotreba virtuelnih alata za 3D prezentacije nafte i gasa. V: RISTOVIĆ, Ivica (ur.). Savremene tendencije u razvoju energetskog rudarstva: zbornik radova = proceedings. Beograd: Rudarsko-geloološki fakultet Univerziteta, str. 220–230.

Differential thermal analysis (DTA) and differential scanning calorimetry (DSC) as a method of material investigation

Diferenčna termična analiza (DTA) in diferenčna vrstična kalorimetrija (DSC) kot metoda za raziskavo materialov

Grega Klančnik[1,*], Jožef Medved[1], Primož Mrvar[1]

[1]University of Ljubljana, Faculty of natural science and engineering, Department of materials and metallurgy, Aškerčeva 12, SI-1000 Ljubljana, Slovenia

*Corresponding author. E-mail: grega.klancnik@ntf.uni-lj.si

Received: August 17, 2009 **Accepted:** December 8, 2009

Abstract: Thermal analysis is used to establish thermodynamic properties which are essential for understanding the behavior of material under different heating and cooling rates, under inert, reduction or oxidation atmosphere or under different gas pressures. Thermal analysis comprises a group of techniques in which a physical property of a substance is measured to a controlled temperature program. In this paper only two methods are presented: differential thermal analysis (DTA) and differential scanning calorimetry (DSC). The results given from the DTA or DSC curves depend on the preparation of the material, and on the instrument sensitivity. The sensitivity is in close relation to the apparatuses design. Several types of DTA and DSC apparatuses are described as well as the use. New types of DSC devices are being developed which will have the capability of high heating / cooling rates and with shorter response time.

Izvleček: Termična analiza podaja termodinamske lastnosti materiala, ki so pomembne za razumevanje vedenja materiala pri različnih segrevalnih in ohlajevalnih hitrostih, bodisi v inertni, redukcijski ali oksidacijski atmosferi ali pri različnih tlakih. Termična analiza združuje skupino tehnik, kjer je preiskovan vzorec izpostavljen kontroliranemu temperaturnemu programu. V tem članku sta predstavljeni le dve metodi: diferenčna termična analiza (DTA) in simultana termična analiza (STA). Rezultati so bolj ali manj odvisni od priprave

Professional Paper

vzorca in nazadnje tudi od občutljivosti naprave. Občutljivost merjenja je v ozki povezavi s konstrukcijo naprave. V tem članku so opisani različni tipi DTA- in DSC-naprav ter možna uporaba le-teh. Novi tipi DSC-naprav se razvijajo v smeri visokih hitrostih segrevanja in ohlajevanja z majhnimi odzivnimi časi.

Key words: DTA, DSC, thermal analysis
Ključne besede: DTA, DSC, termična analiza

Introduction

Thermal analysis (TA)

Thermal analysis comprises a group of techniques where the properties of material are studied as they change with temperature. To determine the thermo-physical properties several methods are commonly used: differential thermal analysis (DTA), differential scanning calorimetry (DSC), thermogravimetric analysis (TGA), dilatometry (DIL), evolved gas analysis (EGA), dynamic mechanical analysis (DMA), dielectric analyse (DEA) etc. In metallurgy, material science, pharmacy and food industry the main application of the DTA and DSC is used for studying phase transition under different atmospheric influences, temperatures and heating / cooling rates. Common laboratory equipment has a combination of two thermal analysis techniques. Most common is the simultaneous thermal analysis (STA) apparatus as the combination of thermogravimetric analysis (TGA) and differential thermal analysis (DSC).

Definitions of DTA and STA methods

The two methods (DTA and DSC) are defined as followed:

Differential thermal analysis (DTA): Thermal analysis using a reference. The sample and the reference material (sample) are heated in one furnace. The difference of the sample temperature and the reference material temperature is recorded during programmed heating and cooling cycles.[1]

Differential Scanning Calorimetry (DSC): Differential Scanning Calorimetry (DSC) measures the change of the difference in the heat flow rate to the material (sample) and to a reference material while they are subjected to a controlled temperature program.[1]

Like differential thermal analysis (DTA), differential scanning (DSC) is also an alternative technique for determining the temperatures of the phase transitions like melting point, solidification onset, re-crystallization onset, evaporation temperature etc. With differential thermal analysis DTA, which

is an older technique than differential scanning calorimetry, the result is a DTA curve (Figure 1b). DTA curve is a curve of temperature difference between the sample material and the reference material versus temperature or time. The result of DSC is a curve of heat flux versus time or temperature and is therefore used also for determination of the enthalpy, specific heat (c_p) etc.[2] Heat flow rate signal (DSC signal) is internally calculated from the temperature difference between the sample material and the reference material. The important difference between DSC and DTA equipment is that the latter is mostly used for the qualitative measurements and it is more robust because of less sensitive materials used for sample holders, heat conduction path etc. The sample holder in the DTA apparatus is much cheaper than the sample holder in the DSC apparatus and is recommended for the investigation of materials with an unknown relation to contamination between the crucible and the sample holders. Sample holders are commonly made of Al_2O_3 with integrated thermocouples. In the case of DSC the technique is more sensitive and allows several modifications which make it possible to measure the thermal conductivity, evolved gas analysis, thermogravimetry and activation energy for the grain growth, precipitation, etc. Sampler holders are commonly made of platinum.

It is typical for the DTA that the sample and the reference material are under identical temperature regime. This is not true in the case of the DSC method. In this case the method with two furnaces can also be used (Power compensation DSC).

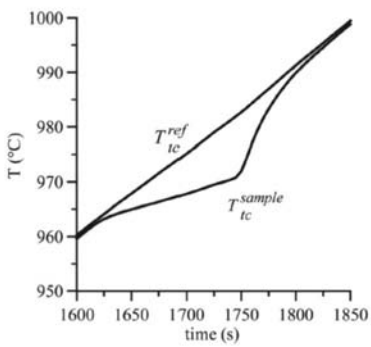

(a)

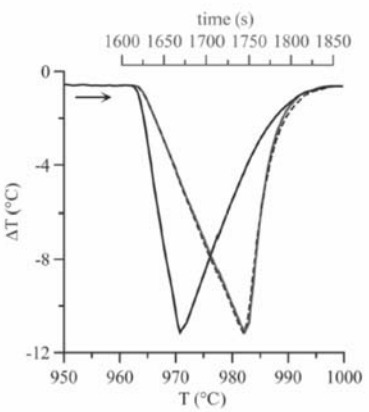

(b)

Figure 1. DTA heating curve for pure Ag (10 K/min): the sample and the reference temperature (a) and DTA signal as dependence of time and temperature (b)

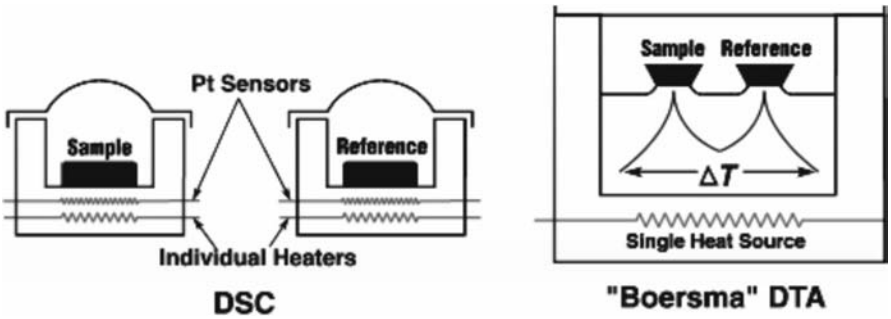

(a) (b)

Figure 2. Shematic layout of the DSC apparatus: PC-DSC (a) and quantitative (Boersma) DTA or HF-DSC[3] (b)

Two basic types of Differential Scanning Calorimetry (DSC) must be distinguished: the heat flux DSC and the power compensation DSC. Sometimes a third basic type is also distinguished called the Hyper DSC which is an apparatus for rapid solidification based on power compensation DSC. Figure 2 represents both basic types of DSC apparatuses.

The power compensation DSC or PC – DSC has an individual heater for each chamber (figure 2 a). In the case of the heat flux or HF – DSC, both the sample and the reference material are inside the same furnace. The HF - DSC is also known as a type of Boersma DTA. The PC – DSC is more effective because the time constants (characteristic response time) are shorter. The characteristics of each device can be described with three characteristic times:

$$t_{S,C} = m_C C_p^C / h_{S,C} A_{S,C} \quad (1)$$

$$t_{W,C} = m_C C_p^C / h_{W,C} A_{W,C} \quad (2)$$

$$t_{S,C} = m_T C_p^T / h_{T,C} A_{T,C} \quad (3)$$

Where:

$t_{S,C}$, $t_{W,C,}$ $t_{T,C}$ – characteristic times for the heat flow between the metal sample and the crucible cup, the furnace wall and the crucible cup, the thermocouple and the crucible cup

$h_{T,C}A_{T,C}$, $h_{W,C}A_{W,C}$, $h_{S,C}A_{S,C}$ - products of heat transfer coefficient and areas of heat flow

m_C, m_T – mass of the crucible (C) and the thermocouple (T)

C_P^c, C_P^t - heat capacity (J/K)

DIFFERENTIAL THERMAL ANALYSIS (DTA)

Differential thermal analysis (DTA) was constructed soon after the development of the thermocouple (1887, Le

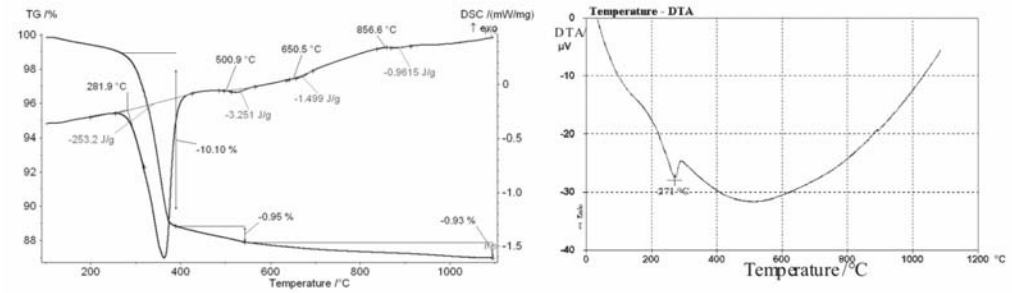

(a) (b)

Figure 3. DSC/TG heating curve (a) and DTA heating curve for the limonite (b)

Chatelier). It was made for the examination of different materials. Most of the research efforts were made on clay and carbonate materials. The limitation in the DTA apparatuses is its sensitivity. This is shown by the next mineral called limonite. The difference in the DTA and DSC heating curves are represented in figure 3.

In figure 3 a at least three separate decompositions were determined by the DSC and TG curve. The DTA curve showed only one because the quantity of the released heat was too small to be detected.

Nevertheless, the DTA curves can record the transformations where the heat is either absorbed or released (dehydration, decarbonation, burning of materials, ordering etc.). DTA is helpful for better understanding of given results by x-ray diffraction, chemical analysis and microscopy.[4]

The most important advantages of the DTA are its simplicity and a possibility to create different experimental conditions (high pressure or vacuum).

DTA can also be used for quantitative measurements (enthalpy measurements). The DTA has advantages over DSC because it allows simultaneous recording of changes in the sample mass, while DSC requires a constant mass during the enthalpy change measurement. DSC directly measures the energy change of a sample while DTA measures the temperature difference between the reference and the sample, which is converted to enthalpy change (ΔH) through conversion factors (which are difficult to determine). The enthalpy calculation with DTA is done using the mass difference baseline method. An inert sample must be used (e.g. sapphire) for estimating the conversion factors K1 and K2. The relation for estimating the conversion

factors is represented with equation 4:[5]

$$\frac{dH}{dt} = K1K2\frac{(DTA1 - DTA2)}{(ms,1 - ms,2)} \quad (4)$$

Where;
$K1$ – determined by the heat transfer from the furnace to the sample – depends on the heat transfer coefficient α_s (by fixed operation conditions it is estimated to be temperature independent)
$K2$ – apparatus related parameter (temperature dependent)
$DTA1 - DTA2$ – the area between two DTA curves
$m_s,1$; $m_s,2$ – mass of the inert sample
dH/dt – specific heat capacity of the sample (sapphire)

Because the DTA allows the sample mass loss during the measurement, it is considered useful for the materials with intensive decomposition (elastomers, exothermic materials etc.). As already discussed the classical DTA apparatus, because of inexpensive materials (main elements are mostly made of ceramics) used, more volatile and reactive systems can be analyzed. Temperature regions are commonly up to 1500 °C with heating and cooling rates up to 50 K/min. Crucibles are mostly made of Al_2O_3, platinum or graphite with 85 µL volumes or less. Different atmosphere can be used. When decomposition of clays or other decompounding samples is analyzed, the measurements are often done under an oxidation atmosphere. High performance modular DTA are DTA systems with widest temperature range –150–2400 °C. Crucibles here are made of tungsten or graphite. It is important to use inert atmosphere to prevent degradation of the crucibles.

Micro differential thermal analysis (µ-DTA)

Just like classical DTA, the DSC also has the same disadvantages, especially when bigger masses are used. With heavier loads the responding time is longer and the interpretation of such a curve is more difficult. A new device called µ-DTA was developed, presented in figure 4.[6]

The sample masses are around 50 µg. Minimum load depends on the system itself and on the type of the sample. Literature (Senesac, Yi etc. [7]) also describes a load of 600×10^{-12} g of explosive adsorbed molecules with characteristic responce time 50 ms which is extremely low and makes this system special than the others.[7]

The system consists of two micro hotplates with two integrated heaters (figure 4) to ensure a homogenous temperature distribution. The wetting of the membrane surface is the most important characteristics to ensure an optimal heat transfer. Integrated TiW thermistors are used for the temperature measurement and are located under the specimen. One

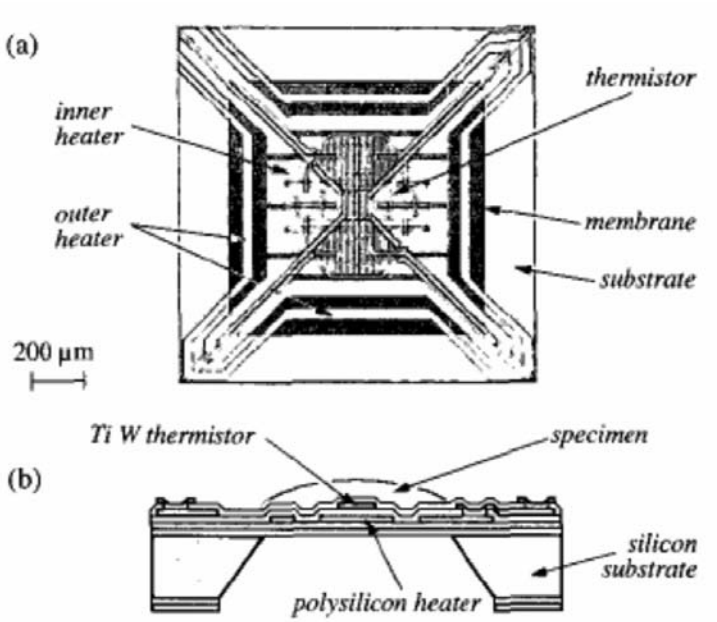

Figure 4. Schematic representation of µ-DTA: optical micrograph of a membrane with inner and outer polysilicon heaters and central TiW thermistor (a) and schematic cross section of the membrane with melted specimen (b) [6]

of the membranes is used as a reference. [6] A big disadvantage of this method although that it is not possible to process metals because of high specific surface tension (small or no wetting of the membrane), is high oxidation process caused by high specific surface of the sample. For this system it is necessary not to use oxidising atmosphere. Many apparatuses are used for differential thermal analysis of frozen food systems, especially at lower temperatures (down to –180 °C). [8] Classical temperature ranges are between –45 °C and 120 °C (maximum up to 200 °C). Heating cooling rates are up to 2 K/min which is much slower than at the common DTA apparatuses. Also the maximal pressure for this type of design is much lower than at the classic DTA apparatus which is higher than 1 bar.

High pressure differential thermal analysis HP - DTA

Excessive evaporation can reduce the sample mass and change the chemical composition which leads to incorrect measurement of the characteristic temperatures. For studying the thermodynamics of different systems by using different gas pressure, the (high pressure differential scanning calorimetry) HP-DTA apparatuses were designed. Multi component systems can decompose if required gas pressure (normally by using argon) is not as close as possible to the synthesis conditions. Pressure range

for the HP-DTA are often wide up to several hundreds bars, but with a narrow temperature range (–150 °C to 600 °C). Heating and cooling rates are normally around 20 K/min. [1, 9] New apparatuses have heating and cooling rates up to 50 K/min at maximum pressure 150 bar. For understanding phase transitions during high pressure, HP DSC apparatuses were designed with a higher sensitivity.[10] HP-DSC experiments can be performed using 2–4 mg samples sealed in aluminium pans which have better response (as platinum, graphit, gold etc.). Cylindrical tin pans are used for most HP-DTA experiments. The dependence of the melting temperature to the pressure is described by the Clausius - Clapeyron equation:

$$\frac{dP}{dTm} = \frac{\Delta Hm}{Tm \cdot \Delta Vm} \tag{5}$$

Where:
ΔH_m – melting enthalpy
ΔV_m – volume difference between solid and liquid
dP – pressure difference
dT_m – Difference in melting temperatures

Equation 5 states that the melting temperature will change with changing the pressure, which can be determined from the DTA curve. Calculation of the change in the melting enthalpy can be calculated from equation 5. Investigation of the sample can be done under atmospheric pressure or by the hydrostatic pressure were different oils are used as pressure transmitting medium. The electronic pressure control device as well as exact regulation of the purge gas (oil) flow is the main feature for outstanding accuracy and reproducibility of the measurements.

Differential Scanning Calorimetry (DSC)

DSC measures the rate of the heat flow to the sample and the reference. DSC is useful in making the same measurements as DTA and has the capability to measure heat capacities and thermal conductivity. Three basic types of DSC must be distinguished:

- heat flux DSC
- power compensation DSC
- Hyper DSC

The primary measurement signal for all three types is a temperature difference; it determines the intensity of the exchange of the heat between the furnace and the sample-reference part. The resulting heat flow rate Φ is proportional to the temperature difference. In the case of power compensation DSC, the apparatus consists of two identical micro-furnaces, one for the sample and the other for the reference. Both furnaces are separately heated; the sample furnace is heated with a temperature – time program, while the reference furnace tries

to follow this program. This includes increment-decrement of the temperature in the reference furnace, when a reaction takes place. In this case the compensating heating power is measured which is actually the heat flow difference.[12]

One of the problems in measuring the heat flow signal is the artefact, which is related to the instrumentation.[11] When a base line is run, one sees a start-up hook, offset, slope and curvature. An ideal baseline would be flat and without any artefacts. Base line artefacts are inherent in the design and manufacture of DSC instrumentation. Typical artefacts are related to the: crucible moving, sudden change in the heat flow rate between crucible and sensors, high frequency disturbance etc.

Heat Flux DSC

The most fundamental types are:

- The disk type measuring system
- The turret type measuring system
- The cylinder-type measuring system

The heat flux within the DSC takes place via a well defined heat conduction path with a low thermal resistance from furnace to the samples.[12] The disk type measuring system heat exchange takes place trough a disk which is solid sample support. Its features are high sensitivity and small sample volume. With turret type heat exchange takes place via small hollow cylinders which also serve as sample support. The turret type has higher sensitivity and faster response with large heating and cooling rates. Like with the disk type sample volume is small. In the case of the cylinder type measuring system the heat exchange takes place between the (big) cylindrical sample cavities and the furnace with a low thermal conductivity (termopile). Only low heating and cooling rates are possible. The sensitivity per unit volume is high even with a large sample volume. This system has a larger time constant than the first two measuring systems.

The disk type measuring system – Heat flux DSC

Figure 5 represents the Disk type DSC. The disk is designed to act as a sample support and the heat exchange measurement. The main heat flow from the furnace passes symmetrically trough the disk with a medium thermal conductivity; this is its main characteristic.[1] In some cases the disks are made with combination of metal (e.g. platinum) and covered with ceramics.

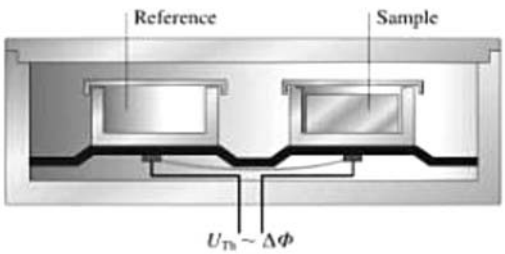

Figure 5. Schematic presentation of the heat flux DSC with a disk type measuring system[12]

In the heat flux DSC the connecting metal strip is often used as a sensor to obtain the temperature difference by measuring the voltage. The heat exchange from the furnace to the sample is limited and it allows only medium heating and cooling rates. Modification of the disk type of DSC is very common. One is HF-DSC with a triple measuring system. With three separate locations the measurement of specific heat is measured with just one run.[1] In the classic HF-DSC device three measurements must be made (with an empty crucible, with a sapphire or a known inert sample and with the investigated sample). Another modification is high pressure HF-DSC, which is used to determine vapour pressures and heats of evaporation.[1]

Typical crucible materials for the DSC apparatuses are made of Al, Al_2O_3, graphite, Y_2O_3, Pt/Rh with Al_2O_3 inside the crucible, gold etc. Different atmospheres can be used. Common heating or cooling rate is 10 K/min. Typical time constant is between 3 s and 10 s which is much longer than with μ-DTA. For special applications (measurement under high pressure) the crucibles are made of stainless steel with a golden cover or titan with 0.19 mL volume.

The Cylinder measuring system – Heat flux DSC

The heat flux DSC operating on Calvet principle is using a cylinder type measuring system by two sintered alumina cylinders set parallel and symmetrical in the heating furnace. The crucible used here is produced from stainless steel.[13] The HF-DSC with the cylinder measuring system is appropriate for large samples. In the case of inhomogeneous alloys large samples are needed because of local differences in the chemical composition. In comparison to micro DTA the characteristic time is much larger, which can cause problems in determining temperatures of small phases with small quantities. In the figure 6, the heat which is conducted to the sample via a large number of thermocouples, changing the sample temperature is shown

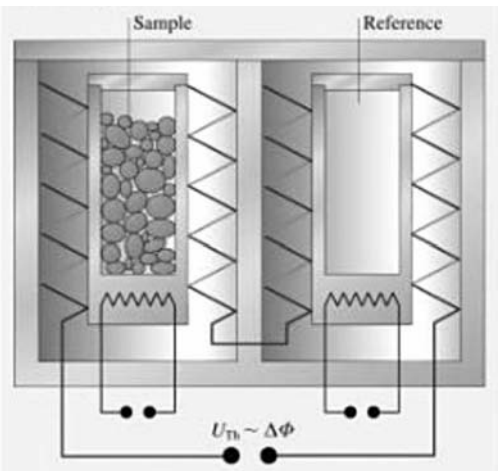

Figure 6. The heat flux DSC with a cylinder-type measuring system (Calvet)[12]

The temperature difference ΔT of both sample containers is generated by differential connection to both thermo-

couples. The problem can appear if the height of a sample is not sufficient enough. Compared with the other apparatuses, the cylinder type has a much larger volume and therefore a longer time constant which can be as long as 40 min. Nevertheless a measurement can also be done in a wide temperature range (–196–1500 °C).[1] Sample volumes of the crucibles are approximately 10 mL larger than those used for classical disk type measuring system. Larger crucibles (100 cm^3) are also used for investigation in biology. These DSC's can usually have the maximum heating rate up to 1 K/min.

Micro differential DSC – modified HF DSC

This method is a combination of an isothermal calorimeter and a HF-DSC mode device. In an isothermal calorimeter, the heat generated by the sample, flows trough the thermal resistance into a water jacket (Figure 7). The temperature difference across the thermal resistance is measured.[3]

Micro DSC has the same ability to measure the thermal properties as an ordinary DSC device. One of the advantages is a very high sensitivity but on the other hand the temperature range is very narrow (–20 °C to ≈120 °C). With this type of device it is ideal to study crystallisation because the cooling and heating rates can be even lower than 0.001 °C/min (with a response time of few seconds) and is also suitable to determine phase transitions like intermediate phases between solid and liquid in Liquid crystals.[15]

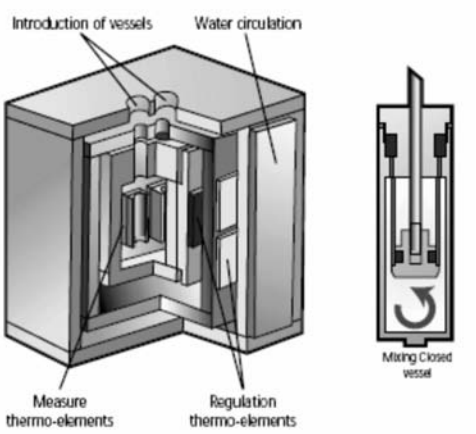

(a) (b)

Figure 7. The heat flux Micro differential DSC: the setup of the device (a) and mixing vessel for determination of the mixture heat (b)

Different vessels are usually needed for the measurement. A special vessel is used for studying the amounts of heat mixture between two liquids or between a liquid and a solid.

The energy of mixing is absorbed or released heat, where the changes in the volume (V) under pressure (p) are negligible ($H = U + pV$). It represents the difference in internal energy (U) before and after mixing.[16]

The mixing vessel is represented in figure 7b. The vessels are made of Hastel-

loy C276 and their volume is 1 cm^3. The measurement of adsorption heat can also be done. With modification this type of DSC can be made into a high pressure micro DSC (HP micro DSC) with maximum pressure of 20 bar. The classical micro DSC like micro DTA apparatuses is applied for 1bar. Modified HF-DSC is a powerful technique, but with existing technology it is limited to heating rates of no more than 5 K/min. As a response to that disability a new Tzero technology was developed with a turret type measuring system.

The turret-type measuring system – HF DSC

Small hollow cylinders are used for sample support and for the heat exchange. The turret type of the HF DSC is represented in figure 8. The turret measuring system is ideal for determining the purity of metals.

This type of the HF-DSC is still one of the options of possible leading DSCs on the market in the future. The advantage of the turret system is in the heat transfer from the jacket to the sample, because it goes through a thin-walled cylinder. This way a very short heat conducting path is achieved. The system is very small thus the characteristic time is very short. No interference between the sample and the reference is present. The turret type is special because of a third thermocouple which measures the thermal inertia. This is a so-called Tzero DSC technology.[1]

The DSC causes the distortion in the DSC curves (in the true shape of the peak) because of a: sample-reference side asymmetry, thermal resistance and thermal capacitance gap of the cell, pan. The temperature reference sensor (figure 9) allows the detection of these effects and they are compensated with an original DSC curve.

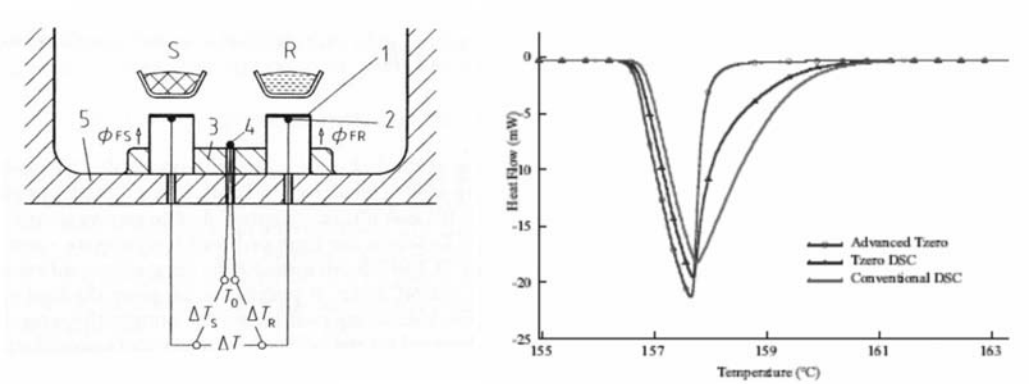

(a) (b)

Figure 8. The turret type measuring system HF-DSC [1] (a) and effect by melting indium[1, 18] (b) specimen[6]

The result is the real (actual) DSC curve (figure 8 b) shown as a dependence of the sample and not of the instrument. [18] Crucibles for this type of DSC (also known as Tzero DSC) apparatuses are made of similar or same material as for the classical DSC apparatuses. This system is relatively new and is due to good results a good competition to the, so far, predominant power compensation DSC and also micro-DSC. New Tzero design is able to detect the glass transition temperature (Tg) of polypropylene, normally not detectable by any current DSC.[19] Heating rates are up to 200 K/min. Theoretically a time constant in this case should be zero but is close to values of the micro DSC and lower.

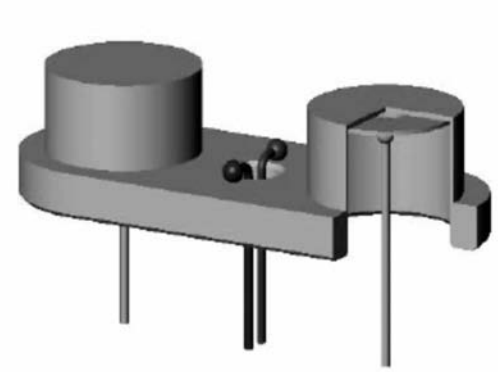

Figure 9. Position of the reference sensor: Tzero™ sensor[17]

Power Compensation DSC

Sample and reference are each held in a separate, self contained calorimeter with its own heater (Figure 10).

The advantage of the PC DSC over the HF-DSC is a very light individual furnace. The power compensated furnaces weigh 1 g. The furnaces for HF DSC weigh up to 200 g.[21] The effect of a low mass furnace is an extremely short responding time. The heating and cooling rates can be up to 500 °C/min. When a reaction appears (exothermal or endothermal) the energy is accumulated or released to compensate the

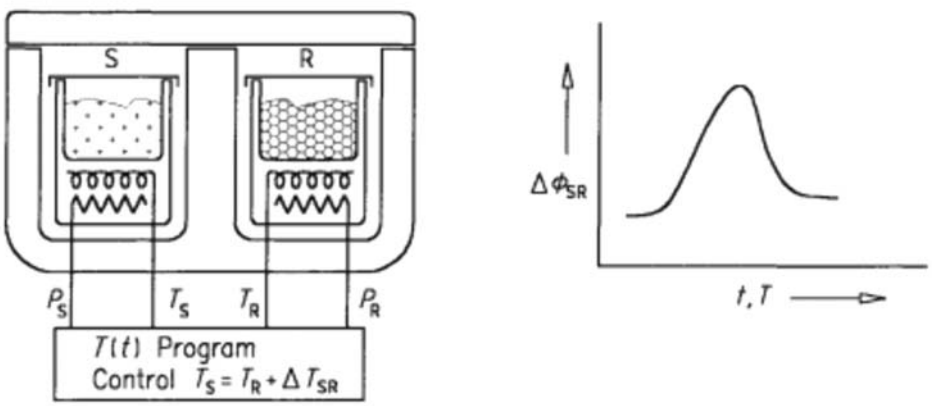

Figure 10. Power compensating DSC (Perkin – Elmer Instruments)[20]

energy change in both furnaces. The power required to maintain the system in equilibrium is proportional to the energy changes occurring in the sample. [1, 21]

All PC DSC are in basic principles the same. But special PC DSC has also been presented in the past. One of them is Photo DSC where direct measurements of radiation flow occur under a light source. This way the degradation of material can also be observed. The maximum heating rate for not modified PC DSC is up to 500 K/min and the maximum cooling rate is up to 400 K/min. Temperature range of measurement is up to 400 °C with time constant of only 1.5 s or lower. Sample masses are around 20 mg. Crucibles of different volumes (lower than several ten cubic millimetres) are made mostly of aluminium.

Hyper DSC

The high resolution of PC-DSC or new type of power compensating DSC provides the best results for an analysis of melting and crystallisation of metals or detection of glass transition temperature (T_g) in medications. Fast scan DSC has the ability to perform valid heat flow measurements with fast linear controlled rates (up to 500 K/min) especially by cooling, where the rates are higher than with the classical PC DSC. Standard DSC operates under 10 K/min. The benefits of such devices are increased sensitivity at higher rates (which enables a better study of the kinetics in the process), suppression of undesired transformation like solid – solid transformation etc. [22] It has a great sensitivity also at a heating rate of 500 K/min with 1 mg of sample material. This technique is specially proper for the pharmaceutics industry for testing medicaments at different temperatures where fast heating rates are necessary to avoid other unwanted reactions etc.

CONCLUSIONS

Several types of the DSC and also DTA devices have been developed in order to achieve as good sensitivity as possible. This depends on the type of the sample or material and its preparation. In some cases the sensitivity can be improved by using smaller samples, if and when it is possible. When this is not possible, the sensitivity mostly depends on the mechanical parts which are used as a thermal path from the furnace to the sample and from the sample to the thermocouples or other detectors. For minimal mechanical effect, different types of measurement devices are constructed. Best results are expected to be achieved by the so called PC DSC apparatuses and hyper DSC.

References

[1] Höhne, G. W. H., Hemminger, W. F., Flammersheim, H. J. (2003): Differential Scanning Calorimetry; Springer Verlag Heidelberg, New York.

[2] Boettinger, W. J., Kattner, U. R., Moon, K. W. (2006): DTA and Heat-flux DSC Measurements of Alloy Melting and Freezing; Metallurgy Division, Material Science and Engineering Laboratory, National Institute of Standards and Technology.

[3] http://personal.cityu.edu.hk/~bhtan/PerkinElmerThermal.ppt

[4] Richards A. Rowland: Differential Thermal Analysis of clays and carbonates

[5] Yang, J., Roy, C. (199): Using DTA to quantitatively determine enthalpy change over a wide temperature range by the mass-difference baseline method; Thermocimica Acta 333; pp. 131–140.

[6] Patrick Ruther, Markus Herrscher, Oliver Paul; A micro differential thermal analysis (μDTA) system; IEEE (2004); pp. 165–168.

[7] L. R. Senesac, D. Yi, A. Greve, J. H. Hales, Z. J. Davis, D. M. Nicholson, A. Boisen, T. Thundat; Micro-differential thermal analysis detection of absorbed explosive molecules using microfabricated bridges; Rev. Sci. Instrum.; 80; 2009

[8] L. G. Parducci, R. B. Duckworth (2007): International Journal of Food Science and Technology, Vol. 7, No. 4; pp. 423–430.

[9] S. L. Johnson, S. Guggenheim & A. F. K. van Gross; Thermal stability of halloysite by high-pressure differential thermal analysis; Clays and Clay Minerals,Vol. 38, No. 5, pp. 477–484,1990

[10] S. Zhu, S. Bulut, A. Le Bail & H. S. Ramaswamy;High-pressure differential scanning calorimetry (DSC): equipment and technique validation using water-ice phase transition data; Journal of Food Process Engineering:vol.27,5; pp. 359–376;2005

[11] Robert L. Danley; New heat flux DSC measurement technique; Thermochimica acta 395 (2003); pp. 201–208.

[12] Czichos, Saito, Smith; Materials Measurement Methods; Springer 2006; pp. 411–413.

[13] C. M. Santos, M. M. S. Ribeiro, M. J. V. Lourence, F. J. V. Santos & C. A. Nieto de Costro; Recent Advances on TG-DSC Accurate measurement;17th Europian Conference on thermophysical Properties, Bratislava, Slovakia, 2005

[14] L. L. Van Zyl; An isothermal calorimeter with sample temperature control. J. Sci. Instr. Vol. 41; 1964; pp.197–202

[15] http://www.ices.a-star.edu.sg/ices/documents/MicroDSC.pdf

[16] Vasilij Gontarev; Termodinamika materialov; Naravoslovnotehniška

fakulteta, Oddelek za materiale in metalurgijo, 2004

[17] http://www.tainstruments.co.jp/application/pdf/Thermal_Library/Applications_Briefs/TA295a.PDF

[18] Cassel Bruce; How Tzero™ Technology Improves DSC performens Part 11. Peak Shape and Resolution; TA278; pp. 1–3

[19] http://www.tainstruments.com/library_download.aspx?file=TA271.pdf

[20] Michael E. Brown; Handbook of Thermal Analysis and Calorimetry: Principles and practice; Elsevier, 1998

[21] W. J. Sichina; Benefits and applications of the Power Compensated Pyris 1 DSC; PE Tech-51 Thermal Analysis; 2000

[22] Pijpers, M. F. J., Mathot, V. B. F. (2008): Optimisation of instrument response and resolution of standard – and high speed power compensation DSC; Journal of Thermal Analysis and Calorimetry; Vol. 93; pp. 319–327.

Author`s Index, Vol. 57, No. 1

Bisht Sandeep	
Breda Mirtič	breda.mirtic@guest.arnes.si
Denić Miodrag	miodrag.denic@yahoo.com
Dervarič Evgen	evgen.dervaric@ntf.uni-lj.si
Dolenec Matej	matej.dolenec@ntf.uni-lj.si
Dolenec Tadej	tadej.dolenec@ntf.uni-lj.si
Đukanović Duško	ugaljprojekt@sezampro.rs
Ganatea Marco Francesco	
Giavazzi Silvia	
Gusain Manju P.	
Gusain Om P.	
Helmut Pristacz	
Klančnik Grega	grega.klancnik@ntf.uni-lj.si
Klenovšek Bojan	bojan.klenovsek@rth.si
Kniewald Goran	kniewald@irb.hr
Kovačič Miha	miha.kovacic@store-steel.si
Kramar Sabina	sabina.kramar@rescen.si
Kumar Vivek	
Lambaša Belak Živana	
Lojen Sonja	sonja.lojen@ijs.si
Macuh Borut	borut.macuh@uni-mb.si
Malenković Vladimir	vladimir.malenkovic@rlv.si
Mauko Alenka	
Medved Jožef	jozef.medved@ntf.uni-lj.si
Mladenović Ana	ana.mladenovic@zag.si
Mrvar Primož	primoz.mrvar@ntf.uni-lj.si
Pandey Piyush	
Petrović David	
Placer Ladislav	

Rodič Tomaž	tomaz.rodic@ntf.uni-lj.si
Senčič Sandra	sandra.sencic@kova.si
Sharma Punam	
Sharma Shivesh	
Sood Anchal	
Šuštarič Primož	
Trkov Mitja	
Urosevic Maja	
Vodopija Josip	
Vukelič Željko	zeljko.vukelic@ntf.uni-lj.si
Žlender Bojan	bojan.zlender@uni-mb.si
Žvab Petra	petra.zvab@guest.arnes.si

INSTRUCTIONS TO AUTHORS

RMZ-MATERIALS & GEOENVIRONMENT (RMZ- Materiali in geookolje) is a periodical publication with four issues per year (established 1952 and renamed to RMZ-M&G in 1998). The main topics of contents are Mining and Geotechnology, Metallurgy and Materials, Geology and Geoenvironment.

RMZ-M&G publishes original Scientific articles, Review papers, Preliminary notes, Professional papers **in English**. In addition, evaluations of other publications (books, monographs,...), In memoriam, Professional remarks and reviews are welcome. The Title, Abstract and Key words in Slovene will be included by the author(s) or will be provided by the referee or the Editorial Office.

**** Additional information and remarks for Slovenian authors:***
Only Professional papers, Publications notes, Events notes, Discussion of papers and In memoriam, will be exceptionally published in the Slovenian language.

Authorship and originality of the contributions. Authors are responsible for originality of presented data, ideas and conclusions as well as for correct citation of data adopted from other sources. The publication in RMZ-M&G obligate authors that the article will not be published anywhere else in the same form.

Specification of Contributions

RMZ-M&G will publish papers of the following categories:

Full papers (optimal number of pages is 7 to 15, longer articles should be discussed with Editor prior to submission). An abstract is required.

- **Original scientific papers** represent unpublished results of original research.
- **Review papers** summarize previously published scientific, research and/or expertise articles on the new scientific level and can contain also other cited sources, which are not mainly result of author(s).

- **Preliminary notes** represent preliminary research findings, which should be published rapidly.
- **Professional paper**s are the result of technological research achievements, application research results and information about achievements in practice and industry.

Short papers (the number of pages is limited to 1 for Discussion of papers and 2 pages for Publication note, Event note and In Memoriam). No abstract is required for short papers.

- **Publication notes** contain author's opinion on new published books, monographs, textbooks, or other published material. A figure of cover page is expected.
- **Event notes** in which descriptions of a scientific or professional event are given.
- **Discussion of papers (Comments)** where only professional disagreements can be discussed. Normally the source author(s) reply the remarks in the same issue.
- **In memoriam** (a photo is expected).

Supervision and review of manuscripts. All manuscripts will be supervised. The referees evaluate manuscripts and can ask authors to change particular segments, and propose to the Editor the acceptability of submitted articles. Authors can suggest the referee but Editor has a right to choose another. **The name of the referee remains anonymous.** The technical corrections will be done too and authors can be asked to correct missing items. The final decision whether the manuscript will be published is made by the Editor in Chief.

The Form of the Manuscript

The manuscript should be submitted as a complete hard copy including figures and tables. The figures should also be enclosed separately, both charts and photos in the original version. In addition, all material should also be provided in electronic form on a diskette or a CD. The necessary information can conveniently also be delivered by E-mail.

Composition of manuscript is defined in the attached Template

The original file of Template is available on RMZ-Materials and Geoenvironment Home page address:

http://www.rmz-mg.com

References - can be arranged in two ways:
- first possibility: alphabetic arrangement of first authors - in text: (Borgne, 1955), or
- second possibility: [1] numerated in the same order as cited in the text: example[1]

Format of papers in journals:

Le Borgne, E. (1955): Susceptibilite magnetic anomale du sol superficiel. *Annales de Geophysique*, 11, pp. 399–419.

Format of books:

Roberts, J. L. (1989): Geological structures, *MacMillan*, *London*, 250 p.

Text on the hard print copy can be prepared with any text-processor. The electronic version on the diskette, CD or E-mail transfer should be in MS Word or ASCII format.
Captions of figures and tables should be enclosed separately.
Figures (graphs and photos) and tables should be original and sent separately in addition to text. They can be prepared on paper or computer designed (MSExcel, Corel, Acad).
Format. Electronic figures are recommended to be in CDR, Al, EPS, TIF or JPG formats. Resolution of bitmap graphics (TIF, JPG) should be at least 300 dpi. Text in vector graphics (CDR, Al, EPS) must be in MSWord Times typography or converted in curves.
Color prints. Authors will be charged for color prints of figures and photos.
Labeling of the additionally provided material for the manuscript should be very clear and must contain at least the lead author's name, address, the beginning of the title and the date of delivery of the manuscript. In case of an E-mail transfer the exact message with above asked data must accompany the attachment with the file containing the manuscript.

Information about RMZ-M&G:
Editor in Chief prof. dr. Peter Fajfar (phone: ++386 1 4250-316) or
Secretary Barbara Bohar Bobnar, univ. dipl. ing. geol. (phone: ++386 1 4704-630),
Aškerčeva 12, 1000 Ljubljana, Slovenia
or at E-mail addresses:
peter.fajfar@ntf.uni-lj.si,
barbara.bohar@ntf.uni-lj.si

Sending of manuscripts. Manuscripts can be sent by mail to the **Editorial Office** address:

- RMZ-Materials & Geoenvironment
  Aškerčeva 12,
  1000 Ljubljana, Slovenia

or delivered to:

- **Reception** of the Faculty of Natural Science and Engineering (for RMZ-M&G)
  Aškerčeva 12,
  1000 Ljubljana, Slovenia
- E-mail - addresses of Editor and Secretary
- You can also contact them on their phone numbers.

These instructions are valid from August 2009

NAVODILA AVTORJEM

RMZ-MATERIALS AND GEOENVIRONMENT (RMZ- Materiali in geookolje) – kratica RMZ-M&G - je revija (ustanovljena kot zbornik 1952 in preimenovana v revijo RMZ-M&G 1998), ki izhaja vsako leto v štirih zvezkih. V reviji objavljamo prispevke s področja rudarstva, geotehnologije, materialov, metalurgije, geologije in geookolja.

RMZ- M&G objavlja izvirne znanstvene, pregledne in strokovne članke ter predhodne objave samo v angleškem jeziku. Strokovni članki so lahko izjemoma napisani v slovenskem jeziku. Kot dodatek so zaželene recenzije drugih publikacij (knjig, monografij …), nekrologi In Memoriam, predstavitve znanstvenih in strokovnih dogodkov, kratke objave in strokovne replike na članke objavljene v RMZ-M&G v slovenskem ali angleškem jeziku. Prispevki naj bodo kratki in jasni.

Avtorstvo in izvirnost prispevkov. Avtorji so odgovorni za izvirnost podatkov, idej in sklepov v predloženem prispevku oziroma za pravilno citiranje privzetih podatkov. Z objavo v RMZ-M&G se tudi obvežejo, da ne bodo nikjer drugje objavili enakega prispevka.

Vrste prispevkov

Optimalno število strani je 7 do 15, za daljše članke je potrebno soglasje glavnega urednika.
Izvirni znanstveni članki opisujejo še neobjavljene rezultate lastnih raziskav.
Pregledni članki povzemajo že objavljene znanstvene, raziskovalne ali strokovne dosežke na novem znanstvenem nivoju in lahko vsebujejo tudi druge (citirane) vire, ki niso večinsko rezultat dela avtorjev.
Predhodna objava povzema izsledke raziskave, ki je v teku in zahteva hitro objavo.
Strokovni članki vsebujejo rezultate tehnoloških dosežkov, razvojnih projektov in druge informacije iz prakse.
Recenzije publikacij zajemajo ocene novih knjig, monografij, učbenikov, razstav …(do dve strani; zaželena slika naslovnice in kratka navedba osnovnih podatkov - izkaznica).

In memoriam (do dve strani, zaželena slika).
Strokovne pripombe na objavljene članke ne smejo presegati ene strani in opozarjajo izključno na strokovne nedoslednosti objavljenih člankov v prejšnjih številkah RMZ-M&G. Praviloma že v isti številki avtorji prvotnega članka napišejo odgovor na pripombe.
Poljudni članki, ki povzemajo znanstvene in strokovne dogodke (do dve strani).

Recenzije. Vsi prispevki bodo predloženi v recenzijo. Recenzent oceni primernost prispevka za objavo in lahko predlaga kot pogoj za objavo dopolnilo k prispevku. Recenzenta izbere Uredništvo med strokovnjaki, ki so dejavni na sorodnih področjih, kot jih obravnava prispevek. Avtorji lahko sami predlagajo recenzenta, vendar si uredništvo pridržuje pravico, da izbere drugega recenzenta. **Recenzent ostane anonimen**. Prispevki bodo tudi tehnično ocenjeni in avtorji so dolžni popraviti pomanjkljivosti. Končno odločitev za objavo da glavni in odgovorni urednik.

Oblika prispevka

Prispevek predložite v tiskanem oštevilčenem izvodu (po možnosti z vključenimi slikami in tabelami) ter na disketi ali CD, lahko pa ga pošljete tudi prek E-maila. Slike in grafe je možno poslati tudi risane na papirju, fotografije naj bodo originalne.

Razčlenitev prispevka:

Predloga za pisanje članka se nahaja na spletni strani:

http://www.rmz-mg.com/predloga.htm

Seznam literature je lahko urejen na dva načina:
-po abecednem zaporedju prvih avtorjev ali
-po [1]vrstnem zaporedju citiranosti v prispevku.

Oblika je za oba načina enaka:
Članki:

> Le Borgne, E. (1955): Susceptibilite magnetic anomale du sol superficiel. *Annales de Geophysique*; Vol. 11, pp. 399–419.

Knjige:

ROBERTS, J. L. (1989): Geological structures, *MacMillan*, *London*, 250 p.

Tekst izpisanega izvoda je lahko pripravljen v kateremkoli urejevalniku. Na disketi, CD ali v elektronskem prenosu pa mora biti v MS Word ali v ASCII obliki.
Naslovi slik in tabel naj bodo priloženi posebej. Naslove slik, tabel in celotno besedilo, ki se pojavlja na slikah in tabelah, je potrebno navesti v angleškem in slovenskem jeziku.
Slike (ilustracije in fotografije) in tabele morajo biti izvirne in priložene posebej. Njihov položaj v besedilu mora biti jasen iz priloženega kompletnega izvoda. Narejene so lahko na papirju ali pa v računalniški obliki (MS Excel, Corel, Acad).
Format elektronskih slik naj bo v EPS, TIF ali JPG obliki z ločljivostjo okrog 300 dpi. Tekst v grafiki naj bo v Times tipografiji.
Barvne slike. Objavo barvnih slik sofinancirajo avtorji
Označenost poslanega materiala. Izpisan izvod, disketa ali CD morajo biti jasno označeni – vsaj z imenom prvega avtorja, začetkom naslova in datumom izročitve uredništvu RMZ-M&G. Elektronski prenos mora biti pospremljen z jasnim sporočilom in z enakimi podatki kot velja za ostale načine posredovanja.

Informacije o RMZ-M&G: urednik prof. dr. Peter Fajfar, univ. dipl. ing. metal. (tel. ++386 1 4250316) ali tajnica Barbara Bohar Bobnar, univ. dipl. ing. geol. (tel. ++386 1 4704630), Aškerčeva 12, 1000 Ljubljana
ali na E-mail naslovih:
peter.fajfar@ntf.uni-lj.si
barbara.bohar@ntf.uni-lj.si

Pošiljanje prispevkov. Prispevke pošljite priporočeno na naslov **Uredništva:**

- RMZ-Materials and Geoenvironment
  Aškerčeva 12,
  1000 Ljubljana, Slovenija

oziroma jih oddajte v

- **Recepciji** Naravoslovnotehniške fakultete (pritličje) (za RMZ-M&G)
  Aškerčeva 12,
  1000 Ljubljana, Slovenija
- Možna je tudi oddaja pri uredniku oziroma pri tajnici.

Navodila veljajo od avgusta 2009.

TEMPLATE

The title of the manuscript should be written in bold letters (Times New Roman, 14, Center)

Naslov članka (Times New Roman, 14, Center)

Name Surname[1], …. , & Name Surname[X] (Times New Roman, 12, Center)

[x] University of ..., Faculty of ..., Address…, Country ... (Times New Roman, 11, Center)

*Corresponding author. E-mail: ... (Times New Roman, 11, Center)

Abstract (Times New Roman, Normal, 11): The abstract should be concise and should present the aim of the work, essential results and conclusion. It should be typed in font size 11, single-spaced. Except for the first line, the text should be indented from the left margin by 10 mm. The length should not exceed fifteen (15) lines (10 are recommended).

Izvleček (Times New Roman, navadno, 11): Kratek izvleček namena članka ter ključnih rezultatov in ugotovitev. Razen prve vrstice naj bo tekst zamaknjen z levega roba za 10 mm. Dolžina naj ne presega petnajst (15) vrstic (10 je priporočeno).

Key words: a list of up to 5 key words (3 to 5) that will be useful for indexing or searching. Use the same styling as for abstract.
Ključne besede: seznam največ 5 ključnih besed (3–5) za pomoč pri indeksiranju ali iskanju. Uporabite enako obliko kot za izvleček.

Introduction (Times New Roman, Bold, 12)

Two lines below the keywords begin the introduction. Use Times New Roman, font size 12, Justify alignment.

There are two (2) admissible methods of citing references in text:

1. by stating the first author and the year of publication of the reference in the parenthesis at the appropriate place in the text and arranging the reference list in the alphabetic order of first authors; e.g.:
   "Detailed information about geohistorical development of this zone can be found in: Antonijević (1957), Grubić (1962), ..."
   "… the method was described previously (Hoefs, 1996)"
2. by consecutive Arabic numerals in square brackets, superscripted at the appropriate place in the text and arranging the reference list at the end of the text in the like manner; e.g.:
   "... while the portal was made in Zope environment. [3]"

Materials and methods (Times New Roman, Bold, 12)

This section describes the available data and procedure of work and therefore provides enough information to allow the interpretation of the results, obtained by the used methods.

Results and discussion (Times New Roman, Bold, 12)

Tables, figures, pictures, and schemes should be incorporated in the text at the appropriate place and should fit on one page. Break larger schemes and tables into smaller parts to prevent extending over more than one page.

Conclusions (Times New Roman, Bold, 12)

This paragraph summarizes the results and draws conclusions.

Acknowledgements (Times New Roman, Bold, 12, Center - optional)

This work was supported by the ****.

References (Times New Roman, Bold, 12)

In regard to the method used in the text, the styling, punctuation and capitalization should conform to the following:

FIRST OPTION - in alphabetical order

Casati, P., Jadoul, F., Nicora, A., Marinelli, M., Fantini-Sestini, N. & Fois, E. (1981): Geologia della Valle del'Anisici e dei gruppi M. Popera - Tre Cime di Lavaredo (Dolomiti Orientali). *Riv. Ital. Paleont.*; Vol. 87, No. 3, pp. 391–400, Milano.

Folk, R. L. (1959): Practical petrographic classification of limestones. *Amer. Ass. Petrol. Geol. Bull.;* Vol. 43, No. 1, pp. 1–38, Tulsa.

SECOND OPTION - in numerical order

[1] Trček, B. (2001): *Solute transport monitoring in the unsaturated zone of the karst aquifer by natural tracers.* Ph. D. Thesis. Ljubljana: University of Ljubljana 2001; 125 p.

[2] Higashitani, K., Iseri, H., Okuhara, K., Hatade, S. (1995): Magnetic Effects on Zeta Potential and Diffusivity of Nonmagnetic Particles. *Journal of Colloid and Interface Science, 172*, pp. 383–388.

Citing the Internet site:

CASREACT-Chemical reactions database [online]. Chemical Abstracts Service, 2000, updated 2. 2. 2000 [cited 3. 2. 2000]. Accessible on Internet: http://www.cas.org/CASFILES/casreact.html.

Texts in Slovene (title, abstract and key words) can be written by the author(s) or will be provided by the referee or by the Editorial Board.

PREDLOGA ZA SLOVENSKE ČLANKE

Naslov članka (Times New Roman, 14, Na sredino)

The title of the manuscript should be written in bold letters (Times New Roman, 14, Center)

Ime Priimek[1], …, Ime Priimek[X] (Times New Roman, 12, Na sredino)

[X]Univerza…, Fakulteta…, Naslov…, Država… (Times New Roman, 11, Center)

*Korespondenčni avtor. E-mail: ... (Times New Roman, 11, Center)

Izvleček (Times New Roman, Navadno, 11): Kratek izvleček namena članka ter ključnih rezultatov in ugotovitev. Razen prve j bo tekst zamaknjen z levega roba za 10 mm. Dolžina naj ne presega petnajst (15) vrstic (10 je priporočeno).

Abstract (Times New Roman, Normal, 11): The abstract should be concise and should present the aim of the work, essential results and conclusion. It should be typed in font size 11, single-spaced. Except for the first line, the text should be indented from the left margin by 10 mm. The length should not exceed fifteen (15) lines (10 are recommended).

Ključne besede: seznam največ 5 ključnih besed (3–5) za pomoč pri indeksiranju ali iskanju. Uporabite enako obliko kot za izvleček.
Key words: a list of up to 5 key words (3 to 5) that will be useful for indexing or searching. Use the same styling as for abstract.

Uvod (Times New Roman, Krepko, 12)

Dve vrstici pod ključnimi besedami se začne Uvod. Uporabite pisavo Times New Roman, velikost črk 12, z obojestransko poravnavo. Naslovi slik in tabel (vključno z besedilom v slikah) morajo biti v slovenskem jeziku.

Slika (Tabela) X. Pripadajoče besedilo k sliki (tabeli)

Obstajata dve sprejemljivi metodi navajanja referenc:

1. z navedbo prvega avtorja in letnice objave reference v oklepaju na ustreznem mestu v tekstu in z ureditvijo seznama referenc po abecednem zaporedju prvih avtorjev; npr.:

"Detailed information about geohistorical development of this zone can be found in: Antonijević (1957), Grubić (1962), ..."

"… the method was described previously (Hoefs, 1996)"

ali

2. z zaporednimi arabskimi številkami v oglatih oklepajih na ustreznem mestu v tekstu in z ureditvijo seznama referenc v številčnem zaporedju navajanja; npr.;

"... while the portal was made in Zope[3] environment."

Materiali in metode (Times New Roman, Krepko, 12)

Ta del opisuje razpoložljive podatke, metode in način dela ter omogoča zadostno količino informacij, da lahko z opisanimi metodami delo ponovimo.

Rezultati in razprava (Times New Roman, Krepko, 12)

Tabele, sheme in slike je treba vnesti (z ukazom Insert, ne Paste) v tekst na ustreznem mestu. Večje sheme in tabele je po treba ločiti na manjše dele, da ne presegajo ene strani.

Sklepi (Times New Roman, Krepko, 12)

Povzetek rezultatov in sklepi.

Zahvale (Times New Roman, Krepko, 12, Na sredino - opcija)

Izvedbo tega dela je omogočilo ……

Viri (Times New Roman, Krepko, 12)

Glede na uporabljeno metodo citiranja referenc v tekstu upoštevajte eno od naslednjih oblik:

PRVA MOŽNOST (priporočena) - v abecednem zaporedju

Casati, P., Jadoul, F., Nicora, A., Marinelli, M., Fantini-Sestini, N. & Fois, E. (1981): Geologia della Valle del'Anisici e dei gruppi M. Popera – Tre Cime di Lavaredo (Dolomiti Orientali). *Riv. Ital. Paleont.*; Vol. 87, No. 3, pp. 391–400, Milano.

Folk, R. L. (1959): Practical petrographic classification of limestones. *Amer. Ass. Petrol. Geol. Bull.;* Vol. 43, No. 1, pp. 1–38, Tulsa.

DRUGA MOŽNOST - v numeričnem zaporedju

[1] Trček, B. (2001): *Solute transport monitoring in the unsaturated zone of the karst aquifer by natural tracers.* Ph. D. Thesis. Ljubljana: University of Ljubljana 2001; 125 p.

[2] Higashitani, K., Iseri, H., Okuhara, K., Hatade, S. (1995): Magnetic Effects on Zeta Potential and Diffusivity of Nonmagnetic Particles. *Journal of Colloid and Interface Science, 172*, pp. 383–388.

Citiranje spletne strani:

CASREACT-Chemical reactions database [online]. Chemical Abstracts Service, 2000, obnovljeno 2. 2. 2000 [citirano 3. 2. 2000]. Dostopno na svetovnem spletu: http://www.cas.org/CASFILES/casreact.html.

Znanstveni, pregledni in strokovni članki ter predhodne objave se objavijo v angleškem jeziku. Izjemoma se strokovni članek objavi v slovenskem jeziku.


RTH

industrijski forum IRT

www.forum-irt.si

Industrijski forum 2010
Inovacije, razvoj, tehnologije

Forum znanja in izkušenj

V dveh dneh se je na Industrijskem forumu IRT 2009 družilo in tkalo nove vezi več kot 250 strokovnjakov, ki so lahko prisluhnili več kot 50 prispevkom o strokovnih, inovacijskih in tehnoloških dosežkih domačega znanja zadnjih nekaj let. Ob forumu se je predstavilo tudi več deset podjetij iz industrije, ki so na razstavnih prostorih na ogled postavili svoje najnovejše dosežke. Udeleženci so se strinjali, da je zaradi gospodarske krize še toliko pomembnejše druženje na dogodkih, saj se na njih sklene veliko novih poznanstev, ki omogočajo izmenjavo mnenj, izkušenj in znanj, pogosto pa pomenijo tudi začetek uspešnega sodelovanja. Zato snovalci revije IRT3000 na krilih uspeha prvega foruma in v ustvarjalnem sodelovanju z industrijo pripravljajo Industrijski forum IRT 2010.

Dogodek je namenjen predstavitvi dosežkov in novosti iz industrije, inovacij in inovativnih rešitev iz industrije in za industrijo, primerov prenosa znanja in izkušenj iz industrije v industrijo, uporabe novih zamisli, zasnov, metod tehnologij in orodij v industrijskem okolju, resničnega stanja v industriji ter njenih zahtev in potreb, uspešnih aplikativnih projektov raziskovalnih organizacij, inštitutov in univerz, izvedenih v industrijskem okolju, ter primerov prenosa uporabnega znanja iz znanstveno-raziskovalnega okolja v industrijo.

Osrednje teme IFIRT

- inoviranje
- razvoj
- izdelovalne tehnologije
- orodjarstvo in strojegradnja
- toplotna obdelava in spajanje
- napredni materiali
- umetne mase in njihova predelava
- organiziranje in vodenje proizvodnje
- menedžment kakovosti
- avtomatizacija
- robotizacija
- informatizacija
- mehatronika
- proizvodna logistika
- informacijske tehnologije
- napredne tehnologije
- ponudba znanja

Portorož, 7. in 8. junij 2010

Organizatorja dogodka: PROFIDTP, d. o. o., Gradišče nad Pijavo Gorico 204, 1291 Škofljica; ECETERA, d. o. o., Motnica 7 A, 1236 Trzin | **Partner dogodka:** Obrtno-podjetniška zbornica Slovenije,
Organizacijski vodja dogodka: Darko Švetak, darko.svetak@forum-irt.si | **Programski vodja dogodka:** dr. Tomaž Perme, tomaz.perme@forum-irt.si

Dodatne informacije in prijava na dogodek: Industrijski forum IRT 2010, Motnica 7 A, 1236 Trzin | tel.: 01/600 1000 | faks: 01/600 3001 | e-pošta: info@forum-irt.si | www.forum-irt.si

www.forum-irt.si

Univerza v Ljubljani, Naravoslovnotehniška fakulteta

Oddelek za materiale in metalurgijo

Aškerčeva cesta 12
1000 Ljubljana

Telefon: (01) 470 46 08,
E-pošta: omm@ntf.uni-lj.si

internetni naslov:
http://www.ntf.uni-lj.si/

Če se premakne, boste izvedeli prvi

Leica Geosystems rešitve za opazovanje premikov

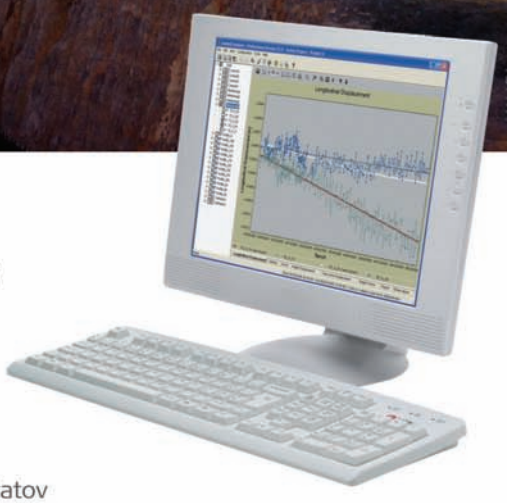

- **Geodetski senzorji**
  samodejni tahimetri, GPS in GNSS senzorji
- **Geotehnični senzorji**
  senzorji nagiba, Campbell datalogger
- **Drugi senzorji**
  meteo, senzorji nivoja
- **Programska oprema**
  za zajem in obdelavo podatkov, analizo opazovanj, alarmiranje, predstavitev rezultatov

geo servis

Geoservis, d.o.o.
Litijska cesta 45, 1000 Ljubljana
t. (01) 586 38 30, i. www.geoservis.si

■ Authorized Leica Geosystems Distributor

- when it has to be **right**

Leica Geosystems